View metadata, citation and similar papers at core.ac.uk
brought to you by CORE
provided by Sydney eScholarship

THE UNIVERSITY OF
SYDNEY

# COPYRIGHT AND USE OF THIS THESIS

This thesis must be used in accordance with the provisions of the Copyright Act 1968.

Reproduction of material protected by copyright may be an infringement of copyright and copyright owners may be entitled to take legal action against persons who infringe their copyright.

Section 51 (2) of the Copyright Act permits an authorized officer of a university library or archives to provide a copy (by communication or otherwise) of an unpublished thesis kept in the library or archives, to a person who satisfies the authorized officer that he or she requires the reproduction for the purposes of research or study.

The Copyright Act grants the creator of a work a number of moral rights, specifically the right of attribution, the right against false attribution and the right of integrity.

You may infringe the author's moral rights if you:

- fail to acknowledge the author of this thesis if you quote sections from the work
- attribute this thesis to another author
- subject this thesis to derogatory treatment which may prejudice the author's reputation

For further information contact the University's Director of Copyright Services

**sydney.edu.au/copyright**

# Channel Estimation, Synchronisation and Contention Resolution in Wireless Communication Networks

Qiong Zhao

A thesis submitted in fulfilment of
requirements for the degree of Doctor of Philosophy

THE UNIVERSITY OF SYDNEY

School of Electrical & Information Engineering
The University of Sydney

July 2014

# Abstract

In the past decade, the number of wireless communications users is increasing at an unprecedented rate. However, limited radio resources must accommodate the increasing number of users. Hence, the efficient use of radio spectrum is a critical issue that needs to be addressed. In order to improve the spectral efficiency for the wireless communication networks, we investigate two promising technologies, the relaying and the multiple access schemes. In the physical (PHY) layer of the open systems interconnect (OSI) model, the relaying schemes are capable to improve the transmission reliability and expand transmission coverage via cooperative communications by using relay nodes. Hence, the two-way relay network (TWRN), a cooperative communications network, is investigated in the first part of the thesis. In the media access control (MAC) layer of the OSI model, the multiple access schemes are able to schedule multiple transmissions by efficiently allocating limited radio resources. As a result, the contention-based multiple access schemes for contention resolution are explored in the second part of the thesis.

In order to achieve the optimal decoding at the destination node, one of the challenges is the estimation of the time-varying channel impairments. In the first part of the thesis, the channel estimation for the two-way relay networks (TWRNs) is investigated. Firstly, the channel estimation issue is considered under the assumption of the perfect synchronisation. Then, the channel estimation is conducted, by relaxing the assumption of perfect synchronisation. Assum-

ing perfect synchronisation in the TWRNs, most works on channel estimation problem focus on training-based approaches which impose a significant training overhead that reduces the spectral efficiency of the system. Some works propose semi-blind channel estimation algorithms, named the deterministic maximum likelihood (DML) and modified constrained maximum likelihood (MCML), which reduce the training overhead of the training-based algorithms. However, the DML and MCML channel estimators depend on optimisation tools to achieve the channel estimation. As a result, the computational complexity of the DML and MCML algorithms are high, which makes them impractical. To make the blind channel estimation algorithm practical, we propose two low complexity semi-blind channel estimation algorithms, referred to as the low complexity maximum likelihood (LCML) estimator and the modified low complexity maximum likelihood (MLCML) estimator. The two algorithms estimate non-reciprocal flat-fading channels by using only one training symbol per estimation in the amplify-and-forward two-way relay networks (AF-TWRNs). We propose the LCML algorithm with a convex maximum likelihood estimation function that produces a closed-form channel estimator. By taking into account the modulation structure, the MLCML channel estimation algorithm with the closed-form channel estimation is proposed to further improved the mean squared error (MSE) performance of the LCML algorithm in BPSK. The MSE performances evaluation shows that the derived channel estimators approach the true channel in either high signal-to-noise ratio (SNR) or large frame length scenarios. Analysis shows that the LCML channel estimator is consistent and unbiased. Due to the convex optimisation function and the derived closed-form channel estimation, the computational complexity of the DML and MCML channel estimators is remarkably reduced to $\mathcal{O}(N)$, where $N$ is the frame length of signals. In addition to a lower computational complexity, the LCML algorithm achieves a better MSE performance than the DML algorithm for the BPSK modulation scheme. To relax the assumption of the perfect synchronisation in the TWRNs, we explored the joint channel estimation and synchronisation issues in the asynchronous two-way relay networks, where there are timing offsets between nodes. In the asynchronous amplify-and-forward (AF) TWRNs, the joint synchronisation and channel estimation algorithm with few training symbols have not been investigated and we develop a generalised low complexity maximum likelihood (GLCML) algorithm to perform channel estimation in the presence of a timing offset using one training symbols per estimation. Then a joint synchronisation and channel estimation (JSCE) algorithm is proposed to estimate the timing offset, using one training symbols per estimation. The low computational complexity is achieved by the GLCML and JSCE algorithms by deriving closed-form solutions. Monte-Carlo simulations demonstrate that the GLCML algorithm always select the optimal channel estimation in the cases of varying timing offsets and the JSCE algorithm is able to achieve accurate timing offset estimations.

Another challenge facing the wireless communication systems is the contention and interference due to multiple transmissions from multiple nodes, sharing the common communication medium. To improve the spectral efficiency in the media access control layer, the backoff algorithm is employed to resolve contention and mitigate signal interference in the multiple access networks. The challenge here is to adjust the contention window length according to the average local packet arrival rate and the channel congestion. We propose a self-adaptive backoff (SAB) algorithm to resolve contention in the contention-based multiple access networks by deriving the optimal contention window length, which maximises the system throughput by considering the number of nodes, the average local packet arrival rate and the channel congestion condition. Given the average local packet arrival rate and the total number of nodes in the network, the expression of the contention window length is derived from the discrete-time Markov chain model

and network contention analysis. Then based on the derived contention window length expression, we formulate the system throughput as the optimisation function and use it to achieve the optimal contention window length. Thus each node is able to adjust the contention window (CW) length adaptively to network conditions. Compared with the existing backoff algorithm, the proposed algorithm significantly saves energy of sensors, while achieving a better system throughput with a lower collision rate.

# Acknowledgement

This doctoral thesis would not have been possible without the inspiration, encouragement and support from many people, to whom I am greatly indebted. Foremost, I would like to express my sincere gratitude to my supervisor, Professor Branka Vucetic, for her academic advice, continuous support and patience during my study at the University of Sydney. Her guidance helped me in all the time of research and writing of this thesis. I feel honoured to have been given the opportunity to work under her supervision.

I would like to express my special thanks to my associate supervisor, Dr.Zhendong (Kyle) Zhou, for his constant encouragement and guidance. I am really grateful to him, not only for contributing many valuable suggestions and improvements to this thesis, but most importantly for his support along the way. I could not have imagined having a better advisor and mentor for my Ph.D study.

Next, I would like to express my gratitude to my co-supervisor, Dr.Wibowo Hardjawana, for his innumerable comments, discussions, and encouragements.

Besides my supervisors, I would like to express my deepest gratitude to my parents for their unreserved love, patience, support, encouragement and understanding that no words can express. I am extremely grateful to them to have sacrificed themselves to give me the warmest care and the best education.

I also thank my friend Keov Kolyan Teav, for sharing joys and sorrows all the time, and Dr.Jun Li, for his insightful comments on my research. My sincere thanks also goes to Tao Yang and Hui Miao, who are the best room mates in the world, for cheering me up every time when I am upset.

The final warmest thanks go to my fiance, who really changed my life to the best in everything. I thank him for his love and spiritual support.

*Qiong Zhao*

*Sydney, NSW, Australia*

*March 2014*

# Statement of Originality

I hereby declare that this thesis, submitted in fulfilment of the requirements for the award of Doctor of Philosophy, in the School of Electrical and Information Engineering, the University of Sydney, is my own work unless otherwise referenced or acknowledged. The document has not been previously submitted for the award of any other qualification at any educational institution. Most of the results contained herein have been published, accepted for publication, or submitted for publication, in journals or conferences of international standing.

The original motivation to pursue research in this field was provided by thesis supervisor, Professor Branka Vucetic from the University of Sydney. The novel ideas and the author's contributions are described in Chapters 3, 4 and 5. The novel ideas and the author's contributions are summarised as follows:

1. In Chapter 3, "Semi-Blind Low Complexity Channel Estimation Algorithms in AF-TWRNs", we present two new semi-blind low complexity channel estimation algorithms, referred to as the low complexity maximum likelihood (LCML) estimator and the modified low complexity maximum likelihood (MLCML) estimator. The contributions of this chapter include formulating a convex maximum likelihood estimation function and deriving the closed-form channel estimation using approximations. By exploring the modulation structure, the mean-squared error (MSE) performance of the LCML algorithm is improved by the MLCML algorithm. The theoretical MSE

expression is derived and the MSE performance of the proposed algorithms in the scenarios of a high signal-to-noise ratio (SNR) and a large signal frame length is analysed. This work is presented in Conference paper [1] and Journal paper [1].

2. In Chapter 4,"Joint Synchronisation and Channel Estimation in AF-TWRNs", we propose two channel estimation algorithms in the asynchronous two-way relay networks (TWRNs), referred to as the generalised low complexity maximum likelihood (GLCML) algorithm and the joint synchronisation and channel estimation (JSCE) algorithm. The contributions of this chapter include formulating a convex maximum likelihood estimation function to estimate the channel parameters, the frame offset and the symbol offset jointly. In the GLCML algorithm, the estimation sample selection criteria (ESSC) is proposed to select the optimal channel estimation based on the MSE expressions. Two sub-algorithms of the JSCE algorithm are proposed to estimate the frame offset and the symbol offset. Furthermore, the JSCE algorithms achieve low computational complexity with closed-form solutions. This work is presented in Journal paper [1].

3. In Chapter 5,"Contention Resolution Algorithm", we propose a backoff algorithm to resolve contention in the contention-based multiple access networks. The contributions of this chapter include deriving the contention window length expression with respect to the average local packet arrival rate and the number of nodes in the system. We model the states of a node as a discrete-time Markov chain and use the queue theory to analyse the traffic load. As the average local packet arrival rate is considered, the assumption that all the nodes always have packets to transmit is relaxed in the proposed algorithm.

# Journal papers

[1] Q. Zhao, Z. Zhou, J. Li, and B. Vucetic, "Joint semi-blind channel estimation and synchronization in two way relay networks," *IEEE Transactions on Vehicular Technology*, vol. PP, no. 99, pp. 1–1, 2014.

# Conference papers

[1] Q. Zhao, Z. Zhou, and B. Vucetic, "Low complexity semi-blind channel estimation algorithm in two-way relay networks," in *22nd International Symposium on Personal Indoor and Mobile Radio Communications (PIMRC), 2011 IEEE*. IEEE, 2011, pp. 1443–1447.

# Table of Contents

# List of Figures

# List of Tables

# Glossary of Notations

| | |
|---|---|
| $\lvert X \rvert$ | Absolute value of X |
| $\Re\{X\}$ | Real part of X |
| $\Im\{X\}$ | Imaginary part of X |
| $\hat{X}$ | Estimation of X |
| $\lvert \mathbf{X} \rvert$ | $l_2$ norm of vector $\mathbf{X}$ |
| $\mathbf{X}$ | Absolute value of the elements of vector $\mathbf{X}$ |
| $\mathbf{X}^H$ | Conjugate transpose of $\mathbf{X}$ |
| $\mathbf{X}^T$ | Transpose of $\mathbf{X}$ |
| $\mathbf{I}_N$ | $N \times N$ identity matrix |
| $\in$ | Is an element of |
| $\triangleq$ | Defined as |
| $\propto$ | Is proportional to |
| **ln** | Natural logarithm |
| **log** | Logarithm |
| **Max** | Maximum |
| **Min** | Minimum |
| $\mathbb{C}$ | Complex number |

# List of Acronyms

| | |
|---|---|
| **AF** | Amplify-and-forward |
| **AWGN** | Additive white Gaussian noise |
| **BPSK** | Binary phase-shift-keying |
| **BEB** | Binary exponential backoff |
| **BS** | Base station |
| **BER** | Bit error rate |
| **CDMA** | Code division multiple access |
| **CPM** | Continuous-phase modulation |
| **CM** | Constant-modulus |
| **CSMA** | Carrier sense multiple access |
| **CSI** | Channel state information |
| **CW** | Contention window |
| **DF** | Decode-and-forward |
| **DML** | Deterministic maximum likelihood |
| **EDGE** | Enhanced Data Rates for GSM Evolution EDGE |
| **EIED** | Exponential increase and exponential decrease |
| **ESSC** | Estimation sample selection criterion |
| **FACE** | Frame asynchronous channel estimation |
| **FDMA** | Frequency division multiple access |

| | |
|---|---|
| **GLCML** | Generalised low complexity maximum likelihood |
| **GSM** | Global system for mobile communications |
| **JSCE** | Joint synchronisation and channel estimation |
| **LANs** | Local area networks |
| **LCML** | Low complexity maximum likelihood |
| **LS** | Least-squares |
| **LTE** | Long Term Evolution |
| **MAC** | Media access control |
| **MANs** | Metropolitan area networks |
| **MCML** | Modified continuous maximum likelihood |
| **ML** | Maximum-likelihood |
| **MLCML** | Modified low complexity maximum likelihood |
| **MIMO** | Multi-input multi-output |
| **MSE** | Mean squared error |
| **MPSK** | M-ary phase-shift-keying |
| **OSI** | Open systems interconnect |
| **PHY** | Physical layer |
| **PLL** | Phase-locked loop |
| **SNR** | Signal-to-noise ratio |
| **SACE** | Symbol asynchronous channel estimation |

| | |
|---|---|
| **SAB** | Self-adaptive backoff |
| **SER** | Symbol error rate (SER) |
| **TDMA** | Time division multiple access |
| **TWRNs** | Two-way relay networks |
| **3GPP** | 3rd Generation Partnership Program |

# Chapter 1

# Introduction

## 1.1 Preliminary

In the past decade, the number of wireless communications users is increasing at an unprecedented rate. However, the radio resources, accommodating the increasing number of users, are limited. Therefore, the efficient use of radio spectrum is a critical issue that needs to be addressed. The pursuit for spectral efficiency is always one of the primary goals of wireless communications. A number of techniques have been proposed or already implemented to improve the spectral efficiency. Among them, two promising technologies are the relaying schemes [1], employed in the physical (PYH) layer of the open systems interconnect (OSI) model [2], and the media access schemes [3], employed in the media access control (MAC) layer [2] of the OSI model.

In the relay communications networks, data transmission from a source node can be overheard by other nodes, due to the broadcast nature of the wireless medium. As a result, it is possible for the source node to cooperate with these overhearing nodes in transmitting their signals to the destination[4]. As shown in Fig.1.1, if the destination node is out of the transmission range of the source node, the relay can help forward the information from the source to the destination. Therefore, the relay transmission can effectively extend the transmission coverage and improve the overall data rate [1]. If the destination node is in the transmission range of the source node, the combined signal of the relayed signal and the direct signal is transmitted to the destination node, as shown in Fig.1.2 [5]. In this case, the relay node can cooperate with the source node to transmit information to the destination node and the transmission reliability can be improved by exploiting the user diversity.

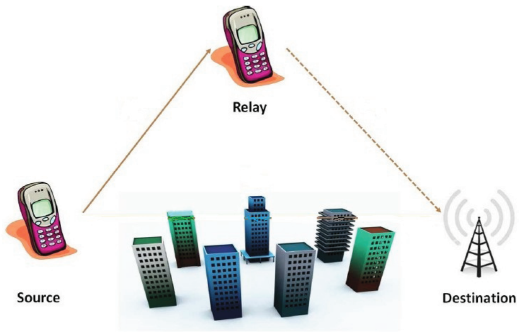


Figure 1.1: Relay assisted communication network that expands the transmission coverage.

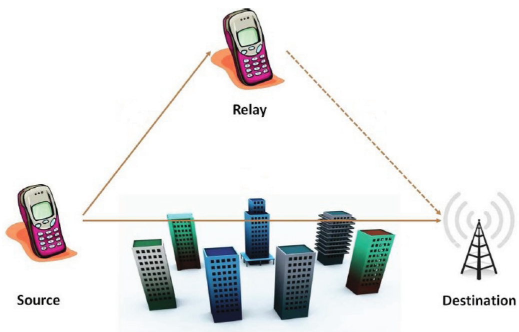


Figure 1.2: Relay assisted communication network that improves the transmission reliability.

The media access schemes are used in the media access control (MAC) layer [2] for resource allocation in order to efficiently utilise the resources. For the purpose of communications, multiple nodes, attempting to utilise common wireless medium, may transmit simultaneously. Hence, the concurrent transmissions may interfere with each other and lead to transmission collisions. To avoid such destructive interference, the primary task of the MAC layer is to coordinate the transmissions of multiple nodes. The cooperation among multiple nodes, contending for their access, can be achieved by resource allocation or scheduling. The typical way to share the wireless medium is channel allocation [6], in which the wireless channel resource is partitioned in a certain dimension, e.g., time, frequency, or spreading code. Consequently, there are time division multiple access (TDMA), frequency division multiple access (FDMA), and code division multiple access (CDMA) [7], as shown in Fig.1.3.

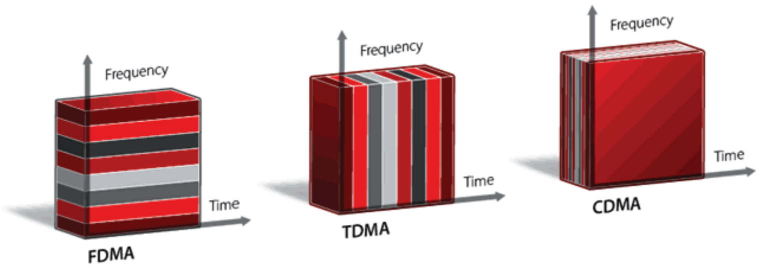


Figure 1.3: Channel access methods: FDMA, TDMA and CDMA.

### 1.1.1 Relaying Schemes

Relaying schemes can effectively extend the transmission coverage and reliability by exploiting the cooperative diversity, which is a cooperative multiple antenna technique, which exploits user diversity by decoding the combined signal of the relayed signal and the direct signal in wireless multi-hop networks, for improving or maximising total network channel capacities for any given set of bandwidths [8]. Hence, it is expected to play a significant role in the next generation wireless cellular systems [9]. In energy constrained wireless sensor networks (WSNs) [10], relaying schemes can be exploited to extend network lifetime. Moreover, relay transmission has been incorporated into many wireless standards, such as IEEE 802.11s (mesh networking) [11], IEEE 802.11j (wireless multi-hop relay)

[12], 802.16m (WiMAX2) [13], Femtocell [14] and LTE advanced [15, 16, 17].

The relay channel was first introduced in [4], and initial research studied the rates achieved in relay channels [1, 18]. [19] proposed cooperative protocols, with amplify-and-forward (AF) and decode-and-forward (DF) being the two basic relaying schemes. In AF relaying schemes, the relay node amplifies the received signal and then forwards the amplified signal to the destination. In DF relaying schemes, the relay node decodes, re-encodes, and retransmits the received signal. A spectral efficient relaying technique called two-way relaying has been proposed in [20], in which two nodes exchange information via the help of a relay node, as shown in Fig. 1.4 [5]. Two-way relaying method consists of two phases: the multiple access phase, in which the source nodes simultaneously transmit their signal to the relay, and the broadcast phase, in which the relay forwards the received signal to the source nodes. The attractive feature of this two-way relay model is that it can improve the spectral inefficiency of one-way relaying under a half-duplex constraint[20, 21, 22, 23, 24]. With one-way relaying, it takes four time slots to exchange information between two nodes via a half-duplex relay node. However, the spectral efficiency can be improved by using only two time slots to exchange information in the two-way relay networks (TWRNs) [25], by exploiting the knowledge of the nodes' own transmitted signals and the broadcast nature of the wireless medium. The two-way relay networks (TWRN) can be applied in many practical scenarios. In smart grid [26], demand response applications require high data rate two-way communications between the customers and the utility's head-end system [27]. In cellular networks, examples of the TWRNs are the base station communicates with a mobile user via a dedicated relay, or two mobile users exchange data via the access point in a WLAN [5].


Figure 1.4: Relay assisted two-way communication network with two user terminals and a relay.

### 1.1.2 Multiple Access Schemes

The multiple access schemes allow multiple users to share the available spectrum simultaneously. In this way, the spectrum can be effectively utilised. In local area networks (LANs) [28] and metropolitan area networks (MANs) [29], multiple access methods enable bus networks, ring networks, hubbed networks, wireless networks and half duplex point-to-point communication [30, 31, 32, 33]. In satellite communications [34], code-division [35], frequency-division [7], and time-division [36] multiple access are presently used, which enable the capability of a communications satellite to function as a portion of a communications link between more than one pair of satellite terminals concurrently [6].

Multiple access schemes can be classified as reservation-based multiple access (e.g., FDMA, TDMA, CDMA)[7] and contention-based multiple access, e.g., ALOHA and carrier sense multiple access (CSMA)) [37, 38]. The reservation-based multiple access schemes, which allocate different channel resources to different users, have a disadvantage in that once the channel is assigned, it remains idle if the user has nothing to transmit, while other users may have data waiting to be transmitted. This problem is critical when data generation is random. In this situation, the contention-based multiple access schemes, which allow each user to access the network whenever the user has information to send, are more efficient and flexible. This results from the fact that a communication channel is shared by many users and users transmit their data in a random or partially coordinated fashion [30]. In the wireless sensor networks, the contention-based access control scheme has been employed to schedule random traffic. Additionally, the contention-based multiple access scheme has been incorporated into communication standards, such as IEEE 802.11s (WiFi) [11], IEEE 802.3(Ethernet) [39] and IEEE 802.15.4(ZigBee) [40].

## 1.2 Motivations

### 1.2.1 Research Problems in TWRNs

In TWRNs, synchronisation [41] and channel estimation [42] are two essential issues for signal detection. Efficient channel estimation in AF-TWRNs poses a big challenge in order to do coherent demodulation [43]. In the case of asynchronous TWRNs, the existence of relative frequency and timing offsets between signals from two source nodes makes the coherent demodulation more challenging.

#### 1.2.1.1 Channel Estimation

The received signal at the relay node suffers from severe random variations of signal strength and phase [43], as the two users' signals undergo different wireless channels. The channel state information is required not only for data recovery, but also for self-interference cancellation [44], in which the source nodes subtract their own forwarded signals from the received signal. As a result, channel estimation for TWRNs is more challenging, compared with the channel estimation of point-to-point communications [45] and one-way relay networks [46].

Most work on two-way relay channels have assumed the availability of perfect channel state information at the receivers. Based on the common assumption that the channel state information (CSI) is perfectly known, the optimal power allocation of two-way relay systems is explored in [47, 48, 49] and the beam forming designs for multi-antenna two-way relay systems is considered in [50, 51].

The existing channel estimation methods use either training-based [52, 53, 54] approaches, which estimate the channel by using training symbols known to both the transmitter and receiver, or blind [55] approaches, which do not depend on training symbols.

In [56], a training-based maximum-likelihood (ML) estimator was developed for the single-antenna single-relay system to estimate the flat-fading channels. In [57], the relay and the two source nodes are equipped with multiple antennas and the multi-input multi-output (MIMO) channels were acquired at each node using a training-based least-squares (LS) algorithm. Channel estimation for TWRNs in frequency selective environments has also been considered in [58]. It has been stated in [52, 56, 57] that training-based channel estimation approaches achieve good performance and are practical. Nevertheless, the spectral efficiency is significantly reduced by training overheads.

Unlike training-based channel estimation, blind channel estimation approaches [59, 60] remarkably decrease undesirable training overheads. Thus, they offer a superior trade-off between estimation accuracy and spectral efficiency. In [59], under M-ary phase-shift-keying (MPSK) modulation [43], a semi-blind channel estimation algorithm, which employs only one training symbol per estimation, is proposed for estimation of reciprocal flat-fading channels [61] in single-relay AF-TWRNs. Since reciprocal channels are not always practical, a deterministic maximum likelihood (DML) channel estimator considering non-reciprocal channels is proposed in [60]. As the DML estimator is unsuitable for binary phase-shift-keying (BPSK), an alternative estimator called the modified constrained maximum likelihood (MCML) estimator is proposed for this case in [60]. The MCML channel estimator takes into account the BPSK structure and approaches the true channel with high probability at high SNR. The approaches in [59, 60] noticeably reduce training overheads and achieve accurate mean squared error (MSE) performances. However, the proposed objective functions are non-convex [62]. Due to the non-convex optimisation function, the DML and MCML algorithms have to rely on numerical solutions by using optimisation tools [62].

In Chapter 3 of the thesis, two semi-blind low complexity channel estimation algorithms are proposed for the TWRN. The proposed algorithms significantly reduce the computational complexity of the existing semi-blind channel estimation algorithm by achieving a closed-form channel estimator.

#### 1.2.1.2 Joint Synchronisation and Channel Estimation

In wireless communications, signals pass through a physical channel, where the signal is distorted and noise is added [61]. In order to recover the transmitted signal at the receiver, the carrier frequency, the carrier phase, and the symbol timing [41] of the transmitted signal are required. However, in many practical situations, a receiver node does not have prior knowledge of the physical wireless channel or the propagation delay associated with the transmitted signal. Moreover, the low cost oscillators of the receivers inherently have some drift [63, 64]. Therefore, the information of the carrier frequency, the carrier phase, and the symbol timing of the transmitted signal needs to be estimated for signal recovery.

In the TWRN, due to the superposition of signals at the relay node, the two users' signals may not be aligned in time and frequency [65]. Consequently, the superimposed signal broadcast from the relay node is affected by multiple impairments, e.g., channel gains, timing offsets, and carrier frequency offsets [65]. Therefore, in order to achieve the optimal decoding at the destination node, one challenge facing the TWRN is the estimation of the time-varying channel impairments such as, channel gains, timing offsets, and carrier frequency offsets.

Recent research has focused mainly on communication strategies for two-way relay networks, assuming perfect synchronisation [66, 67]. However the synchronisation techniques, which enable accurate synchronisation among cooperating nodes, have not been largely addressed. A training-based estimation method is proposed in [53, 68] to estimate channel parameters and the frequency offset in OFDM modulated TWRNs. However, the perfect timing synchronisation is assumed and significant training overheads are still required for the estimation. Moreover, the use of training sequences can give rise to significant overhead with data rate reduction and may become unrealistic or impractical in certain scenarios. For instance, no training signal may be available to receivers in military communication scenarios and defence applications [69]. Consequently, there is a strong and practical need for blind estimation of channel parameters and time offsets without training symbols [70]. In [71], a blind joint maximum likelihood (ML) estimator for time offsets and channel estimation is developed. However, the ML estimator in [71] requires exhaustive search and is computationally complex. In order to reduce the complexity of ML estimation, new iterative estimation schemes are proposed in [72]. Nevertheless, the algorithms in [71, 72] are limited to DF cooperative networks.

In Chapter 4 of the thesis, a joint synchronisation and channel estimation algorithm is proposed for the AF TWRNs and achieves semi-blind timing offset and channel estimation.

### 1.2.2 Research Problems in Media Access

Under the contention-based access methods (e.g. ALOHA and CSMA), each user has the freedom to gain access to the network, whenever the user has information to send. Due to the lack of central control, the transmitted signals interfere with each other, which leads to packet collisions, if multiple users transmit simultaneously over the same channel. As a result, these schemes result in contention among users accessing the network. Contention may cause collisions and require retransmission of the information, which decrease the spectral utilisation. Therefore, the contention resolution algorithm to schedule multiple access in the contention-based access protocol is essential.

A widely used contention resolution algorithm is the binary exponential backoff (BEB) algorithm [73], which is employed in ZigBee, WiFi and WiMax for access control. The basic idea of the BEB algorithm is to delay the transmission by a random amount of time after a collision, so that individual nodes are able to access the channel with a lower collision probability. After $c$ times collisions, a backoff time is chosen randomly from a uniform distribution $[1\ CW]$, where CW denotes the contention window (CW) length, which is $2^c - 1$, and the minimum and maximum value of $c$ depend on the network setting. For a new packet transmission, the CW length is initialised to be the minimum value. The BEB algorithm is widely used due to its simplicity. However, the performance evaluation in [73] demonstrates that the BEB algorithm incurs a high collision probability and low channel utilisation in congested networks. To overcome the shortcoming of BEB, [74] proposes a backoff algorithm, referred to as the exponential increase and exponential decrease (EIED) algorithm, in which the CW length is doubled after a collision and halved after a successful transmission. As a result, frequent collisions are avoided at a cost of a higher latency. As the CW length in [73] and [74] of a transmission starts from 1, this initial value is set without taking account the current channel congestion level.

Unlike [73] and [74], the channel congestion level is considered to adjust the CW length of a transmission in [75, 76, 77, 78]. In [75], the CW length is tuned adaptively to the number of contending nodes, which represents the channel congestion level and is estimated from the transmission history. Whereas, simulation results in [75] show that the estimations of the contending nodes tend to be inaccurate in the scenario of a large number of nodes. In [76], the backoff window size is tuned by observing the status of the channel and estimating the network traffic, in order to improve the efficiency of the BEB and EIED algorithms. However, the number of active nodes needs to be estimated as well. Without relying on the estimate of the number of active nodes, each node adjusts its CW based on the observed average number of idle slots in [77]. In [78], the average contention window length expression is derived by analysing the transmission collision probability, which is obtained by letting the node continuously sense the channel. Although the estimation of the number of the contending nodes in [75] is avoided by [77, 78], the energy consumption of the node in [77, 78] increases significantly due to the continuous channel sensing.

In [75, 76, 77, 78], the contention window length is analysed assuming that all the nodes always have packets to transmit. However, this assumption restricts their practicality. For most real-time traffic, the demanded transmission rate is variable with significant idle periods, i.e., nodes are usually far from being saturated [79, 80]. There exist previous modelling works for non saturated operation [81, 82], but their focus is not on tuning the backoff algorithm. In [82], the queue model [83] is used to analyse the traffic load in ZigBee network. However, the expression of the CW length with respect to the traffic load is not available. As a result, the results in [82] are not adequate to provide specific directions on the CW length adjustment.

In Chapter 5 of the thesis, a new backoff algorithm is proposed for the contention-based multiple access networks to resolve contention. Considering the packet arrival rate and the number of the nodes in the system, the proposed backoff algorithm obtains the expression of the contention window length, which optimises the system throughput.

## 1.3 Contributions

The objective of the thesis is to improve the spectral efficiency of wireless communication networks, by applying novel signal processing techniques in the physical (PHY) layer and the media access control (MAC) layer of the open systems interconnect (OSI) model.

The algorithms proposed in the first part of the thesis (Chapters 3 and 4) for the PHY layer, i.e. the channel estimation and synchronisation algorithms for two-way relay networks, allow signal collisions to improve the spectral efficiency of wireless communications. The contributions of the first part include

- formulating a convex maximum likelihood estimation function and deriving the closed form channel estimation in the synchronous two-way relay networks,
- formulating a convex maximum likelihood estimation function to estimate the channel parameters, the frame offset and the symbol offset jointly, in the asynchronous two-way relay networks,
- providing analysis to verify the performance of the proposed algorithms theoretically.

The proposed algorithms avoid training symbols and reduce the computational complexity of other known methods. In addition, the channel estimation and synchronisation are performed with additional signal processing in a two-time-slot transmission, without occupying extra time slots.

The algorithms proposed in the second part of the thesis (Chapter 6) for the MAC layer, i.e. the self-adaptive backoff algorithm, avoid signal collisions and resolve contention in the contention-based multiple access networks, in order to improve the network throughput and spectral efficiency of the wireless communications. The contributions include

- representing the system and traffic by Markov models,
- deriving the contention window length expression with respect to the average local packet arrival rate and the number of nodes in the system.

Therefore, the two parts of the thesis contribute to the spectral efficiency improvement, by solving problems from different aspects. Moreover, the two parts are related in terms of the system models. In particular, the two scenarios share the common feature in that multiple nodes intend to communicate with one access point.

### 1.3.1 Semi-blind Low Complexity Channel Estimation

In Chapter 3 of the thesis, we propose two low complexity semi-blind channel estimation algorithms, referred to as the low complexity maximum likelihood (LCML) estimator and modified low complexity maximum likelihood (MLCML) estimator, in order to make the existing blind channel estimation algorithms practical. The two algorithms estimate general non-reciprocal flat-fading channels by using only one training symbol per estimation in AF-TWRNs. Assuming MPSK modulation, we formulate a convex [62] maximum likelihood estimation function and derive a closed-form channel estimator in the LCML algorithm. With the channel state information, only one training symbol is necessary to resolve phase ambiguity [84] in signal demodulation. To further improve the MSE performance of the LCML algorithm, we propose the MLCML algorithm by taking into account the modulation structure. Compared to the DML and MCML algorithms, which depends on optimisation tools to derive channel estimation, the computational complexity of the LCML and MLCML estimation algorithms are $\mathcal{O}(N)$, where $N$ is the frame length of signals. Thus, the computational complexity of the existing blind channel estimators is remarkably reduced. In addition, the LCML channel estimator noticeably decreases the average MSE of the DML channel estimator by 89.84% in BPSK. We analyse the proposed algorithms theoretically and prove that the LCML channel estimator is consistent and unbiased [85]. The mean squared error (MSE) performance of the proposed channel estimators are evaluated theoretically and numerically. It has been shown that the derived channel estimators approach the true channel in either high signal-to-noise ratio (SNR) or large frame length scenario.

The main contributions of Chapter 3 are as follows,

1. In synchronous AF-TWRNs, a convex optimisation function for blind channel estimation is not available in the open literature [59, 60]. We propose the LCML algorithm with a convex optimisation function that produces a closed-form channel estimator. By taking into account the modulation structure, a modified LCML(MLCML) channel estimation algorithm with the closed-form channel estimation is proposed to further improved the MSE performance of the LCML algorithm in BPSK. Furthermore, the availability of the closed-form channel estimation enables us to derive the analytical estimation MSE;

2. We analyse the performance of the LCML algorithm in the scenarios of high SNR and large frame length of signals, respectively. In the case of a high SNR, the LCML and MLCML channel estimation algorithms approach the real channel parameter values with the probability of $1-\left(\frac{2}{M}\right)^{N-1}(M-1)$ and $1-\frac{1}{M^{N-1}}$, respectively, where M is the modulation order and $N$ denotes

the frame length; we further conclude that the LCML channel estimator is unbiased. On the other hand, in the case of a large frame length, the LCML channel estimator is consistent if channel parameters belong to compact sets (closed and bounded sets) [85];

3. We derive a closed-form MSE expression of the LCML and MLCML channel estimator with respect to the SNR and $N$, $MSE \propto \frac{2}{SNR\ N}$ and $MSE \propto \frac{1}{SNR\ N}$, respectively, which are consistent with the simulation results. Both the theoretical and numerical MSE performances demonstrate that the LCML and MLCML channel estimator approach the true channel for either high SNR or in a large frame length scenario;

4. The deterministic maximum likelihood (DML) channel estimator and the modified constrained maximum likelihood (MCML) estimator in [60] are the best performing semi-blind channel estimators for TWRNs in the literature. The LCML algorithm noticeably decreases the average MSE of the DML channel estimator by 89.84% in BPSK. The DML and MCML algorithms depend on optimisation tools to derive channel estimation, while the proposed LCML and MLCML estimation algorithms achieve closed-form channel estimators. The computational complexity of the LCML and MLCML estimation algorithms are $\mathcal{O}(N)$, where $N$ is the frame length of signals. Hence, the computational complexity of the existing blind channel estimators is remarkably reduced.

### 1.3.2 Joint Synchronisation and Channel Estimation

In Chapter 4 of the thesis, we consider the joint synchronisation and channel estimation in the asynchronous AF-TWRNs and propose algorithms to estimate the timing offsets and channel parameters jointly. In the asynchronous AF-TWRNs, we develop a generalised low complexity maximum likelihood (GLCML) algorithm to perform channel estimation in the presence of a timing offset. We derive two channel estimations from the overlapped and non-overlapped signals, respectively. Then, we devise an estimation sample selection criterion (ESSC) to choose the channel estimation with the minimum MSE. Then a joint synchronisation and channel estimation (JSCE) algorithm is proposed to estimate the timing offset. We firstly propose a sub-algorithm to achieve frame synchronisation, referred to as the frame asynchronous channel estimation (FACE) algorithm, to estimate the frame offset (integer timing offset) by energy detection and the cross correlation of the received and transmitted signals. Then, channel estimation is performed in the frame asynchronous system. After frame boundaries are determined by the frame synchronisation algorithm, we propose a sub-algorithm, named the symbol asynchronous channel estimation (SACE) algorithm, to estimate the symbol offset (fractional timing offset) based on the overlapped signals. In addition, the SACE algorithm achieves joint symbol synchronisation and channel estimation. Monte-Carlo simulations are employed to evaluate the MSE performance of the GLCML and JSCE algorithms. The simulation results demonstrate that the GLCML algorithm always select the optimal channel estimation in the cases of varying timing offsets and the JSCE algorithm is able to achieve accurate timing offset estimations.

The main contributions of Chapter 4 are as follows.

1. Based on the analytical MSE expression, the optimal channel estimation is achieved in GLCML algorithm by comparing the estimation MSE of the overlapped and non-overlapped samples. Based on the MSE analysis, we make the proposed algorithm more practical by relaxing the assumption of perfect synchronisation and propose the GLCML algorithm for the asynchronous system, where there exists a relative timing offset between both the source nodes.

2. We formulate the channel estimation and timing synchronisation as an overall maximum likelihood estimation problem, which is solved by the JSCE algorithm, which includes two sub-algorithms, the FACE and SACE algorithms. The analysis shows that the error probability of the FACE algorithm approaches zero in a large frame length scenario. The symbol offset is estimated jointly with the channel estimation by the SACE algorithm. Therefore, the JSCE algorithm is capable to achieve accurate timing offset estimation and channel estimation even in the absence of perfect timing synchronisation.

3. Compared with the best known channel estimation algorithm for TWRNs, the modified constrained maximum likelihood (MCML) estimator in [60], the proposed GLCML and JSCE algorithm are capable to achieve a similar MSE performance of channel parameter estimation in the presence of the timing offset. Different from the MCML algorithm, which depends on optimisation tools to derive channel estimation, the GLCML and JSCE algorithm derive the closed-form channel estimation. Thus, the computational complexity of the MCML algorithm is reduced. Moreover, the timing offset and channel parameters can be jointly estimated for the AF-TWRNs in the proposed GLCML and JSCE algorithms.

### 1.3.3 Contention Resolution

In Chapter 5, we propose a self-adaptive backoff (SAB) algorithm to resolve contention in the contention-based multiple access networks. We model the states of a node as a discrete-time Markov chain [86] to derive the contention window (CW) length, given the local packet arrival rate and the total number of nodes in the network. In the first step, the mathematical relationship of the contention window length, the total number of nodes, the Markov state probability and the Markov transition probability is derived, by analysing the state transitions of the Markov chain model. In the second step, the mathematical relationship of the Markov transition probability, the local packet arrival rate, the contention window length and the total number of nodes is derived, according to the queue theory [83]. As a result, we obtain the relationship of the contention window length, the local packet arrival rate, the total number of nodes in the network and the Markov state probability. Then based on the derived contention window length expression, we formulate the system throughput as the optimisation function and use it to achieve the optimal contention window length. Thus each node is able to adjust CW length adaptively to network conditions. Compared with the existing backoff algorithm, the proposed algorithm significantly saves energy of sensors, while achieving better throughput with a lower collision rate.

The contributions are as follows,

1. The SAB algorithm derives the expression of the CW with respect to the average local packet arrival rate and the total number of nodes in the network. This expression provides specific directions on the CW length adjustment.

2. The assumption that all the nodes always have packets to transmit is relaxed in the proposed algorithm, by considering the packet arrival rate. Hence, the CW length is adaptive to the traffic load.

3. As the channel congestion condition is analysed according to the Markov chain model, the CW length increases if channel is estimated to be busy and decreases when channel is estimated to be idle. Thus, the continuous channel sensing to detect the channel congestion level in [78] is avoided. Therefore, the proposed algorithm significantly saves energy consumed by avoiding continuous channel sensing in [78].

4. Compared with the Avg CW algorithm proposed in [78], the proposed algorithm significantly reduces the collision rate by 37% and the energy con-

sumption by 50%, when the number of nodes is 40, while achieving an 11% higher throughput than [78].

## 1.4 Thesis Outline

This thesis consists of six chapters, presenting the background material, reviews of the relevant literature, critical analysis and research results, as well as the conclusions we reach through the research.

Chapter 1 explains the research motivation, states the research problems and presents a brief overview of some promising approaches for increasing the spectral efficiency of wireless communication networks.

Chapter 2 introduces the background information to aid the understanding and analysis in subsequent chapters and presents the system models used in the following chapters.

Chapter 3 presents low complexity semi-blind channel estimation algorithms, referred to as the low complexity maximum likelihood (LCML) estimator and modified low complexity maximum likelihood (MLCML) estimator, to estimate general non-reciprocal flat-fading channels by using only one training symbol per estimation in AF-TWRNs.

Chapter 4 extends the the low complexity maximum likelihood channel estimation algorithm in Chapter 3 to a generalised low complexity maximum likelihood (GLCML) algorithm, which performs channel estimation in the presence of a timing offset. In the asynchronous AF-TWRNs, a joint synchronisation and channel estimation (JSCE) algorithm is proposed to estimate the timing offset. Two sub-algorithms are proposed in the JSCE algorithm. one is the frame asynchronous channel estimation (FACE) algorithm for the frame offset estimation, the other is the symbol asynchronous channel estimation (SACE) algorithm for the joint symbol and channel estimation.

Chapter 5 presents a self-adaptive backoff (SAB) algorithm to resolve contention in the contention-based multiple access networks. In the proposed algorithm, the states of a node is modelled as a discrete time Markov chain and the queue theory is employed to analyse the traffic load. The contention window length is obtained given the local packet arrival rate and the total number of nodes in the network.

Chapter 6 concludes the thesis by summarising the major findings.

# Chapter 2

# System Model

The first part of this chapter provides a brief review of the background of the investigated system models. The basics of two-way relay networks is introduced and the multiple access schemes are reviewed.

In the second part of this chapter, the investigated system models, including synchronous TWRN, asynchronous TWRN and contention-based multiple access networks, are discussed.

## 2.1 Background

### 2.1.1 Two-Way Relay Networks

Relaying technologies have been nominated as a promising solution to spectrum scarcity issues in the physical (PHY) layer, due to their capability of enhancing spectral efficiency, as well as channel capacity and coverage. In relay assisted communication networks, also known as cooperative communication networks, a relay node helps to forward user information from neighbouring nodes to a local base station (BS). In doing this, a relay node can effectively extend the signal and service coverage of a BS and enhance the overall throughput performance of a wireless communication system [18]. As a result, the radio spectral resources can be efficiently utilised in the relay assisted communication networks.

Improving the spectral efficiency is always a major goal of communications. Historically, Shannon introduced the two-way communication channel model and showed how to efficiently design message structures to enable simultaneous bidirectional communication between two terminals at the highest possible data rates [18]. Recently, this model has regained significant interest by introducing an additional relay, which is working in amplify-and-forward (AF) mode, to support the exchange of information between the two communicating terminals. In the amplify-and-forward two-way relay network (see Fig. 1.4), each terminal transmits its signal to the relay simultaneously during the first time slot, where two signals get combined due to the broadcast nature of the wireless medium. The relay then amplifies the received signals and forwards the scaled version to both terminals in the second time slot. The two-way relay model is capable to compensate the spectral inefficiency of one-way relaying under a half-duplex constraint[20, 21, 22, 23, 24].

In one-way relaying schemes, it takes four time slots to exchange information between two terminals via a half-duplex relay, i.e., it takes two time slots to send information from one terminal to the other terminal and two time slots for the reverse direction (see Fig. 2.1). However, exploiting the knowledge of the nodes' own transmitted signals and the broadcast nature of the wireless medium, spectral efficiency can be improved by using only two time slots to exchange information in the two-way relay networks (TWRNs) [25], as shown in Fig. 2.2. Based on the channel state information (CSI), each terminal can extract the desired signal from its own interference upon receiving the combined signals.

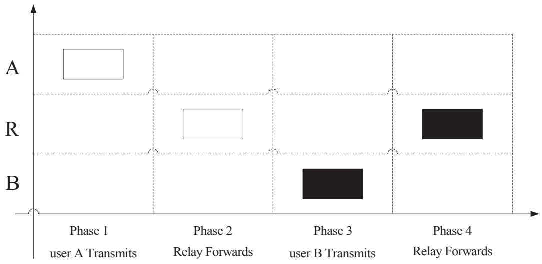


Figure 2.1: Traditional Four-phase two-way relay communication.

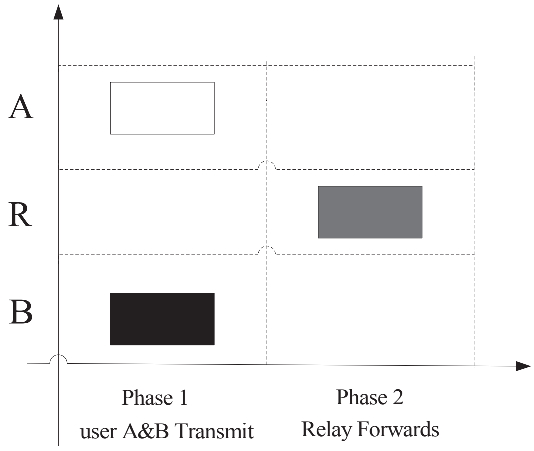


Figure 2.2: Two-phase relay assisted two-way communication.

### 2.1.2 Contention-Based Multiple Access Network

In response to the increasing size of communication networks and the scarcity of network resources, the multiple access schemes has emerged and enable multiple wireless communications users to share the finite physical medium efficiently in the media access control (MAC) layer. Multiple access schemes can be classified as reservation-based multiple access (e.g., FDMA, TDMA, CDMA)[7] and contention-based multiple access (e.g., ALOHA, CSMA) [37, 38].

The family of reservation-based multiple access includes frequency division multiple access (FDMA) [7], time division multiple access (TDMA)[87], and code division multiple access (CDMA) [88]. When each user has a steady flow of information to transmit, reservation-based access methods are useful as they make an efficient use of communication resources. However, once the channel is assigned, it remains idle if the user has nothing to transmit, while other users may have data waiting to be transmitted.

In the situation that the data generation is random, the contention-based multiple access is more efficient, as the communication channel is shared by many users and users transmit their data in a random or partially coordinated fashion [30]. However, the schemes result in contentions among users, due to the fact that each user can access the network whenever it has information to send. Contention may cause collisions and may require retransmission of the information. The commonly used contention-based access protocols are ALOHA [37] and carrier sense multiple access (CSMA) [38].

In the ALOHA scheme, each user transmits information whenever the user has information to send. After sending a packet, the user waits a length of time equal to the round-trip delay for an acknowledgement (ACK) of the packet from the receiver. If no ACK is received, the packet is assumed to be lost in a collision and it is retransmitted with a randomly selected delay to avoid repeated collisions. The ALOHA scheme is widely used in wireless communications networks due to its simplicity. However, the main drawback of the ALOHA scheme is the lack of efficiency caused by the collision and retransmission process. This disadvantage results from the fact that, users do not take into account the actions of the other users when they attempt to transmit data packets and there are no mechanisms to avoid collisions [38].

To decrease the probability of collisions, the carrier sense multiple access (CSMA) [89] protocols provide enhancements over the ALOHA protocol. The enhancements are achieved through the use of the additional capability at each user to sense the transmissions of other users. In CSMA, the transmitting node senses the channel before sending a packet. If the channel is idle (i.e., no user is transmitting), the packet is transmitted. If the channel is busy (i.e., some other user is transmitting), the backoff mechanism is employ to delay the packet transmission for a random amount of time to avoid collisions [38].

The contention-based multiple access scheme allows many users to use the same radio channel without pre-coordination, which has been incorporated into communication standards, such as IEEE 802.11s (WiFi) [11], IEEE 802.3(Ethernet) [39] and IEEE 802.15.4(ZigBee) [40]. In the wireless sensor networks, the contention-based access control scheme has been employed to schedule random traffic with low energy consumption. In Chapter 5 of the thesis, the contention-based multiple access network is considered.

## 2.2 System Model

Multiple access networks are widely deployed in modern wireless and wire line telecommunications networks, to enable multiple users to share the limited spectral resources effectively. In these scenarios, multiple nodes intend to communicate with one access point, as shown in Fig. 2.3.

We consider two cases of multiple access networks in subsequent chapters. In Chapter 3 and Chapter 4, we consider a two-way relay network, which is a special case of the multiple access networks. In the TWRN, two nodes exchange information via a relay node and the relay node can be considered as the access point in phase 1 (the multiple access phase). In Chapter 5, we consider a typical multiple access network with $N$ nodes communicating with one access point.

Figure 2.3: Multiple Access Network.

### 2.2.1 TWRN Model

The two-way relay network is considered as the system model in Chapter 3. The system shown in Fig. 2.4 is composed of three nodes, two source nodes $T_1$ and $T_2$ and one relay node $R$. Each node is equipped with a single antenna. Two source nodes are out of each other's transmission range. In the TWRNs, the relay node assists both source nodes to exchange messages in two phases. In phase 1, also known as the multiple access phase, both source nodes send their messages simultaneously to the relay node. In phase 2, also known as the broadcasting phase, the relay sends back the overheard messages to the source nodes.

The following assumptions have been made throughout Chapter 3 of the thesis:

1. Amplify-and-Forward relaying scheme: The relaying scheme employed in the system is the amplify-and-forward (AF) relaying scheme. In the AF relaying scheme, the relay transmits an amplified version of its received signal from the source to the destination. This leads to low-complexity relay transceivers and low processing power consumption at the relay, since there is no need for decoding at the relay. Furthermore, AF relaying schemes are transparent to modulation and coding techniques which are employed

at the source nodes[5].

2. MPSK: In the AF-TWRN, we employ MPSK modulation and demodulation schemes.

3. Channel Model: Quasi-static and frequency flat-fading channels are considered and the channel is assumed to be fixed and flat over one frame. The quasi-static flat-fading channel model is commonly assumed in the literature. However, the proposed algorithms can still be applied to the time-varying channel scenarios. In the scenario of a frequency selective channel, the proposed channel estimation algorithms can be applied to estimate channel parameters of different frequency sub-bands one by one.

4. We assume three nodes are perfectly synchronised in the AF-TWRN. The perfect synchronisation means that there is no carrier frequency offset and carrier phase offset among all the nodes. Moreover, all the nodes are time synchronised, that is, they can transmit simultaneously without the timing offset and they know when to sample the received signal. The synchronisation among nodes in the TWRNs is often assumed in the literature. However, this assumption will be relaxed in Chapter 4.

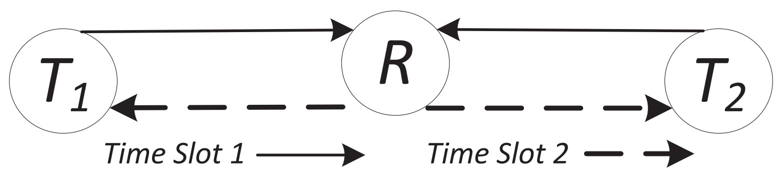


Figure 2.4: The two-time-slot two-way relay network with two source nodes and one relay node

### 2.2.2 Asynchronous TWRN model

The asynchronous TWRN is studied in Chapter 4, where we assume perfect carrier frequency synchronisation and focus on the carrier phase and timing synchronisation in the AF-TWRNs. The asynchronous TWRN model is illustrated in Fig. 2.5. Due to the lack of synchronisation, signals transmitted by source nodes do not perfectly align. One signal starts first with a few symbols that do not interfere with the other signal, while the second signal ends last with a few symbols that do not interfere with the first signal. As shown in Fig. 2.5, there are overlapped and non-overlapped symbols in the received signal at relay. The carrier phase synchronisation is performed based on the whole signal in Chapter 4. In addition, the symbols of each signal do not perfectly align in the asynchronous TWRNs. As a result, there exists a symbol offset and the estimation of this symbol offset is known as symbol synchronisation. In the special case, where the symbols of each signal align, there only exists a frame offset between signals. This case is referred to as the frame asynchronous TWRNs, as shown in Fig. 2.6. The estimation of the frame offset is known as frame synchronisation.

The following assumptions have been made throughout Chapter 4 of the thesis:

1. Amplify-and-Forward relaying scheme at relay node.
2. MPSK: In the asynchronous AF-TWRN, we employ MPSK modulation and demodulation schemes.
3. Channel Model: Quasi-static and frequency flat-fading channels are considered and the channel is assumed to be fixed and flat over one frame. For frequency-selective fading channel, orthogonal-frequency-division multiplexing (OFDM) technique effectively converts a single frequency-selective fading channel into multiple parallel quasi-static flat fading sub-channels. The proposed synchronisation and channel estimation algorithms can be applied to estimate channel parameters and the time offset of different frequency sub-bands one by one;

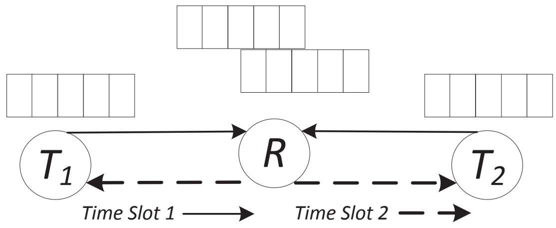


Figure 2.5: Asynchronous two-way relay network.

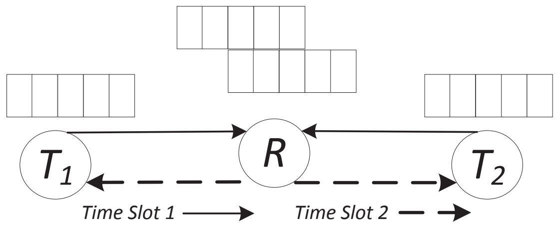


Figure 2.6: Frame asynchronous two-way relay network.

4. Over one frame, the timing offsets are modelled as deterministic but unknown parameters. Perfect carrier frequency synchronised is assumed. Typically, carrier frequency can be recovered from the received noisy signal by means of a suppressed carrier phase-locked loop (PLL) [84].

### 2.2.3 Contention-Based Multiple Access Network

The contention-based multiple access network considered in Chapter 5 has $N$ nodes, contending to communicate with the access point over a single communication channel, as shown in Fig. 2.7. We study the local medium access process of a node under the carrier sense multiple access (CSMA) random access mechanism, given the local packet arrival rate $\lambda$ and the total number of nodes $N$.

The following assumptions have been made throughout Chapter 5 of the thesis:

1. There is no communication between $N$ nodes, which only transmit to the access point under contention-based media access scheme CSMA. Under CSMA access scheme, each user performs carrier sensing before sending a

packet, in order to sense the actions of other users. If the channel is sensed idle (i.e., no user is transmitting), the packet is transmitted. If the channel is busy (i.e., some other user is transmitting), the backoff mechanism is employed to delay the packet transmission for a random amount of time to avoid collisions.

2. The backoff algorithm is employed to resolve contention among transmitting nodes. If the node senses a busy channel or has a transmission failure, it waits a random amount of time before the next channel access in order to avoid repeated collisions. However, the binary exponential backoff (BEB) algorithm is not considered and we employ the proposed backoff algorithm for contention resolution.

3. The total number of the nodes in the network is assumed known to all the nodes and all the nodes share the same average packet arrival rate $\lambda$.

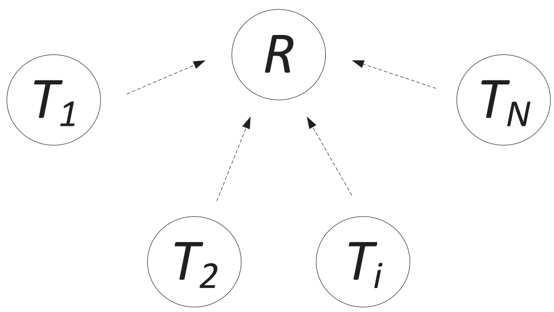


Figure 2.7: Multiple Access Model with N nodes transmitting to one Access Point.

# Chapter 3

# Semi-Blind Low Complexity Channel Estimation Algorithms in AF-TWRNs

In order to improve the spectral efficiency in the physical (PHY) layer of the open systems interconnect (OSI) model, the relay schemes are considered in this chapter. Under the assumption that the carrier frequency, carrier phase and timing are synchronised among all the nodes, we investigate the channel estimation issues in the amplify-and-forward two-way relay networks (AF-TWRNs). To our best knowledge, a deterministic maximum likelihood (DML) channel estimator and a modified constrained maximum likelihood (MCML) estimator are proposed in [60] for semi-blind channel estimation in the synchronous AF-TWRNs. However, the DML and MCML algorithms have to rely on numerical solutions by using optimisation tools, due to the non-convex optimisation functions for channel estimation. In order to make the existing semi-blind channel estimators practical, we propose a low complexity semi-blind channel estimation algorithm, referred to as the low complexity maximum likelihood (LCML) estimator, to estimate general non-reciprocal flat-fading channels by using only one training symbol per estimation in AF-TWRNs. We formulate a convex maximum likelihood estimation function and derive a closed-form channel estimator. Then we propose the modified low complexity maximum likelihood (MLCML) channel estimator, by employing the BPSK modulation structures, to improve the MSE performance of the LCML channel estimator in the case of BPSK. The MLCML channel estimator not only achieves a closed-form channel estimation, but also improves the MSE performance of the LCML estimator for BPSK. We analyse the proposed LCML and MLCML algorithms theoretically and prove that the LCML channel estimator is consistent and unbiased. The MSE performance evaluation shows the derived channel estimators approach the true channel in either high signal-to-noise ratio (SNR) or large frame length scenario.

## 3.1 System Model

A typical half-duplex TWRN over quasi-static flat-fading [90] channels is considered in this chapter. The system is composed of three nodes, two source nodes $T_1$ and $T_2$ and one relay node $R$. Each node is equipped with a single antenna. Two source nodes are out of each other's transmission range. We assume perfect frequency and timing synchronisation [84] among these nodes. In the scenario of a frequency selective channel, the proposed channel estimation algorithms can be applied to estimate channel parameters of different frequency sub-bands one by one.

Each signal transmission process occupies two time slots. In the first time slot, two source nodes $T_1$ and $T_2$ simultaneously transmit signals to the relay node $R$. As MPSK modulation and demodulation are employed, the transmitted base band signals are $s_1 = \sqrt{P_1}e^{j\phi_1}$ and $s_2 = \sqrt{P_2}e^{j\phi_2}$, respectively. $P_1$ and $P_2$ are transmit powers of $T_1$ and $T_2$, respectively. In TWRNs, the most common convention is to set $P_1 = P_2$. $\phi_1$ and $\phi_2$ are MPSK modulated phases, which are independent and uniformly distributed in the set $S_M = \{\frac{2\pi(l-1)}{M}, l = 1, ..., M\}$ where $M$ is the modulation order and $j \triangleq \sqrt{-1}$.

In the first time slot, the received signal at the relay node is given by

$$r_1 = h_1 s_1 + g_1 s_2 + n_1. \tag{3.1}$$

In (3.1), $n_1$ is additive white Gaussian noise (AWGN) distributed in $\mathcal{CN}(0, \sigma_n^2)$, which represents the complex normal distribution with zero mean and variance $\sigma_n^2$. $h_1$ and $g_1$ are complex coefficients of flat-fading channels $T_1 \to R$ and $T_2 \to R$, respectively. Since non-reciprocal channels are considered in this paper, the complex channel coefficients of $R \to T_1$ and $R \to T_2$ are denoted as $h_2$ and $g_2$, respectively. Channel coefficients $h_1$, $h_2$, $g_1$ and $g_2$ are modelled as independent and identically distributed (i.i.d) in $\mathcal{CN}(0, \sigma_c^2)$ and remain fixed during one estimation process.

In the second time slot, the relay node purely amplifies the received signal $r_1$ and then broadcasts the amplified signal $A_r = Kr_1$, where $K$ is the power scaling factor. To maintain an average power of $P_r$ at the relay node over a long term, the expression $K = \sqrt{\frac{P_r}{\sigma_c^2 P_1 + \sigma_c^2 P_2 + \sigma_n^2}}$ is used in this chapter, where $P_r$ denotes the transmit power of $R$. Here, we assume $P_1$, $P_2$, $\sigma_c^2$ and $\sigma_n^2$ are prior known to $R$. Without loss of generality, channel estimation and signal detection at $T_1$ are studied. The received signal at $T_1$ is obtained as

$$r = Kh_1 h_2 s_1 + Kg_1 h_2 s_2 + Kh_2 n_1 + n_2, \tag{3.2}$$

where $n_2$ is AWGN distributed in $\mathcal{CN}(0, \sigma_n^2)$.

Due to the fact that $T_1$ knows its own transmitted signal $s_1$ and the phase modulation scheme, as long as the power scaling factor $K$ and channel coefficients $h_1$, $h_2$, $g_1$ and $g_2$ are perfectly known to $T_1$, demodulation of $s_2$ can be conducted after cancelling self-interference term $Kh_1h_2s_1$ from $r$. However, it is complicated to get the knowledge of these unknown variables individually. By inspecting (3.2), it is sufficient for signal demodulation purpose to estimate the composite channel parameters $H \triangleq Kh_1h_2$, $G \triangleq Kg_1h_2$ and $\sigma^2 \triangleq \left(K^2 |h_2|^2 + 1\right) \sigma_n^2$ jointly under MPSK modulation scheme.

## 3.2 Maximum Likelihood Channel Estimation Algorithm

Channel estimation is performed at source node $T_1$ using $N$ received samples $r_i, i = 1, ..., N$, of the form given by (3.2). The time index $i$ is used to indicate the realisations of $s_1$, $s_2$, $\phi_1$, $\phi_2$, $n_1$ and $n_2$ that give rise to each sample $r_i$. Let $\mathbf{r} \triangleq [r_1, r_2, ..., r_N]^T$ be the vector of the received samples. It is expressed as,

$$\mathbf{r} = H\mathbf{s}_1 + G\mathbf{s}_2 + \mathbf{n}, \tag{3.3}$$

where $\mathbf{s}_1 \triangleq [s_{11}, s_{12}, ..., s_{1N}]^T$, $\mathbf{s}_2 \triangleq [s_{21}, s_{22}, ..., s_{2N}]^T$ and $\mathbf{n} \triangleq [n(1), n(2), ..., n(N)]^T$. The noise term $\mathbf{n}$ is distributed as $\mathcal{CN}(0, \sigma^2)$ where $\sigma^2 = (K^2|h_2|^2 + 1)\sigma_n^2$.

Assuming $\mathbf{s}_2$ is deterministic unknown, the vector of unknown parameters $\Theta \triangleq [H, G, \sigma^2, \phi_{21}, ..., \phi_{2N}]^T$ can be estimated by the maximum likelihood estimation method. Since $\mathbf{s}_1$ is a known vector, the received vector $\mathbf{r}$ follows the complex Gaussian distribution with expectation $\mathrm{E}\{\mathbf{r}\} = H\mathbf{s}_1 + G\mathbf{s}_2$ and variance $\mathrm{Var}\{\mathbf{r}\} = \sigma^2\mathbf{I}$. The log likelihood function of the received signal $\mathbf{r}$ is,

$$L(\mathbf{r}; \Theta) = -\frac{\|\mathbf{r} - H\mathbf{s}_1 - G\mathbf{s}_2\|^2}{\sigma^2} - N\log(\pi\sigma^2), \tag{3.4}$$

$$= -N\ln(\pi\sigma^2) - \frac{\sum_{i=1}^{N}\left|r_i - Hs_{1i} - A|G|e^{j(\phi_g+\phi_{2i})}\right|^2}{\sigma^2}.$$

Without loss of generality, the amplitude of $s_1$ and $s_2$ are assumed equal to $A$ and $\phi_g$ is the phase of $G$. The estimated parameters $\hat{H}$, $\hat{G}$ and $\hat{\sigma}$ corresponding to $H$, $G$ and $\sigma$, respectively, can be obtained by maximising the log likelihood function (3.4).

The log likelihood function (3.4) could be maximised, if $\left|r_i - Hs_{1i} - A\left|G\right|e^{j(\phi_g+\phi_{2i})}\right|, i = 1, ..., N$ is minimised. Since $\left|r_i - Hs_{1i} - A\left|G\right|e^{j(\phi_g+\phi_{2i})}\right|$ represents the Euclidean Distance between $r_i - Hs_{1i}$ and $A\left|G\right|e^{j(\phi_g+\phi_{2i})}$, the minimum distance could be achieved if (3.5) is met.

$$\angle\left\{r_i - Hs_{1i}\right\} = \angle\left\{A\left|G\right|e^{j(\phi_g+\phi_{2i})}\right\}, \quad i = 1, ..., N, \tag{3.5}$$

While (3.5) is not always true, as the modulated phases $\phi_1$ and $\phi_2 \in S_M$ and they can't take continuous values in $[0, 2\pi)$. Therefore, it is assumed in [60] that $\phi_1$ and $\phi_2$ are continuously valued in $[0, 2\pi)$, that is, M$\rightarrow\infty$. Then, the condition (3.5) is met and Eq.(3.4) is approximated as,

$$L(\mathbf{r}; \Theta) = -N\ln(\pi\sigma^2) - \frac{\sum_{i=1}^{N}\left(\left|r_i - Hs_{1i}\right| - A\left|G\right|\right)^2}{\sigma^2}. \tag{3.6}$$

Maximizing (3.6), $\hat{G}$ is estimated as

$$|\hat{G}| = \frac{\sum_{i=1}^{N}\left|r_i - Hs_{1i}\right|}{AN}, \quad \hat{\phi_g} = \angle\sum_{i=1}^{l}\left(r_i - Hs_{1i}\right)s_{2i}^{*}, \tag{3.7}$$

where $l$ is the number of training symbols. As the channel is assumed to be fixed and flat over one frame, the channel fading and phase shift are the same for each symbol. In the proposed algorithms, we use only one training symbol to find $\hat{\phi}_g$, which will be applied to resolve the phase ambiguity [84] in the signal demodulation. It will be shown in Section 3.4 that one training symbol is sufficient to achieve a near optimal symbol error rate (SER).

Substituting (3.7) into (3.4), the log likelihood function reduces to,

$$L(\mathbf{r}; H, \sigma) = -N \ln(\pi\sigma^2) - \tfrac{1}{\sigma^2}\textstyle\sum_{i=1}^{N} \left(|r_i - Hs_{1i}| - \frac{\sum_{k=1}^{N}|r_k - Hs_{1k}|}{N}\right)^2. \quad (3.8)$$

Since Eq.(3.8) is differentiable with respect to $\sigma^2$, let $\frac{\partial L(\mathbf{r};H,\sigma)}{\partial \sigma^2} = 0$, $\hat{\sigma}^2$ is obtained as,

$$\hat{\sigma}^2 = \frac{\sum_{i=1}^{N} \left(|r_i - Hs_{1i}| - \frac{\sum_{k=1}^{N}|r_k - Hs_{1k}|}{N}\right)^2}{N}. \quad (3.9)$$

Substituting (3.9) into (3.8), the channel estimate $\hat{H}$ is obtained as,

$$\hat{H} = \underset{u\in\mathbb{C}}{\operatorname{argmin}} L(\mathbf{r}; u),$$
$$L(\mathbf{r}; u) = \tfrac{1}{N}\textstyle\sum_{i=1}^{N} \left(|r_i - us_{1i}| - \frac{\sum_{k=1}^{N}|r_k - us_{1k}|}{N}\right)^2. \quad (3.10)$$

In the literature, [60] proposed a semi-blind channel estimation method named the deterministic maximum likelihood (DML) algorithm to estimate $\Theta$. In the DML algorithm, channel parameter $H$ is estimated by solving (3.10). As (3.10) is a non-convex function and its analytical solution is not available, a two-dimensional grid-search [91] is employed to solve $\hat{H}$ in [60]. It is possible to obtain an accurate estimate of $H$ when the grid-search range is asymptotically infinite and the search step-size is sufficiently small. However, the exhaustive grid-search algorithm leads to an extremely high computational complexity. In most realistic applications, the high computational complexity is unacceptable.

### 3.2.1 Low Complexity Maximum Likelihood Channel Estimator

To our best knowledge, all the existing semi-blind channel estimators [59] [60] in TWRNs produce fairly high complexity, due to the unavailability of a convex estimation function. Therefore, we propose a convex optimisation function to estimate non-reciprocal channels in TWRNs. The proposed LCML channel estimator achieves a closed-form channel estimator of $H$.

We still assume $\mathbf{s}_2$ is a deterministic unknown. Nevertheless, the actual statistics of $\mathbf{s}_2$ are considered in analysing the behaviour of the LCML channel estimator theoretically in Section 3.3. Under the assumption M $\rightarrow \infty$, $\hat{G}$ and $\hat{\sigma^2}$ are obtained as (3.7) and (3.9), respectively. In the LCML channel estimator, we use only one training symbol to solve $\hat{\phi}_g$, which will be used to resolve the phase ambiguity [84] in signal demodulation. It will be shown in Section 3.4, one training symbol is sufficient to achieve near optimal symbol error rate (SER).

Letting $y_i(u) \triangleq r_i - us_{1i}, i = 1, ..., N$ and we find the presence of $|y_i(u)|$ makes (3.10) non-convex. Replace $|y_i(u)|$ by $|y_i(u)|^2$, we formulate a convex objective function to estimate $H$,

$$\hat{H} = \underset{u \in \mathbb{C}}{\operatorname{argmin}} \ \mathrm{f}(\mathbf{r}; u),$$
$$\mathrm{f}(\mathbf{r}; u) = \tfrac{1}{N} \textstyle\sum_{i=1}^{N} \left( |y_i(u)|^2 - \frac{\sum_{k=1}^{N} |y_k(u)|^2}{N} \right)^2. \tag{3.11}$$

The theoretical analysis in Section 3.3 demonstrates that $\hat{H}$ is the critical point [85] of the differentiable function $\mathrm{f}(\mathbf{r}; u)$. Letting the first partial derivative $\frac{\partial \mathrm{f}(\mathbf{r};u)}{\partial \Re\{\hat{u}\}} = 0$, we get,

$$\Re\{\hat{H}_{lcml}\} = \quad j\Im\{\hat{H}_{lcml}\}\frac{\left(\mathbf{C}_2^T\mathbf{C}_2 - \mathbf{C}_3^T\mathbf{C}_3\right)}{(\mathbf{C}_2+\mathbf{C}_3)^T(\mathbf{C}_2+\mathbf{C}_3)} - \frac{\mathbf{C}_1^T\mathbf{C}_2+\mathbf{C}_1^T\mathbf{C}_3}{(\mathbf{C}_2+\mathbf{C}_3)^T(\mathbf{C}_2+\mathbf{C}_3)}. \tag{3.12}$$

Substituting (3.12) into (3.11), we derive a closed-form $\Im\{\hat{H}\}$ from $\frac{\partial \mathrm{f}(\mathbf{r};u)}{\partial \Im\{\hat{u}\}} = 0$,

$$\Im\{\hat{H}_{lcml}\} = \quad \frac{\mathbf{C}_1^T\mathbf{C}_2\left(\mathbf{C}_3^T\mathbf{C}_3+\mathbf{C}_2^T\mathbf{C}_3\right)}{2j\left(\mathbf{C}_2^T\mathbf{C}_2\mathbf{C}_3^T\mathbf{C}_3-\left(\mathbf{C}_2^T\mathbf{C}_3\right)^2\right)} - \frac{\mathbf{C}_1^T\mathbf{C}_3\left(\mathbf{C}_2^T\mathbf{C}_2+\mathbf{C}_2^T\mathbf{C}_3\right)}{2j\left(\mathbf{C}_2^T\mathbf{C}_2\mathbf{C}_3^T\mathbf{C}_3-\left(\mathbf{C}_2^T\mathbf{C}_3\right)^2\right)}. \tag{3.13}$$

where

$$\begin{cases} \mathbf{C}_1 \triangleq \left[C_{11}, ..., C_{1N}\right]^T, & C_{1i} = |r_i|^2 - \dfrac{\|\mathbf{r}\|^2}{N}, \\ \mathbf{C}_2 \triangleq \left[C_{21}, ..., C_{2N}\right]^T, & C_{2i} = \dfrac{\mathbf{s}_1^H\mathbf{r}}{N} - s_{1i}^* r_i, \\ \mathbf{C}_3 \triangleq \left[C_{31}, ..., C_{3N}\right]^T, & C_{3i} = \dfrac{\mathbf{s}_1^T\mathbf{r}^*}{N} - s_{1i} r_i^*, i = 1, .., N. \end{cases}$$

The channel estimation in AF-TWRNs is obtained as $\hat{H}_{lcml} = \Re\{\hat{H}_{lcml} + j\Im\{\hat{H}_{lcml}\}$, where $j \triangleq \sqrt{-1}$.

### 3.2.2 Modified LCML Channel Estimator

As we will see shortly, the MSE performance of the proposed LCML algorithm hits an error floor in high SNR scenario for BPSK ($M = 2$). In this section, we propose the modified LCML (MLCML) channel estimation algorithm in the case of BPSK ($M = 2$) to remove the error floor.

The log likelihood function is obtained by the maximum likelihood estimation method as

$$L(\mathbf{r};\Theta) = -\frac{\sum_{i=1}^{N} |r_i - Hs_{1,i} - Gs_{2,i}|^2}{\sigma^2} - N\log(\pi\sigma^2). \tag{3.14}$$

By inspecting (3.14), the estimated parameters that satisfy the following condition

$$r_i - Hs_{1,i} - Gs_{2,i} = 0, \ \ \texttt{for} \quad i = 1, ..., N \tag{3.15}$$

will definitely maximise the log likelihood function (3.14). Based on this fact, we make some approximations and propose a modified low complexity maximum likelihood (MLCML) channel estimation algorithm. In [60], a modified constrained maximum likelihood (MCML) estimator is proposed for BPSK. Different from the MCML estimator, the MLCML estimator produces closed-form channel estimations.

Since $s_{2,i} = \pm 1$ in BPSK, we obtain $\hat{s}_{2,i} = Sign\{(r_i - Hs_{1,i})\, e^{-j\phi_g}\}$, where $Sign(x)$ denotes the sign function and $\phi_g$ is the phase of $G$. Therefore, the signal detection of $s_{2,i}$ depends on the availability of $\hat{H}$ and $\hat{\phi}_g$. Then we propose a convex optimisation function to estimate channel parameters $\hat{H}$ and $\hat{\phi}_g$. As the estimated parameters satisfying condition (3.15) also make $(r_i - Hs_{1,i})^2 - (Gs_{2,i})^2 = 0$ hold for $i = 1, ..., N$, we eliminate $s_{2,i}$ in (3.14) and obtain the optimisation function

$$L_{sync}^{BPSK}(\mathbf{r};\Theta) = -\frac{\sum_{i=1}^{N} \left|(r_i - Hs_{1,i})^2 - G^2\right|^2}{\sigma^2} - N\log(\pi\sigma^2). \tag{3.16}$$

As the proposed optimisation function (3.16) is convex, we derive $\hat{G}$ and $\hat{\sigma}$ by letting the first partial derivative $\frac{\partial L_{sync}^{BPSK}}{\partial G^2} = 0$ and $\frac{\partial L_{sync}^{BPSK}}{\partial \sigma^2} = 0$ and obtain

$$\hat{G}^2 = \frac{\sum_{i=1}^{N} (r_i - Hs_{1,i})^2}{N}, \tag{3.17}$$

$$\hat{\sigma}^2 = \frac{\sum_{i=1}^{N} \left| (r_i - Hs_{1,i})^2 - \frac{\sum_{k=1}^{N} \left( r_k - Hs_{1,k} \right)^2}{N} \right|^2}{N}. \tag{3.18}$$

Substituting Eqs. (3.17) and (3.18) into (3.16), $\hat{H}$ can be obtained by minimizing the following objective function,

$$F_{mlcml}(H) = \frac{\sum_{i=1}^{N} \left| (r_i - Hs_{1,i})^2 - \frac{\sum_{k=1}^{N} \left( r_k - Hs_{1,k} \right)^2}{N} \right|^2}{N}. \tag{3.19}$$

Letting $\frac{\partial F_{sync}^{BPSK}(H)}{\partial H} = 0$, the closed-form channel estimation is obtained as

$$\hat{H}_{mlcml} = \frac{\sum_{i=1}^{N} \left( r_i^2 - \frac{\sum_{k=1}^{N} r_k^2}{N} \right) \left( r_i^* s_{1,i}^* - \frac{\sum_{k=1}^{N} r_k^* s_{1,k}^*}{N} \right)}{2 \sum_{i=1}^{N} \left| r_i s_{1,i} - \frac{\sum_{k=1}^{N} r_k s_{1,k}}{N} \right|^2}. \tag{3.20}$$

To estimate $\hat{\phi}_g$, we use $l$ training symbols and obtain

$$\hat{\phi}_g^{mlcml} = \angle \sum_{i=1}^{l-1} \left( r_i - Hs_{1,i} \right) s_{2i}^*. \tag{3.21}$$

As the channel is assumed to be fixed and flat over one frame, the channel fading and phase shift are the same for each symbol. In the proposed algorithms, we use only one training symbol to find $\hat{\phi}_g$, which will be applied to resolve the phase ambiguity [84] in the signal demodulation. It will be shown in Section 3.4 that one training symbol is sufficient to achieve a near optimal symbol error rate (SER).

## 3.3 Analysis of Low Complexity Channel Estimator

In this section, we will analyse the computational complexity of the LCML and MLCML algorithms and their behaviours in the cases of high SNR and large frame length, as well as its MSE performance.

### 3.3.1 Computational Complexity Analysis

To achieve the objective of the signal demodulation of $\mathbf{s}_2$ from (3.3) in synchronous AF-TWRNs, we first cancel the self-interference term $H\mathbf{s}_1$ in (3.3) with the channel state information of $\hat{H}_{lcml}$, derived in Eqs.(3.12), (3.13), and $\hat{H}_{mlcml}$ derived in Eq.(3.20), and the transmitted signal $\mathbf{s}_1$. Then, $\hat{\phi}_g$ is obtained from (3.7) with the help of only one training symbol, so that the phase ambiguity in MPSK demodulation could be resolved. Due to the phase modulation, $\left|\hat{G}\right|$ and $\hat{\sigma}^2$ are not needed for the signal demodulation [84]. Therefore, the demodulation of $\mathbf{s}_2$ depends only on the availability of $\hat{H}$ and the training symbol. Eqs.(3.12) and (3.13) indicate that the calculation of the closed-form expression of channel estimation involves summation and multiplication operations. The computational complexity is considered in terms of the number of samples $N$. The summation operation leads to a computational complexity of $\mathcal{O}(N)$ and the multiplication operation results in a constant complexity. As a result, the computational complexity of the LCML estimation algorithm is $\mathcal{O}(N)$ in the case of $M > 2$. Similarly, from Eq.(3.20) we obtain that the computational complexity of the MLCML estimation algorithm as $\mathcal{O}(N)$ in the case of $M = 2$.

Since the signal demodulation only depends on the availability of $\hat{H}$ and the training symbol, the following analysis focuses on the channel estimation $\hat{H}_{lcml}$ and $\hat{H}_{mlcml}$. Hereafter, we denote $\hat{H}_{lcml}$ as $\hat{H}$ for simplicity.

### 3.3.2 Large Sample Size

In the large frame length scenario, we will prove that when the channel parameter spaces of $H$ and $G$ are restricted to compact sets [85], the LCML channel estimator is consistent [85]. In other words, if channel parameters $H$ and $G$ are bounded, $\hat{H}$ converges in probability to the real channel value $H$ as the frame length $N$ gets larger.

For simplicity, we define the estimation error $v \triangleq H - \hat{H}$ and $V_N(v) \triangleq \mathrm{f}(\mathbf{r}; H - v)$. Then (3.11) is expressed as,

$$V_N(v) = \frac{1}{N}\sum_{i=1}^{N}\left(|z_i(v)|^2 - \frac{\sum_{k=1}^{N}|z_k(v)|^2}{N}\right)^2, \tag{3.22}$$

where $z_i(v) \triangleq vs_{1i} + Gs_{2i} + n_i, i = 1, ..., N$. In (3.22), $V_N(v)$ represents the sample variance of random variable $|z_i(v)|^2$.

Since the channel estimator (3.22) belongs to the class of extremum estimators [92], we use the fundamental lemma for the consistency of extremum estimators, **Lemma 3.1** [92], to prove the consistency of the proposed LCML channel estimator.

**Lemma 3.1.** *If $v$ belongs to a compact set $\Omega$ and $V_N(v)$ converges uniformly to $F(v)$, where $F(v)$ is continuous and uniquely minimised at $v = v_o$, then $\hat{v}$ converges in probability to $v_o$, where $\hat{v} = \underset{v\in\Omega}{\operatorname{argmin}}\ V_N(v)$.*

In Eq. (3.22), signal terms $s_{1i}$, $s_{2i}$ and noise term $n_i$ are i.i.d for each index $i = 1, ..., N$. As a result, $z_i(v)$ is i.i.d and we define $V(v)$ as the true variance of $|z_i(v)|^2$. $V(v)$ is considered as the function $F(v)$ in **Lemma 3.1**. If **Conditions** [1.1, 1.2, 1.3] are satisfied,

**Conditions**

1.1 The channel parameter $H, G \in$ compact set $\Omega$,

1.2 The optimisation function $V_N(v)$ converges uniformly [93] to $V(v)$,

1.3 $V(v)$ is continuous and has a unique global minimum at $v_o = 0$.

then **Lemma 3.1** could be applied to the LCML channel estimator, which implies that $\hat{v}$ converges in probability to $v_o$. Condition 1.3 shows that estimation error $v_o = 0$. Then we could conclude that $\hat{H}$ converges in probability to the real channel value $H$ (See **Theorem 3.1**), that is, the LCML channel estimator is consistent.

**Theorem 3.1.** *If $H$ and $G \in \Omega$, the following channel estimator*

$$\hat{H} = \underset{u \in \mathbb{C}}{\operatorname{argmin}} \frac{1}{N} \sum_{i=1}^{N} \left( |r_i - us_{1i}|^2 - \frac{\|r - us_1\|^2}{N} \right)^2,$$

*is consistent.*

*Proof.* See **Appendix D**. □

The consistency of the LCML channel estimator suggests that in each estimation process, the estimation gets more accurate with larger frame length $N$.

### 3.3.3 High SNR

**Theorem 3.2.** *For a fixed finite frame length $N$, the proposed LCML channel estimator approaches the true channel as SNR $\to \infty$ with probability $1 - \frac{1}{2^{N-1}}$ for BPSK ($M = 2$) and $1 - (M-1)\left(\frac{2}{M}\right)^{N-1}$ for MPSK ($M > 2$).*

*Proof.* It has been proved in Appendix D of [60] that the DML algorithm approaches the true channel with the probability $1 - \left(\frac{2}{M}\right)^{N-1}(M-1)$ in the scenario of high SNR. As the proposed LCML algorithm for MPSK($M > 2$) behaves exactly the same as the DML estimator, we use the conclusion of [60] and obtain that the LCML algorithm for MPSK($M > 2$) approaches the true channel with the probability $1 - \left(\frac{2}{M}\right)^{N-1}(M-1)$ in the scenario of high SNR. The LCML algorithm for BPSK ($M = 2$) is different from that for MPSK ($M > 2$). Hence, we analyse the behaviour of the LCML channel estimator for BPSK ($M = 2$) in high SNR scenarios in **Appendix E** and conclude that the LCML algorithm for

BPSK approaches the true channel with the probability $1-\frac{1}{2^{N-1}}$ in the scenario of a high SNR. $\square$

### 3.3.4 MSE Performance

In this section, the MSE performance of the proposed LCML channel estimator will be assessed analytically. We derive the expression for the MSE in terms of the SNR and frame length $N$. The definition of the channel estimation MSE is

$$\begin{aligned} MSE_{\hat{H}} &= E\left\{\left|\hat{H}-H\right|^2\right\} = MSE_{\Re\left\{\hat{H}\right\}} + MSE_{\Im\left\{\hat{H}\right\}}, \\ MSE_{\Re\left\{\hat{H}\right\}} &= E\left\{\left(\Re\left\{\hat{H}\right\}-\Re\left\{H\right\}\right)^2\right\}, \\ MSE_{\Im\left\{\hat{H}\right\}} &= E\left\{\left(\Im\left\{\hat{H}\right\}-\Im\left\{H\right\}\right)^2\right\}. \end{aligned} \tag{3.23}$$

We begin with the calculation of $MSE_{\Im\left\{\hat{H}\right\}}$. By expanding (3.13), we obtain $\Im\left\{\hat{H}\right\} = f(x,y) \triangleq \frac{x}{y}$, where

$$\begin{cases} x = \sum_{i=1}^{N} C_{1i}C_{2i}\left(\sum_{i=1}^{N} C_{3i}^2 + \sum_{i=1}^{N} C_{2i}C_{3i}\right) - \\ \sum_{i=1}^{N} C_{1i}C_{3i}\left(\sum_{i=1}^{N} C_{2i}^2 + \sum_{i=1}^{N} C_{2i}C_{3i}\right), \\ y = 2j\left(\sum_{i=1}^{N} C_{2i}^2 \sum_{i=1}^{N} C_{3i}^2 - \left(\sum_{i=1}^{N} C_{2i}C_{3i}\right)^2\right). \end{cases} \tag{3.24}$$

Eq. (3.24) shows that $x$ and $y$ are the summations of $N$ terms. According to the *Central Limit Theorem* [93], $x$ and $y$ are asymptotically complex normal distributed random variables with expectations $\mu_x$ and $\mu_y$ and variances $\sigma_x^2$ and $\sigma_y^2$, respectively.

For the simplicity of $MSE_{\Im\left\{\hat{H}\right\}}$ calculation, we approximate $\Im\left\{\hat{H}\right\}$ as its first degree Taylor polynomial representation [94] $\frac{\mu_x}{\mu_y}+\frac{x}{\mu_y}-\frac{\mu_x y}{\mu_y^2}$ at the point $(\mu_x, \mu_y)$ (See **Lemma 3.2**).

**Lemma 3.2.** *If SNR $\to \infty$, $f(x,y) = \frac{x}{y}$ equals its first degree Taylor polynomial approximation at the point $(\mu_x, \mu_y)$, namely,*

$$f(x,y) = \frac{\mu_x}{\mu_y} + \frac{x}{\mu_y} - \frac{\mu_x y}{\mu_y^2}.$$

*Proof.* See **Appendix F**. □

As proved in **Lemma 3.2**, under the condition SNR $\to \infty$,

$$\Im\left\{\hat{H}\right\} = \frac{\mu_x}{\mu_y} + \frac{x}{\mu_y} - \frac{\mu_x y}{\mu_y^2}. \tag{3.25}$$

After calculating the expectation of (3.25), we obtain the first moment of $\Im\left\{\hat{H}\right\}$ as,

$$E\left\{\Im\left(\hat{H}\right)\right\} = \tfrac{\mu_x}{\mu_y}. \tag{3.26}$$

The expectations of $x$ and $y$ are calculated from (F.5) and we obtain $\frac{\mu_x}{\mu_y} = \Im\{H\}$. That is, $E\left\{\Im\left(\hat{H}\right)\right\} = \Im\{H\}$. Similarly, we derive $E\left\{\Re\left(\hat{H}\right)\right\} = \Re\{H\}$. Therefore, $E\left\{\hat{H}\right\} = H$, which suggests that the LCML channel estimator is unbiased if SNR $\to \infty$ and this helps to proves the following theorem,

**Theorem 3.3.** *If SNR $\to \infty$, the following channel estimator*

$$\hat{H} = \underset{u\in\mathbb{C}}{\operatorname{argmin}} \tfrac{1}{N}\textstyle\sum_{i=1}^{N}\left(|r_i - us_{1i}|^2 - \frac{\|\boldsymbol{r}-u\boldsymbol{s}_1\|^2}{N}\right)^2,$$

*is unbiased.*

It has been proved that $E\left\{\Im\left(\hat{H}\right)\right\} = \Im\{H\}$ on the condition SNR $\to \infty$, replacing $\Im\{H\}$ with $E\left\{\Im\left(\hat{H}\right)\right\}$ in (3.23), we obtain $MSE_{\Im\left\{\hat{H}\right\}}$ as,

$$MSE_{\Im\left\{\hat{H}\right\}} = E\left\{\left[\Im\left(\hat{H}\right) - E\left\{\Im\left(\hat{H}\right)\right\}\right]^2\right\}. \tag{3.27}$$

Substituting (3.25) and (3.26) into (3.27), $MSE_{\Im\{\hat{H}\}}$ is expressed as

$$MSE_{\Im\{\hat{H}\}} = \frac{E\{x^2\}}{\mu_y^2} - 2\frac{\mu_x}{\mu_y}\frac{E\{xy\}}{\mu_y^2} + \left(\frac{\mu_x}{\mu_y}\right)^2 \frac{E\{y^2\}}{\mu_y^2}.$$

Likewise, we derive $MSE_{\Re\{\hat{H}\}}$ and then obtain the expression of $MSE_{\hat{H}}$ by analysing the moments of $x$ and $y$ from (F.5),

$$MSE_{\hat{H}} = \frac{\sigma^2}{A^2N}\kappa, \tag{3.28}$$

where

$$\kappa = \frac{4A^2|G|^2\left(N^4-8N^3+8N^2-4N+1\right)\left(\sigma^4+A^2|G|^2\right)^2}{(N^2-3N+2)^2\left(|G|^2A^2+\sigma^2\right)^4} + \frac{2(N-1)\left(N^3-3N^2+N-1\right)\left(|G|^4A^4+\sigma^4\right)\left(\sigma^4+A^2|G|^2\right)^2}{(N^2-3N+2)^2\left(|G|^2A^2+\sigma^2\right)^4}.$$

Eq. (3.28) shows $\kappa \propto 2 + \frac{\sigma^2}{A^2N}$ and $MSE_{\hat{H}} \propto \frac{2\sigma^2}{A^2N}$, which implies that the LCML channel estimations approach the true channel parameter values in either high SNR or large frame length scenario. In the TWRNs, if channel parameter $G = 0$, source node $T_1$ could estimate the non-reciprocal channel parameter $H$ without interference from the source node $T_2$. Based on the received signal $\mathbf{r}$ in (3.3) with $G = 0$ and its transmitted signal $\mathbf{s}_1$, channel parameter $H$ can be estimated as $\hat{H}_{opt} = \frac{\mathbf{r}^T\mathbf{s}_1^*}{A^2N}$. By taking into account of the statistics of $\mathbf{s}_1$, the estimation MSE of $\hat{H}_{opt}$ is derived as,

$$MSE_{\hat{H}_{opt}} = \frac{\sigma^2}{A^2N}. \tag{3.29}$$

With no interference and prior known signal $\mathbf{s}_1$, this estimation is optimal. On the other hand, in the TWRNs with $G \neq 0$, the presence of source node $T_2$ causes interference to signal detection at source node $T_1$. Comparing (3.28) with the optimal estimation (3.29), $\gamma$ in (3.28) represents the performance penalty produced by interference signal $\mathbf{s}_2$ and the MSE performance degradation is 50%. Furthermore, we derive the MSE expression of the LCML algorithm in the case of BPSK ($M = 2$) from the closed-form channel estimation (3.20) as

$$MSE_{H_{lcml}^{BPSK}} = \frac{\sigma^2}{A^2 N}. \tag{3.30}$$

## 3.4 Simulation Results

In this section, we evaluate the performance of the proposed LCML and MLCML algorithms numerically using Monte Carlo simulations over flat-fading channels. In the simulations, we employ MPSK signal modulation and assume $P_r = P_1 = P_2 = P$. Power scaling factor $K = \sqrt{\frac{P_r}{P_1+P_2+\sigma_n^2}}$ and SNR is defined as $\frac{P}{\sigma_n^2}$, where $\sigma_n^2$ denotes the AWGN noise power. All the simulation results are averaged over 100 independent realisations of the channel parameters $h_1$, $h_2$, $g_1$ and $g_2$, which are modelled as i.i.d in $\mathcal{CN}(0, 1)$ and remain fixed during one channel estimation process.

The commonly adopted Estimation Theoretic Performance Metrics are: Mean Squared Error (MSE) of channel estimation. The expression for MSE depends on the specific channel estimation algorithm employed at the receiver. When using this metric to measure the system performance, the goal of the system designer is to minimise this metric.

We begin by comparing the MSE performance of the DML and LCML channel estimator and the theoretical MSE performance derived in Section 3.3.4 is included as a reference. The MSE performance comparison in different modulation orders is plotted versus SNR for sample size $N = 45$ in Fig. 3.1, which shows the LCML channel estimator noticeably decreases the average MSE by 89.84% in BPSK and is slightly superior to the DML channel estimator in QPSK and 8-PSK. Actually, there is no performance guarantee for the DML estimator when the modulation order M=2. This verifies the analytical results that the DML channel estimator produces infinite number of channel estimates with probability 1 when M=2 [60], while the LCML estimator is capable to achieve a unique estimate in BPSK. However, the MSE performance hits an error floor in the case of a high SNR as shown in Fig. 3.1.

Fig. 3.2 shows the MSE performance of the DML and LCML channel estimators versus sample size $N$ for SNR=20 dB. As mentioned before, the DML channel estimator is invalid in BPSK. In contrast, the LCML channel estimator achieves an accurate estimation and its MSE performance is improved steadily with increasing sample size in BPSK. In the cases of M$\geq$ 4, the MSE performance of the DML estimator is improved by the LCML channel estimator, whose MSE performance approaches the theoretical MSE, derived in Section 3.3.4, with increasing $N$, which verifies **Theorem 3.1** that the LCML is consistent.

The MSE performance illustrated in Figs. 3.1 and 3.2 are consistent with the theoretical analysis in Section 3.3 and MSE analysis in Section 3.3.4. Both of the figures show, in QPSK and 8-PSK, the MSE performance of the LCML channel estimator versus SNR or $N$ outperforms that in the case of BPSK. This results from the fact that the assumption of the proposed algorithm is the modulation order M $\rightarrow \infty$. Obviously, the curves approach the theoretical MSE when M $\geq 4$, which indicates that the estimation is accurate even though the assumption of M$\rightarrow \infty$ is not satisfied.

In QPSK and 8-PSK, the MSE performance of the LCML channel estimator versus SNR or $N$ improves with increasing SNR or $N$. This verifies **Theorem 3.1** and **Theorem 3.2** that the proposed LCML channel estimator approaches the true channel in the case of high SNR or large sample size under the assumption $\mathrm{M} \rightarrow \infty$. In high modulation orders, the numerical MSE performance approaches the theoretical MSE, which verifies the MSE analysis in Section 3.3.4 that the analytical expression of MSE is inversely proportional to SNR and $N$.

The MSE performance of the LCML algorithm presents different patterns versus SNR and $N$, it improves rapidly with increasing SNR in Figs. 3.1, while, steadily when $N$ gets larger in Fig. 3.2. The analytical result in (3.28) gives a specific expression of MSE in terms of SNR and $N$, which implies $MSE_{\hat{H}} \propto \frac{2}{SNR^2 N}$. Both of the results show the MSE performance is more sensitive to SNR than sample size $N$.

The symbol error rate (SER) performance is compared between the LCML and DML channel estimator in Fig. 3.3. After cancelling the self-interference term by $\hat{H}$ as derived in (3.12) and (3.13), we use only one training symbol to recover the phase ambiguity according to (3.7). Fig. 3.3 shows that one training symbol is sufficient to achieve a near optimal SER. It has been concluded that the DML channel estimator offers a better tradeoff between estimation accuracy and spectral efficiency than the Least-Squares channel estimator [60]. In addition to a much lower computational complexity than the DML estimator, the proposed LCML channel estimator remarkably improves the SER performance in BPSK and in QPSK its SER performance approaches the case with perfect channel state information.

Regarding the computational complexity, the DML estimator has to rely on the two-dimensional grid-search algorithm to derive the channel estimation. In contrast, the LCML algorithm proposes a closed-form channel estimator and completely avoids the grid-search algorithm, so that it significantly reduces the computational complexity.

Therefore, the LCML channel estimator outperforms the DML channel estimator by offering even better tradeoff between accuracy and spectral efficiency, as well as a much lower computational complexity. Next, we compare the MSE performance of the MLCML, LCML and MCML channel estimators. Figs. 3.4 and 3.5 show the MSE performance comparison of the three channel estimators versus SNR for frame length $N = 45$ and versus $N$ for SNR=20 dB, respectively. The analytical MSE performance of the MLCML channel estimator is included as a reference in both figures. The MSE performance of the MLCML channel estimator improves with increasing SNR or $N$, as shown in Figs. 3.4 and 3.5. The MSE performance of the LCML channel estimator is improved significantly by the MLCML channel estimator, which achieves as good MSE performances as the MCML estimator. Due to the non-convex optimisation function, the DML and MCML algorithms have to rely on numerical solutions by using optimisation tools. In contrast, the LCML and MLCML algorithms are based on a closed-form channel estimator.

The symbol error rate (SER) performance of the MLCML is shown in Fig. 3.6. In the proposed algorithms, we use only one training symbol to find $\hat{\phi}_g$, which will be applied to resolve the phase ambiguity [16] in the signal demodulation. Fig. 3.6 shows that one training symbol is sufficient to achieve a near optimal SER.

In the scenarios of time-varying channels, the MSE performance of the proposed algorithm versus SNR is shown in Fig. 3.7. The Jakes' channel model [95] is used to simulate the time-varying channel with the normalised Doppler frequency $f_dT$, where $f_d$ is the Doppler shift and $T$ is the input symbol period. In Fig. 3.7, the channel is static when $f_dT = 0$, which is the channel model assumed in this paper. In the case of time-varying channels, the MSE performance degrades, as the LCML algorithm is not designed for time-varying channels. However, in the case where fade rate $f_dT$ is 0.0005, the LCML algorithm achieves a similar MSE performance as in the static channel scenario. This demonstrates that the proposed LCML algorithm is applicable to some slow time-varying channels.

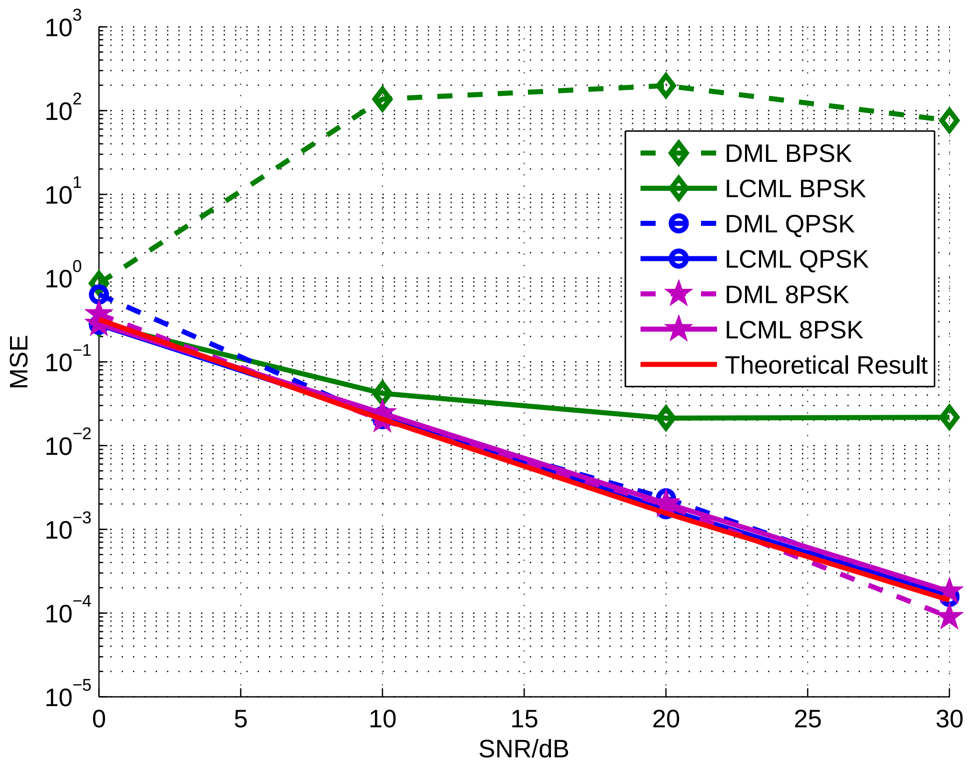


Figure 3.1: The comparison of MSE performance of the LCML and DML channel estimator VS. SNR for $N$=45

## 3.5 Conclusion

In this chapter, we proposed two low complexity semi-blind channel estimators, referred to as the low complexity maximum likelihood (LCML) channel estimators and the modified low complexity maximum likelihood (MLCML) channel

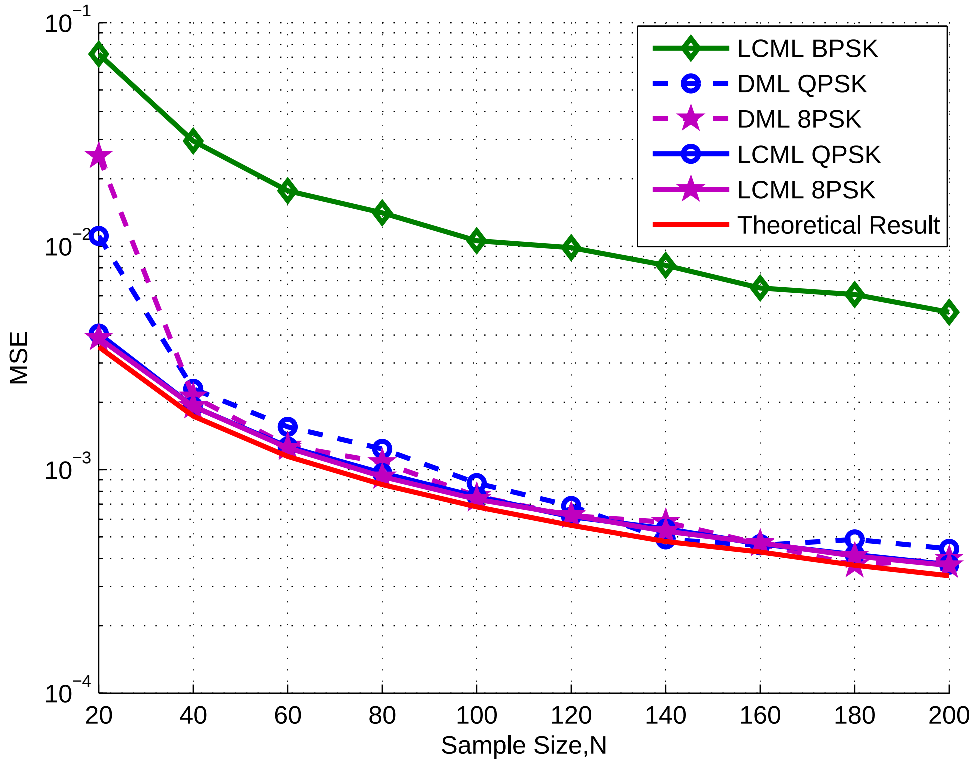


Figure 3.2: The comparison of MSE performance of the LCML and DML channel estimator VS. $N$ for SNR=20dB

estimator. Both channel estimators employ only one training symbol in each channel estimation to estimate general non-reciprocal flat-fading channels in AF-TWRNs. We formulate a convex objective function for the LCML channel estimator, by maximising the log-likelihood function of the received interfered signal. As a result, the closed-form channel estimate is obtained. To remove the mean squared error (MSE) performance error floor of the LCML channel estimator, we proposed the MLCML algorithm by taking into account the modulated signal structure. The MLCML achieves closed-form channel estimation and better MSE performance than the LCML channel estimator. The computational complexity of the LCML and MLCML estimation algorithms are $\mathcal{O}(N)$, where $N$is the frame length. Theoretical analysis proves that the derived channel estimates approach the true channels in high SNR or large frame length scenarios. We analysed the MSE performance theoretically and numerically. Both the analytical MSE ex-

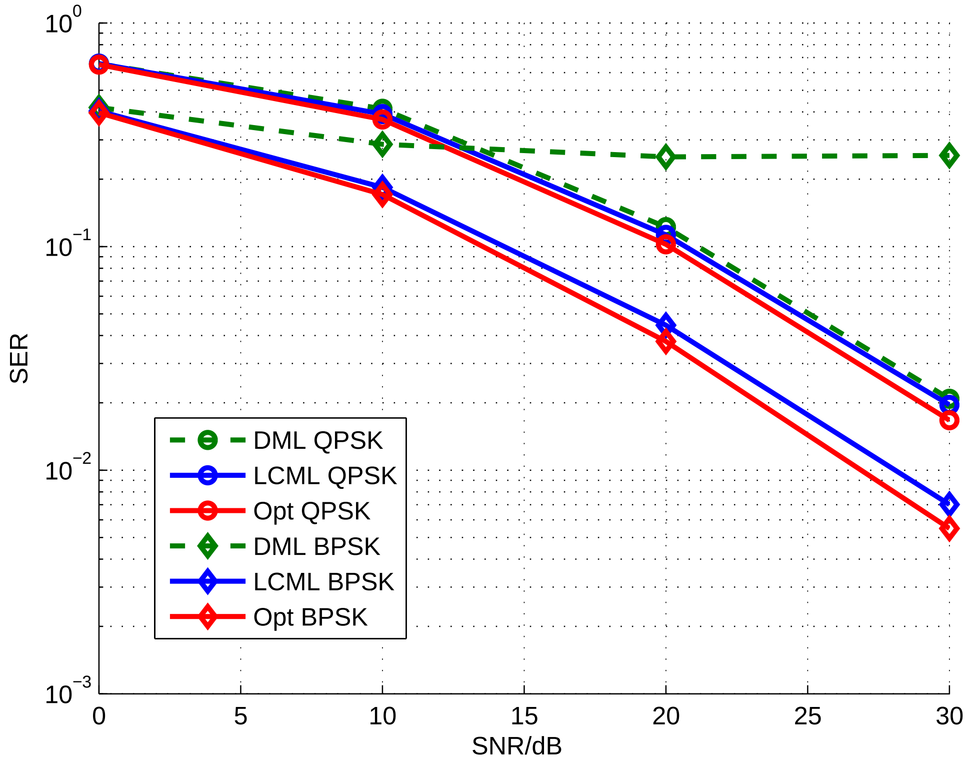


Figure 3.3: The comparison of SER performance of the LCML and DML channel estimator VS. SNR for $N$=20 with 1 training symbol

pression and Monte-Carlo simulations show that the average MSE performance of the LCML channel estimator improves as either SNR, frame length or modulation order increases. Compared with the DML and MCML channel estimators in the literature, the LCML and MLCML estimators not only achieve a better MSE and SER performance, but also significantly reduce the computational load. However, the perfect synchronisation is assumed in this chapter. As a result, the channel impairments result from asynchronization are not considered.

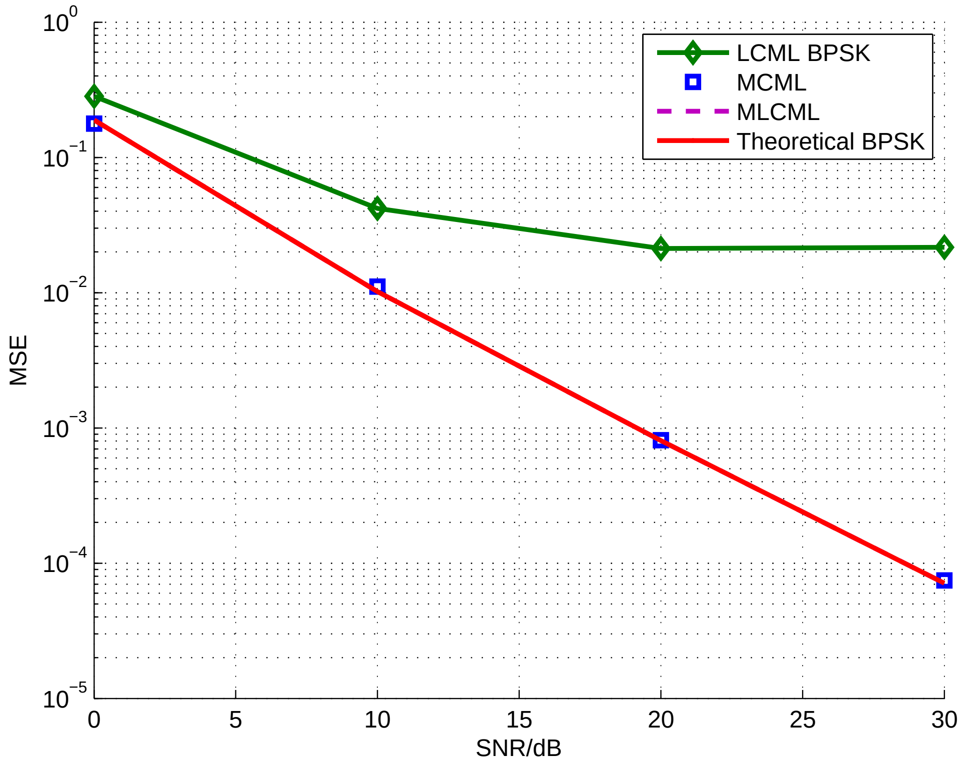


Figure 3.4: The comparison of MSE performance of the LCML, MLCML and MCML channel estimators VS. SNR for $N$=45

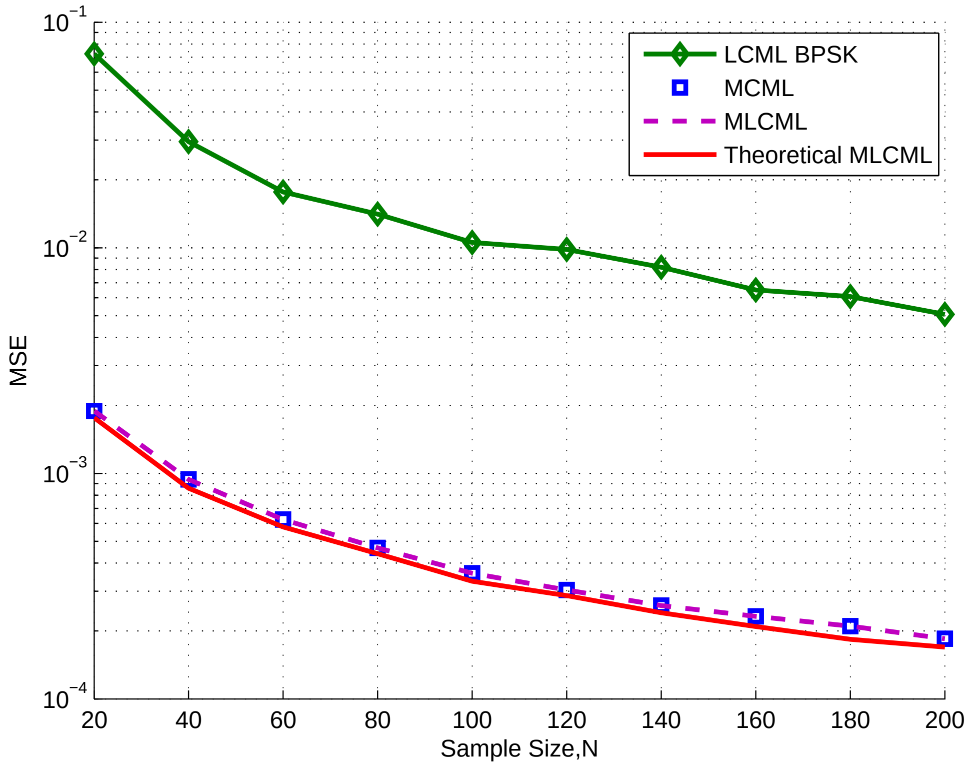


Figure 3.5: The comparison of MSE performance of the LCML, MLCML and MCML channel estimators VS. $N$ for SNR=20dB

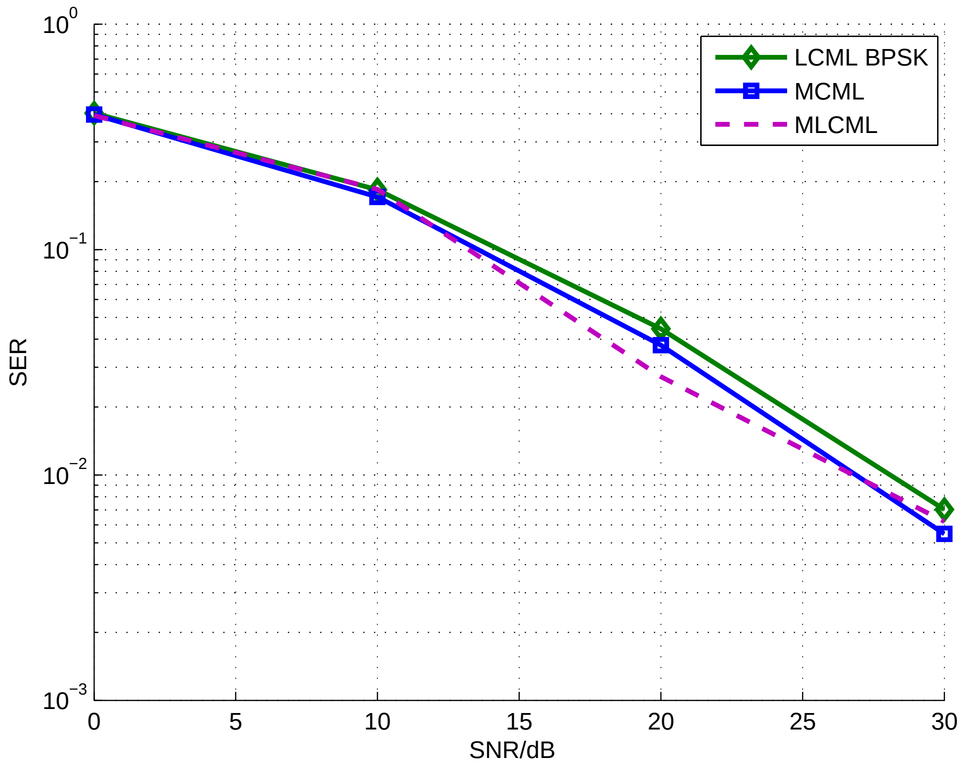


Figure 3.6: The comparison of SER performance of the LCML, MLCML and MCML channel estimators VS. SNR for $N$=20 with 1 training symbol

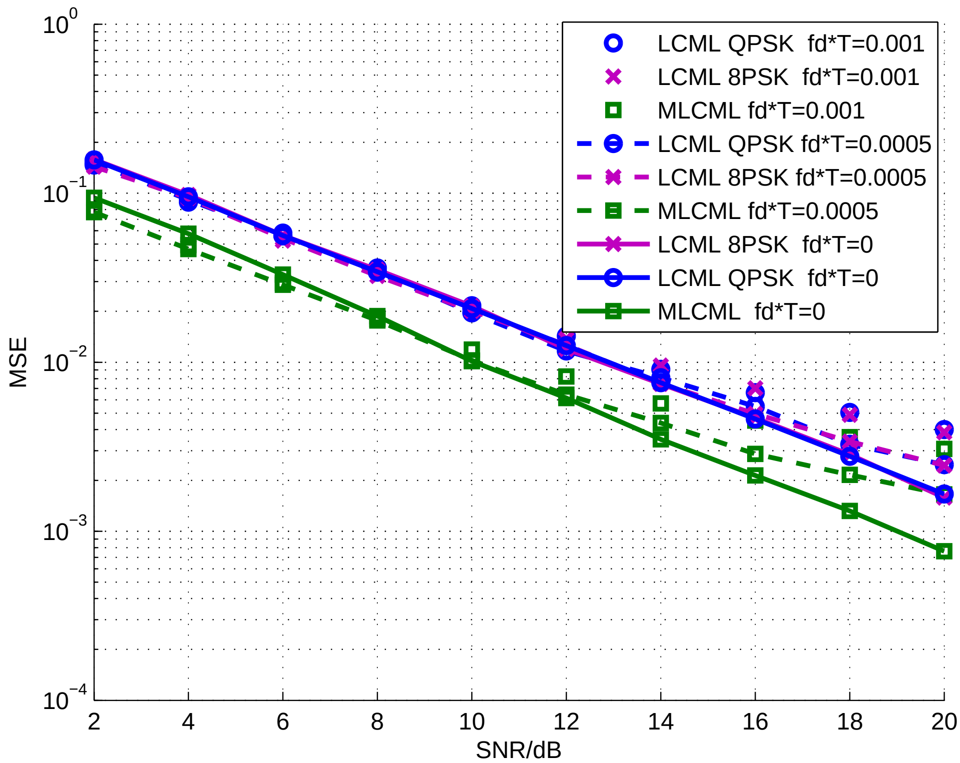


Figure 3.7: The MSE performance of the LCML and MLCML channel estimators in time-varying channels VS. SNR in the case of N=45.

# Chapter 4

# Joint Synchronisation and Channel Estimation in AF-TWRNs

In order to improve the spectral efficiency in the physical (PHY) layer of the open systems interconnect (OSI) model, the relay schemes are considered in Chapter 3 and the low complexity semi-blind channel estimation algorithms have been proposed. As the channel estimation algorithm is proposed assuming the perfect synchronisation among all the nodes, the channel impairments resulting from asynchronisation are not considered. In the asynchronous two-way relay networks (TWRNs), the existence of relative frequency offsets and timing offsets between signals from two source nodes will make the channel estimation more challenging. In the literature, many algorithms have been proposed to estimate the channel in TWRNs assuming perfect synchronisation, while not much attention has been paid to study the joint synchronisation and channel estimation problem for the amplify-and-forward TWRNs.

In this chapter, the assumption of perfect synchronisation is relaxed and we study the joint synchronisation and channel estimation in amplify-and-forward two-way relay networks (AF-TWRNs). We develop a generalised low complexity maximum likelihood (GLCML) algorithm to perform channel estimation in the asynchronous AF-TWRNs, under the assumption that the time offset is assumed as known to both source nodes. To relax the assumption of the GLCML algorithm, we propose the frame asynchronous channel estimation (FACE) algorithm and the joint synchronisation and channel estimation (JSCE) algorithm. The FACE algorithm achieves the frame offset estimation and the JSCE algorithm achieves the symbol offset estimation by performing channel estimate and synchronisation jointly.

## 4.1 System Model

A typical half-duplex AF-TWRN over quasi-static flat-fading [90] channels is considered. The system is composed of three nodes, two source nodes $T_1$ and $T_2$ and one relay node $R$. Each node is equipped with a single antenna. The two source nodes are out of each other transmission range. The assumption of perfect synchronisation among all the nodes is relaxed and the joint synchronisation and channel estimation in the TWRNs will be studied in this chapter. In the scenario of a frequency selective channel, the proposed channel estimation algorithms can be applied to estimate channel parameters of different frequency sub-bands individually.

Each signal transmission process consists of two time slots. In the first time slot, the two source nodes $T_1$ and $T_2$ simultaneously transmit signals to the relay node. The transmitted signals of source nodes $T_1$ and $T_2$ are $s_1(t) = \sum_{i=1}^{N} e^{jw_1Ti}s_{1,i}f(t-iT)$ and $s_2(t) = \sum_{i=1}^{N} e^{jw_2Ti}s_{2,i}f(t-iT)$, respectively. Without loss of generality, both $T_1$ and $T_2$ are assumed to transmit $N$ symbols in a frame. $f(t)$ is the time-invariant pulse shaping transmit filter of source nodes $T_1$ and $T_2$. $w_1$ and $w_2$ are the carrier angular frequencies of the transmitters. The carrier frequency is assumed perfectly synchronised across two source nodes $T_1$ and $T_2$. $T$ is the symbol time interval and $j \triangleq \sqrt{-1}$. As MPSK modulation is employed, we get,

$$s_{1,i} = \begin{cases} \sqrt{P_1} e^{j\phi_{1i}}, & i = 1, 2, ..., N, \\ 0, & else, \end{cases} \qquad s_{2,i} = \begin{cases} \sqrt{P_2} e^{j\phi_{2i}}, & i = 1, 2, ..., N, \\ 0, & else, \end{cases}$$

$P_1$ and $P_2$ are the transmit powers of $T_1$ and $T_2$, respectively. $\phi_{1i}$ and $\phi_{2i}$ are MPSK modulated phases, which are independent and uniformly distributed in the set $S_M = \{\frac{2\pi(l-1)}{M}, l = 1, ..., M\}$, where $M$ is the modulation order.

During the first time slot, the overall signal received by the relay node is given by

$$r(t) = h_1 s_1(t + \tau_1) + g_1 s_2(t + \tau_2) + n_1(t).$$

Due to timing asynchrony, there exist timing offsets $\tau_1$ and $\tau_2$ of source nodes $T_1$ and $T_2$ relative to the relay node $R$, respectively. As the relay node only amplifies the received signal, the timing offsets $\tau_1$ and $\tau_2$ are not needed for synchronisation or channel estimation. $h_1$ and $g_1$ are complex coefficients of flat-fading channels $T_1 \to R$ and $T_2 \to R$, respectively. Since non-reciprocal channels are considered in this paper, the complex channel coefficients of the links $R \to T_1$ and $R \to T_2$ are denoted as $h_2$ and $g_2$, respectively. Channel coefficients $h_1$, $h_2$, $g_1$ and $g_2$ are modelled as independent and identically distributed (i.i.d) in $\mathcal{CN}(0, \sigma_c^2)$ and remain fixed during one frame. Here, $\mathcal{CN}(0, \sigma_c^2)$ represents the complex normal distribution with a zero mean and the variance of $\sigma_c^2$. $n_1(t)$ is a complex additive white Gaussian noise (AWGN) distributed in $\mathcal{CN}(0, \sigma_n^2)$.

In the second time slot, the relay node amplifies the received signal $r(t)$ and then broadcasts the amplified signal $A_r(t) = Kr(t)$, where $K$ is the power scaling factor. To maintain an average power of $P_r$ at the relay node over a long term, the power scaling factor $K = \sqrt{\frac{P_r}{\sigma_c^2 P_1 + \sigma_c^2 P_2 + \sigma_n^2}}$ [52] is used in this paper, where $P_r$ denotes the transmit power of $R$. Here, we assume $P_1$, $P_2$, $\sigma_c^2$ and $\sigma_n^2$ are a priori known to the relay node $R$. However, the rough knowledge of $P_1$ and $P_2$ is sufficient to obtain $K$. In this work, all the estimations are performed at the source nodes, rather than at the relay node.

Without loss of generality, signal detection at source node $T_1$ is considered. The received signal at $T_1$ is obtained as,

$$r_1(t) = h_2 K r(t) + n_2(t).$$

where $n_2(t)$ is AWGN distributed in $\mathcal{CN}(0, \sigma_n^2)$.

Assuming perfect frequency synchronisation, there exists a relative timing offset between $T_1$ and $T_2$ in the time asynchronous AF-TWRNs as shown in Fig. In the timing asynchronous system, the structure of the received signal is shown in Fig. 4.1. The time offset results in different structures in the received signal. As shown in Fig. 4.1, there is one overlapped part in the received signal, which consists of signals $s_1$ and $s_2$ from two source nodes. There are two non-overlapped parts and each one consists of one signal.

Hereafter, we refer the integral timing offset $n_t$ as the frame offset and the fractional timing offset $\tau$ as the symbol offset. In the case that the frame offset $n_t \neq 0$ and the symbol offset $\tau = 0$, the symbols of two signals transmitted by

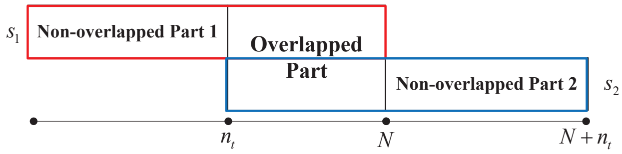


Figure 4.1: The structure of the received signal in the asynchronous system.

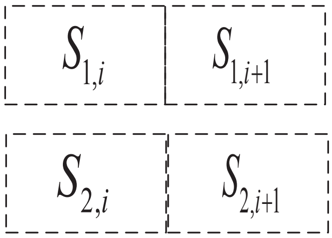


Figure 4.2: The structure of the received signal in the frame asynchronous system.

both source nodes are still aligned, as shown in Fig. 4.2. We refer this case as the frame asynchronous system. On the other hand, if the symbol offset $\tau \neq 0$, the symbols of two signals are not aligned any more, as shown in Fig. 4.3. This case is referred to as the symbol asynchronous system.

## 4.2 Channel Estimation in Asynchronous AF-TWRNs

In this section, we study channel estimation in asynchronous AF-TWRNs, under the assumption that both source nodes have the knowledge of the relative time offset. This assumption will be relaxed. We begin by analysing the received

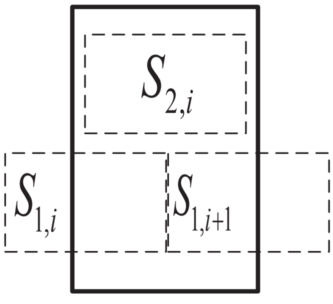


Figure 4.3: The structure of the received signal in the symbol asynchronous system.

signal model at source node $T_1$. Based on the received signal, channel estimation is performed by utilising the different signal structures, resulted from the time offset. Then an Estimation Sample Selection Criterion (ESSC) is proposed to achieve the optimal channel estimation.

### 4.2.1 Received Signal Model

In this case, $n_t \neq 0$ and $\tau \neq 0$. As $s_1(t)$ is the self-transmitted signal of $T_1$, source node $T_1$ can synchronise with $s_1(t)$ by cross-correlation method. Under the assumption that both source nodes know the time offset $n_t$ and $\tau$, $T_1$ can synchronise with $s_2(t)$ with the knowledge of the time offset. This assumption will be relaxed in the following. Hence, $T_1$ is able to synchronise with either $s_1(t)$ or $s_2(t)$.

$T_1$ performs twice samplings to the received signal. Firstly, $T_1$ synchronises with $s_1(t)$ and obtains the non-overlapped samples of $s_1(t)$ as

$$r_{async}(i) = Hs_{1,i} + Kh_2n_{1,i} + n_{2,i}, \quad i = 1, ..., n_t. \tag{4.1}$$

Then $T_1$ synchronises with $s_2(t)$ and obtains the overlapped and non-overlapped samples of $s_2(t)$ as,

$$r_{async}(i) = H\left[f_1(\tau)s_{1,i} + f_2(\tau)s_{1,i+1}\right] + Gs_{2,i-n_t} + Kh_2n_{1i} + n_{2i}, \quad i = n_t + 1, ..., N, \tag{4.2}$$

$$r_{async}(i) = Gs_{2,i-n_t} + Kh_2n_{1,i} + n_{2,i}, \quad i = N + 1, ..., N + n_t. \tag{4.3}$$

where $n_{1i}$ and $n_{2i}$ are AWGN distributed in $\mathcal{CN}(0, \sigma_n^2)$ and the frame length of the received samples is $N + n_t$. $f_1(\tau)$ and $f_2(\tau)$ are the factors resulting from the symbol offset $\tau$ and the use of a matched filter. The values of $f_1(\tau)$ and $f_2(\tau)$ are related to the filter type and symbol offset $\tau$. The analytical expressions of $f_1(\tau)$

and $f_2(\tau)$ are derived in Appendix G. Eq. (4.2) implies that the timing offsets $\tau_1$ and $\tau_2$ between source nodes and relay node are not needed for channel estimation.

Based on the received discrete signal samples, $T_1$ needs to demodulate $s_2$. By inspecting Eqs. (4.1)(4.2)(4.3), it is sufficient for signal demodulation purpose to estimate $f_1(\tau)$, $f_2(\tau)$ and the composite channel parameters $H$, $G$ and $\sigma^2$ jointly in MPSK modulated AF-TWRNs.

### 4.2.2 Generalised Low Complexity Maximum Likelihood Channel Estimation Algorithm

Channel estimation is performed at $T_1$ by using $N+n_t$ received samples $r_{async}(i), i = 1, ..., N+n_t$ given by Eqs. (4.1)(4.2)(4.3). Let

$$\mathbf{r} \triangleq [r_{async}(1), ..., r_{async}(N+n_t)]^T$$

be the vector of the received signals. The overlapped part is denoted by $\mathbf{r}_{n_t+1}^{N}$ and the non-overlapped parts of $s_1(t)$ and $s_2(t)$ are represented by $\mathbf{r}_1^{n_t}$ and $\mathbf{r}_{N+1}^{N+n_t}$, respectively. Due to the timing offset, we can take advantage of different expressions of the received signal and obtain channel estimations from the non-overlapped and overlapped signals, respectively.

#### 4.2.2.1 Channel Estimation Based on Non-overlapped and Overlapped Signals

Based on the non-overlapped signal $\mathbf{r}_1^{n_t}$, channel parameter $H$ can be estimated by training-based method [58] since $s_1(t)$ is known to $T_1$. Therefore, we obtain the estimation of $H$ as $\hat{H}_{no}$,

$$\hat{H}_{no} = \frac{\sum_{i=1}^{n_t} r_{async}(i) s_1^*(i)}{A n_t}. \tag{4.4}$$

Without loss of generality, the amplitude of $s_1$ and $s_2$ are assumed to be equal to $A$.

Overlapped samples in Eq.(4.2) can be expressed in vector form as,

$$\mathbf{r}_{n_t+1}^{N} = \quad H_1\mathbf{s}_1 + G\mathbf{s}_2 + H_2\mathbf{s}_3 + \mathbf{n}, \tag{4.5}$$

where $H_1 \triangleq f_1(\tau)H$, $H_2 \triangleq f_2(\tau)H$, $\mathbf{s}_1 \triangleq [s_{1,n_t+1}, ..., s_{1,N}]^T$, $\mathbf{s}_2 \triangleq [s_{2,1}, ..., s_{2,N-n_t}]^T$ and $\mathbf{s}_3 \triangleq [s_{1,n_t+2}, ..., s_{1,N}, 0]^T$. The noise term $\mathbf{n} \triangleq [n_{n_t+1}, ..., n_N]^T$, where $n_i = Kh_2n_{1i} + n_{2i}$ for $i = 1, ..., N + n_t$.

Assuming that $\mathbf{s}_1$, $\mathbf{s}_2$ and $\mathbf{s}_3$ are deterministic unknown vectors, the actual statistics of $\mathbf{s}_1$, $\mathbf{s}_2$ and $\mathbf{s}_3$ are considered in analysing the behaviour of the proposed algorithm theoretically in Section 3.3. The received vector $\mathbf{r}_{n_t+1}^{N}$ follows a complex Gaussian distribution with the expectation $\mathrm{E}\left\{\mathbf{r}_{n_t+1}^{N}\right\} = H_1\mathbf{s}_1 + G\mathbf{s}_2 + H_2\mathbf{s}_3$ and variance $\mathrm{Var}\left\{\mathbf{r}_{n_t+1}^{N}\right\} = \sigma^2\mathbf{I}$. The vector of unknown parameters $\Theta \triangleq [H_1, H_2, G, \sigma^2, \phi_{2,1}, ..., \phi_{2,N-n_t}]^T$ can be estimated by maximising the likelihood function of $\mathbf{r}_{n_t+1}^{N}$,

$$\Pr(\mathbf{r}_{n_t+1}^{N}; \Theta) = \frac{1}{(\pi\sigma^2)^{N-n_t}} \exp\left[-\frac{\left\|\mathbf{r}_{n_t+1}^{N} - H_1\mathbf{s}_1 - G\mathbf{s}_2 - H_2\mathbf{s}_3\right\|^2}{\sigma^2}\right], \tag{4.6}$$

which can be simplified as the log likelihood function,

$$\begin{aligned} L(\mathbf{r}_{n_t+1}^{N}; \Theta) &= -(N - n_t)\log(\pi\sigma^2) \\ &- \frac{\sum_{i=n_t+1}^{N}\left|r_{async}(i) - H_1s_{1,i} - H_2s_{1,i+1} - A|G|e^{j\left(\phi_g+\phi_{2,i-n_t}\right)}\right|^2}{\sigma^2}, \end{aligned} \tag{4.7}$$

where $\phi_g$ is the phase of $G$. Hereafter, $\hat{H}$, $\hat{H}_1$, $\hat{H}_2$, $\hat{G}$ and $\hat{\sigma}$ represent the estimated values of $H$, $H_1$, $H_2$, $G$ and $\sigma$, respectively.

With the knowledge of $\hat{n}_t$, the log likelihood function (4.7) could be maximised if $\left|r_{async}(i) - H_1 s_{1,i} - H_2 s_{1,i+1} - A\,|G|\,e^{j\left(\phi_g+\phi_{2,i-n_t}\right)}\right|$, $i = n_t+1,...,N$ is minimised. Since $\left|r_{async}(i) - H_1 s_{1,i} - H_2 s_{1,i+1} - A\,|G|\,e^{j\left(\phi_g+\phi_{2,i-n_t}\right)}\right|$ represents the *Euclidean Distance* between $r_{async}(i) - H_1 s_{1,i} - H_2 s_{1,i+1}$ and $A\,|G|\,e^{j\left(\phi_g+\phi_{2,i-n_t}\right)}$, the minimum distance could be achieved, if Eq. (4.8) is met.

$$\angle\left\{r_{async}(i) - H_1 s_{1,i} - H_2 s_{1,i+1}\right\} = \angle\left\{A\,|G|\,e^{j\left(\phi_g+\phi_{2,i-n_t}\right)}\right\}, \quad \forall \quad i = n_t+1,...,N. \tag{4.8}$$

However, in general (4.8) does not hold for all samples, as the modulated phases $\phi_1$ and $\phi_2 \in S_M$ and they cannot take continuous values in $[0, 2\pi)$. In order to derive a simple expression of $|G|$, we assume $\phi_1$ and $\phi_2$ are continuously valued in $[0, 2\pi)$ [60], that is, M$\rightarrow \infty$. Under the condition (4.8), (4.7) is approximated as,

$$L(\mathbf{r}_{n_t+1}^{N};\Theta) = -(N-n_t)\log(\pi\sigma^2) - \tfrac{1}{\sigma^2}\textstyle\sum_{i=n_t+1}^{N}\left(\left|r_{async}(i) - H_1 s_{1,i} - H_2 s_{1,i+1}\right| - A\,|G|\right)^2. \tag{4.9}$$

By maximising (4.9), $\hat{G}$ is estimated as

$$|\hat{G}| = \tfrac{\left\|\mathbf{r}_{n_t+1}^{N} - H_1\mathbf{s}_1 - H_2\mathbf{s}_3\right\|}{A(N-n_t)}, \quad \hat{\phi}_g = \angle\textstyle\sum_{i=0}^{l-1}\left(r_{async}(i) - H_1 s_{1,i} - H_2 s_{1,i+1}\right)s_{2,i-n_t}^{*}, \tag{4.10}$$

where $l$ is the number of training symbols. As the channel is assumed to be fixed and flat over one frame, the channel fading and phase shift are the same for each symbol. In the proposed algorithms, we use only one training symbol to find $\hat{\phi}_g$, which will be applied to resolve the phase ambiguity [84] in the signal demodulation. It will be shown in Section 4.5 that one training symbol is sufficient to achieve a near optimal symbol error rate (SER).

Substituting (4.10) into (4.9), the log likelihood function reduces to,

$$L(\mathbf{r}_{n_t+1}^N;\Theta) = -(N-n_t)\log(\pi\sigma^2) - \frac{1}{\sigma^2}\sum_{i=n_t+1}^N \mathbb{F}_i(H_1,H_2), \tag{4.11}$$

where

$$\mathbb{F}_i(H_1,H_2) \triangleq \left(|r_{async}(i) - H_1 s_{1,i} - H_2 s_{1,i+1}| - \frac{\sum_{k=n_t+1}^N |r_{async}(k) - H_1 s_{1,k} - H_2 s_{1,k+1}|}{N-n_t}\right)^2.$$

Since (4.11) is differentiable with respect to $\sigma^2$, let $\frac{\partial L(\mathbf{r}_{n_t+1}^N;\Theta)}{\partial \sigma^2} = 0$, $\hat{\sigma}^2$ is obtained as,

$$\hat{\sigma}^2 = \frac{\sum_{i=n_t+1}^N \mathbb{F}_i(H_1,H_2)}{N-n_t}. \tag{4.12}$$

Substituting (4.12) into (4.11), we obtain

$$[\hat{H}, \hat{f}_1(\tau), \hat{f}_2(\tau)] = \underset{\alpha\in\mathbb{C},0<a<1,0<b<1}{\operatorname{argmin}} \frac{\sum_{i=n_t+1}^N \mathbb{F}_i(a\alpha, b\alpha)}{N-n_t}. \tag{4.13}$$

Hence, $\hat{H}_1 = \hat{f}_1(\tau)\hat{H}$ and $\hat{H}_2 = \hat{f}_2(\tau)\hat{H}$. Eqs. (4.10) and (4.12) show that $\hat{G}$ and $\hat{\sigma}$ depend on $[\hat{H}_1, \hat{H}_2]$. Hence, the estimation of $\Theta$ can be obtained as long as $[\hat{H}_1, \hat{H}_2]$ is available.

To achieve channel estimation from the optimisation function (4.13), we make an approximation by replacing $|r_{async}(i) - H_1 s_{1,i} - H_2 s_{1,i+1}|$ as $|r_{async}(i) - H_1 s_{1,i} - H_2 s_{1,i+1}|^2$. Then (4.13) is updated as,

$$\begin{aligned}[\hat{H}_o, \hat{f}_1(\tau), \hat{f}_2(\tau)] &= \underset{\alpha\in\mathbb{C},0<a<1,0<b<1}{\operatorname{argmin}} L(\mathbf{r}_{n_t+1}^N;\alpha,a,b),\\ L(\mathbf{r}_{n_t+1}^N;\alpha,a,b) &= \end{aligned} \tag{4.14}$$

$$\frac{1}{N-n_t}\sum_{i=n_t+1}^{N}\left(\left|r_{async}(i)-a\alpha s_{1,i}-b\alpha s_{1,i+1}\right|^2-\frac{\sum_{k=n_t+1}^{N}\left|r_{async}(k)-a\alpha s_{1,k}-b\alpha s_{1,k+1}\right|^2}{N-n_t}\right)^2.$$

Note that we get another estimation of parameter $H$, which is denoted as $\hat{H}_o$. Then we obtain $\hat{H}_1=\hat{f}_1(\tau)\hat{H}_o$ and $\hat{H}_2=\hat{f}_2(\tau)\hat{H}_o$.

#### 4.2.2.2 Estimation Sample Selection Criterion

In the asynchronous system, where $n_t \neq 0$ and $\tau \neq 0$, we obtain two estimations of channel parameter $H$ from the overlapped signal as $\hat{H}_o$ and the non-overlapped signal as $\hat{H}_{no}$. The channel estimation $\hat{H}$ is selected from $\hat{H}_o$ and $\hat{H}_{no}$ as the one with the minimum MSE by the Estimation Sample Selection Criterion (ESSC).

By taking into account the statistics of $\mathbf{s}_1$, the estimation MSE of $\hat{H}_{no}$ is derived as

$$MSE_{\hat{H}_{no}}=\frac{\sigma^2}{A^2 n_t}. \tag{4.15}$$

Under the condition that symbol offset $\tau=0$, $\hat{H}_o=\hat{H}_{mlcml}$ $(M=2)$ and $\hat{H}_o=\hat{H}_{lcml}$ $(M>2)$. Hence, the estimation MSE of $\hat{H}_o$ is approximated as Eqs.(3.28) and (3.30) in Section 3.3.

Comparing Eq. (4.15) and Eqs.(3.28) and (3.30), we find that the frame length $N$ and the frame offset $n_t$ affect the MSE performance of the two channel estimators. Let us define $n_s \triangleq N-n_t$ and we get the ESSC,

$$\begin{cases} n_t > n_s, \quad M=2, \\ n_t > \dfrac{n_s^4-5n_s^3+8n_s^2-4n_s}{2n_s^3-3n_s^2+n_s-1}, \quad M>2. \end{cases} \tag{4.16}$$

If the ESSC (4.16) holds, which is equivalent to $MSE_{\hat{H}_{no}} < MSE_{\hat{H}_o}$, then we use the non-overlapped samples $\mathbf{r}_1^{n_t}$ to estimate the channel parameters as Eq.(4.4), i.e., $\hat{H} = \hat{H}_{no}$. Otherwise, the overlapped samples are selected to obtain the channel estimations by the GLCML algorithm as $\hat{H} = \hat{H}_o$.

## 4.3 Frame Synchronisation and Channel Estimation in AF-TWRNs

In this section, we study channel estimation in frame asynchronous AF-TWRNs, where there exist a frame offset between source nodes $T_1$ and $T_2$. In this case, the frame offset $n_t \neq 0$ and the symbol offset $\tau = 0$. First, we analyse the received signal model at source node $T_1$. Based on the received signal, a frame synchronisation algorithm is proposed in Section to estimate the integral timing offset, that is, the frame offset $n_t$. Then, we propose the frame asynchronous channel estimation (FACE) algorithm in Section, which achieves the channel estimation in the presence of a frame offset.

### 4.3.1 Received Signal Model

In the frame asynchronous system, the transmitted signals $s_1(t)$ and $s_2(t)$ are not aligned due to the frame offset. As a result, there is one overlapped part and two non-overlapped parts in the received signal as shown in Fig. 4.1. The overlapped part consists of two signals and the non-overlapped parts consist of only one signal. However, each symbol of the transmitted signals $s_1(t)$ and $s_2(t)$ are aligned, as shown in Fig. 4.2.

As $s_1(t)$ is the self-transmitted signal of source node $T_1$, $T_1$ can synchronise with $s_1(t)$ by a cross-correlation method [96] even without the knowledge of the frame offset. Then it filters $r_1(t)$ with a matched filter and samples it every $T$ period. The frame length of the resulting signal samples is $N + n_t$ due to the frame offset. As $T_1$ does not know $n_t$ and $0 < n_t < N$, $T_1$ gets $2N$ samples to detect the frame offset. The received $2N$ samples at $T_1$ are

$$r_f(i) = \begin{cases} Kh_1h_2s_{1,i} + Kh_2n_{1i} + n_{2i}, \quad i = 1, ..., n_t, \\ Kh_1h_2s_{1,i} + Kg_1h_2s_{2,i-n_t} + Kh_2n_{1i} + n_{2i}, \quad i = n_t + 1, ..., N, \\ Kg_1h_2s_{2,i-n_t} + Kh_2n_{1i} + n_{2i}, \quad i = N + 1, ..., N + n_t, \\ n_{2i}, \quad i = N + n_t + 2, ..., 2N. \end{cases} \tag{4.17}$$

where $n_{1i}$ and $n_{2i}$ are AWGN distributed in $\mathcal{CN}(0, \sigma_n^2)$.

Based on the received discrete signal samples, $T_1$ needs to demodulate $s_2$. Due to the fact that $T_1$ knows its self-transmitted signal $s_1(t)$ and the employed phase modulation scheme, signal demodulation of $s_2(t)$ can be conducted based on the power scaling factor $K$ and channel coefficients $h_1$, $h_2$, $g_1$ and $g_2$. However, it is complicated to estimate these unknown variables individually. By inspecting Eq. (4.17), it is sufficient for signal demodulation purpose to estimate the composite channel parameters $H \triangleq Kh_1h_2$, $G \triangleq Kg_1h_2$ and $\sigma^2 \triangleq \left(K^2 |h_2|^2 + 1\right) \sigma_n^2$ jointly in MPSK modulated AF-TWRNs. The power scaling factor $K$ is not assumed known to both the source nodes, but estimated jointly with channel coefficients at both the source nodes.

### 4.3.2 Frame Synchronisation Algorithm

Based on the received samples in Eq. (4.17), the frame offset is estimated by the frame synchronisation algorithm. The frame synchronisation algorithm is described in Table 4.1.

In Stage 1, the cross correlation of the received sample $r_1(t)$ and transmitted signal $s_1(t)$ is calculated and $s_1(t)$ begins when $xcorr(r_1(t), s_1(t))$ defined in Table 4.1 reaches its maximum. Under the assumption $N \to \infty$, we get

$Max[xcorr(r_1(t), s_1(t)] = N|H|^2A^2$.

In Stage 2, the total power of every $N$ received samples is denoted as $P_R$ defined in Table 4.1. If $N \to \infty$ and $SNR \to \infty$, the curve of $P_R$ is drew in Fig 4.4 and its slope is represented as

$$\mathbf{slope} = \left[\left(|G|^2 - |H|^2\right) A^2, -\left(|G|^2 + |H|^2\right) A^2\right], \tag{4.18}$$

where $\mathbf{slope}(i)$ denotes the slope of $P_R$ at intervals $i$ and represents the rate at which signal power changes, where $i = 1, 2$. By analysing the pattern of $P_R$, we derive the frame offset $n_t$. The beginning of $s_1(t)$ has been found in Stage 1, whose x-coordinate is $L_1$. Without loss of generality, we assume $n_t > 0$ and $a$ is assumed as the beginning of $s_1(t)$. $c$ is defined as the point whose x-coordinate is $c = L_1 + N$ on curve $P_R$. As illustrated in Fig 4.4, among all the points between $a$ and $c$ on curve $P_R$, the longest distance to the line $ac$ occurs at $b$ that is the beginning of $\mathbf{s}_2$, whose x-coordinate is $L_2$. As a result, $b$ is found by optimising $D(x, y, z)$, which calculates the distance from the point $x$ to the line $yz$. We obtain the frame offset estimation $\hat{n}_t = L_2 - L_1$.

The asymptotic performance of the frame synchronisation algorithm is analysed under the condition $N \to \infty$ and $SNR \to \infty$. In Stage 1, detection error occurs when $|H|$ is sufficiently small so that the maximum cross correlation could not be differentiated. In Stage 2, we utilise the $P_R$ slope differences to locate the beginning of $s_2(t)$. When $|G|^2$ is sufficiently small, there will be no slope difference between two intervals. Hence, detection error occurs if $|G| \to 0$. Since $H \triangleq Kh_1h_2$ and $G \triangleq Kg_1h_2$, $|H|$ and $|G|$ are i.i.d with the cumulative probability function $\mathcal{F}(u) = 1 - e^{\frac{-u}{\sigma_c^2}}, u > 0$. Obviously, the probability that $|H|$ or $|G|$ is arbitrarily small approaches zero. Therefore, the error probability of frame

Table 4.1: Frame Synchronisation Algorithm

| |
|---|
| **Stage 1-Locate the beginning of $\mathbf{s}_1$**<br>$xcorr(r_1(t), s_1(t))(x) = \vert \int_{-\infty}^{\infty} r_1(x), s_1^*(t+x)dx \vert$<br>$L_1 = \underset{x}{\text{argmax}}\ xcorr(r_1(t), s_1(t))(x),$ |
| **Stage 2-Locate the beginning of $\mathbf{s}_2$**<br>$P_R(i) = \sum_{j=0}^{N-1} \vert r_t(i+j)\vert^2 f(j+1),$<br>$f(i) = 1, i = 1, ..., N$<br>$a = [L_1, P_R(L_1)],$<br>$c = [L_1 + N, P_R(L_1 + N)],$<br>$b = \underset{a_x \leq p_x \leq c_x}{\text{argmax}}\ D(p, a, c)$<br>$L_2 = b_x.$ |

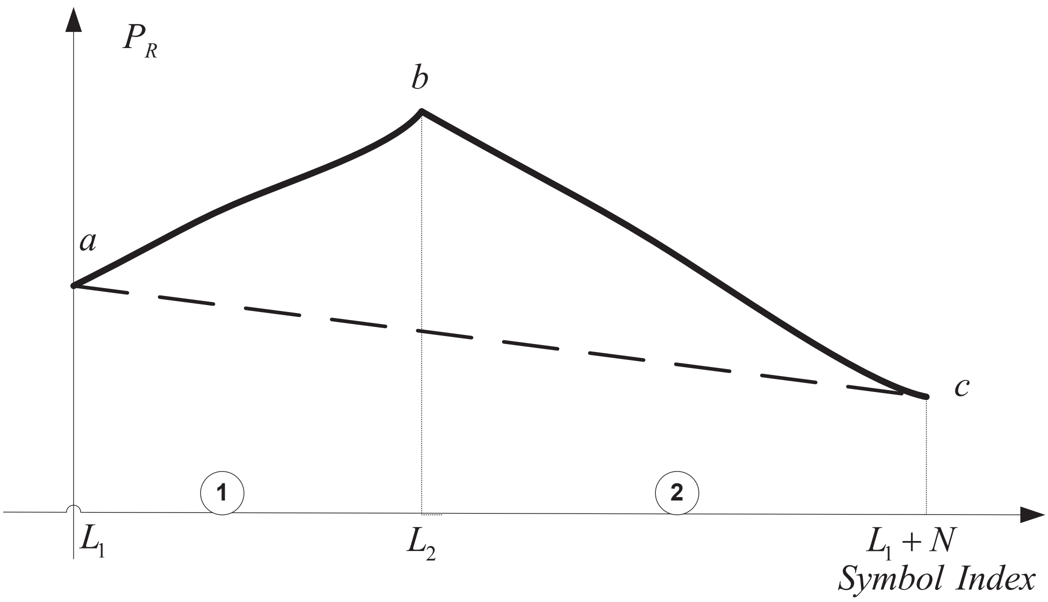


Figure 4.4: The Total Power of N Signals.

synchronisation algorithm approaches zero under the condition of large $N$ and SNR.

### 4.3.3 Channel Estimation In Frame Asynchronous Systems

Based on the estimation of the frame offset $\hat{n}_t$, we propose the frame asynchronous channel estimation (FACE) algorithm to obtain the estimation of $H$. In the FACE algorithm, the channel estimation of $H$ is denoted as $H_f$.

Channel estimation is performed at $T_1$ by using $2N$ received samples $r_f(i), i = 1, ..., 2N$ given by Eq. (4.17). Let $\mathbf{r}_f \triangleq [r_f(1), ..., r_f(2N)]^T$ be the vector of the received signals. Here we denote set $\mathbf{v} \triangleq [v_1, v_2, ..., v_n]$ and subset $\mathbf{v}_i^j \triangleq [v_i, v_{i+1}, ..., v_j]$. The overlapped part is denoted by ${\mathbf{r}_f}_{n_t+1}^N$ and the non-overlapped parts of $s_1(t)$ and $s_2(t)$ are represented by ${\mathbf{r}_f}_1^{n_t}$ and ${\mathbf{r}_f}_{N+1}^{N+n_t+1}$, respectively. Due to the frame offset, we can take advantage of different expressions of the received signal and obtain channel estimations from the non-overlapped and overlapped signals, respectively.

By using the non-overlapped signal ${\mathbf{r}_f}_1^{n_t}$, the channel parameter $H$ can be estimated in a similar way as $\hat{H}_{no}$ derived in Eq.(4.4). The overlapped signal ${\mathbf{r}_f}_{n_t+1}^N$ can be employed to generate the other channel estimation of $H$ as derived in the LCML and MLCML algorithms. As a result, we obtain two estimations of channel parameter $H$ from the overlapped signal and the non-overlapped signal. Then the ESSC algorithm is applied to obtain $H_f$.

If the ESSC (4.16) holds, then we use the non-overlapped samples ${\mathbf{r}_f}_1^{n_t}$ to estimate the channel parameters as Eq.(4.4). Otherwise, the overlapped samples ${\mathbf{r}_f}_{n_t+1}^N$ are selected to obtain the channel estimations by the LCML and MLCML algorithms as Eqs.(3.12), (3.13) and (3.20).

## 4.4 Channel Estimation in Timing Asynchronous AF-TWRNs

In this section, we study channel estimation in asynchronous AF-TWRNs without the assumption of perfect timing synchronisation between source nodes $T_1$ and $T_2$. In this case, the frame offset $n_t \neq 0$ and the symbol offset $\tau \neq 0$. The received signal model at source node $T_1$ is analysed in. Then the joint synchronisation and channel estimation (JSCE) algorithm is proposed to jointly estimate channel and the time offset.

### 4.4.1 Received Signal Model

In the time asynchronous system, the transmitted signals $s_1(t)$ and $s_2(t)$ are not frame-aligned as the frame offset $n_t \neq 0$. In addition, the transmitted signals $s_1(t)$ and $s_2(t)$ are not symbol-aligned due to the symbol offset $\tau \neq 0$, as shown in Fig. 4.3.

The source node $T_1$ tries to synchronise with its own transmitted signal $s_1(t)$ via the cross-correlation method. It calculates the cross correlation of the received sample $r_1(t)$ and the self-transmitted signal $s_1(t)$. Then it filters $r_1(t)$ with a matched filter $f^{'}(t) = f(T - t)$ and samples it every $T$ period. As the frame offset $n_t$ is estimated by the frame synchronisation algorithm, $T_1$ gets $N + n_t + 1$

samples to detect the timing offset. The received samples at $T_1$ are

$$r_t(i) = \begin{cases} Hs_{1,i} + Kh_2 n_{1i} + n_{2i}, \quad i = 1, ..., n_t, \\ Hs_{1,i} + G_1 s_{2,i-n_t} + G_2 s_{2,i-n_t-1} + Kh_2 n_{1i} + n_{2i}, \\ i = n_t + 1, ..., N, \\ G_1 s_{2,i-n_t} + G_2 s_{2,i-n_t-1} + Kh_2 n_{1i} + n_{2i}, \quad i = N+1, ..., N+n_t+1. \end{cases}$$

where $G_1 = f_1(\tau)G$ and $G_2 = f_2(\tau)G$. $f_1(\tau)$ and $f_2(\tau)$ are the factors resulting from the symbol offset $\tau$ and the use of a matched filter. The values of $f_1(\tau)$ and $f_2(\tau)$ are related to the filter type and symbol offset $\tau$. The analytical expressions of $f_1(\tau)$ and $f_2(\tau)$ are derived in Appendix G. $f_1(\tau), f_2(\tau) < 1$ regardless of the type of filters (See Appendix G). Eq. (4.19) implies that the timing offsets $\tau_1$ and $\tau_2$ between source nodes and relay node are not needed for synchronisation and channel estimation. The received discrete signal vector at $T_1$ is denoted as $\mathbf{r}_t \triangleq [r_t(1), ..., r_t(N+n_t+1)]^T$. The overlapped part is denoted by $\mathbf{r}_{t\,n_t+1}^{\,N}$ and the non-overlapped parts of $\mathbf{s}_1$ and $\mathbf{s}_2$ are represented by $\mathbf{r}_{t\,1}^{\,n_t}$ and $\mathbf{r}_{t\,N+1}^{\,N+n_t+1}$, respectively.

### 4.4.2 Joint Synchronisation and Channel Estimation Algorithm

Joint synchronisation and channel estimation is performed at $T_1$ by using $N+n_t+1$ received samples $r_t(i), i = 1, ..., N+n_t+1$ given by Eq. (4.19). As $G_1 = f_1(\tau)G$ and $G_2 = f_2(\tau)G$, we estimate symbol offset $\tau$ as

$$\hat{\tau} = \underset{0<\mu<T}{\operatorname{argmin}} \left| \frac{f_1(\mu)}{f_2(\mu)} - \frac{\hat{G}_1}{\hat{G}_2} \right|. \tag{4.19}$$

If $s_{2,1}$ and $s_{2,N}$ are the pilot symbol known to both the source nodes. We obtain the estimation of $G_1$ and $G_2$ from (4.19) as

$$\hat{G}_1 = \left(r_t(n_t+1) - Hs_{1,n_t+1}\right) s^*_{2,1},$$
$$\hat{G}_2 = r_t(N+n_t+1)s^*_{2,N}. \tag{4.20}$$

Substituting (4.20) into (4.19) yields,

$$\hat{\tau} = \underset{0<\mu<T}{\operatorname{argmin}} \left| \frac{f_1(\mu)}{f_2(\mu)} - \frac{\left(r_t(n_t+1)-Hs_{1,n_t+1}\right)s^*_{2,1}}{r_t(N+n_t+1)s^*_{2,N}} \right|, \tag{4.21}$$

which shows that $\hat{\tau}$ depends on the availability of the estimation of $H$. Note (4.21) is applicable to any type of filters.

In the case that frame offset $n_t \neq 0$, the non-overlapped signal $\mathbf{r}_{t1}^{n_t}$ can be used to derive one estimation of $H$ as $\hat{H}_f$. Then $\hat{\tau}$ is obtained from (4.21) based on $\hat{H}_f$. On the other hand, in the case that frame offset $n_t = 0$, the symbol asynchronous channel estimation (SACE) algorithm is proposed to estimate channel $H$ as Eqs.(4.28) and (4.30) based on the overlapped part $\mathbf{r}_{t n_t+1}^{N}$ of the received sample. As a result, the fractional timing offset, that is, the symbol offset $\tau$ is obtained from (4.21).

If the frame offset $n_t = 0$, the vector of unknown parameters

$$\Theta_s \triangleq \left[H, \sigma^2, \phi_{2,1}, ..., \phi_{2,N-n_t}\right]$$

can be estimated by maximizing the log likelihood function of $\mathbf{r}_{t n_t+1}^{N}$,

$$L(\mathbf{r}_{t n_t+1}^{N}; \Theta_s) = -(N-n_t)\log\left(\pi\sigma^2\right) - \frac{\sum_{i=n_t+1}^{N}\left|r_t(i)-Hs_{1,i}-G_1 s_{2,i-n_t}-G_2 s_{2,i-n_t-1}\right|^2}{\sigma^2}. \tag{4.22}$$

By inspecting (4.22), the estimated parameters that satisfy the following condition

$$r_t(i) - Hs_{1,i} - G_1 s_{2,i-n_t} - G_2 s_{2,i-n_t-1} = 0, \\ \texttt{for} \quad i = n_t + 1, ..., N \tag{4.23}$$

will definitely maximise the log likelihood function (4.22). Based on this fact, we make some approximations and propose a symbol asynchronous channel estimation (SACE) algorithm.

#### 4.4.2.1 BPSK ($M = 2$)

The condition (4.23) implies that the estimated parameters also satisfy

$$(r_t(i) - Hs_{1,i})^2 - (G_1 s_{2,i-n_t} + G_2 s_{2,i-n_t-1})^2 = 0 \\ for i = n_t + 1, ..., N.$$

As $s_{2,i} = \pm 1$ in BPSK, the log likelihood function (4.22) can be approximated as,

$$\begin{aligned} L(\mathbf{r}_{t_{n_t+1}}^N; \Theta_s) &= -(N - n_t) \log(\pi\sigma^2) \\ &- \frac{\sum_{i=n_t+1}^N \left| (r_t(i) - Hs_{1,i})^2 - \left(G_1 s_{2,i-n_t} + G_2 s_{2,i-n_t-1}\right)^2 \right|^2}{\sigma_s^2}, \\ &= -(N - n_t) \log(\pi\sigma^2) \\ &- \frac{\sum_{i=n_t+1}^N \left| (r_t(i) - Hs_{1,i})^2 - G_1^2 - G_2^2 - 2G_1 G_2 s_{2,i-n_t} s_{2,i-n_t-1} \right|^2}{\sigma^2}. \end{aligned} \tag{4.24}$$

If channel parameters satisfy

$$(r_t(i) - Hs_{1,i})^2 - G_1^2 - G_2^2 - 2G_1 G_2 s_{2,i-n_t} s_{2,i-n_t-1} = 0, \\ i = n_t + 1, ..., N, \tag{4.25}$$

then the approximated log likelihood function (4.24) is maximised. As condition (4.25) suggests that channel parameters also make

$$\angle\left(\left(r_t(i) - Hs_{1,i}\right)^2 - G_1^2 - G_2^2\right) = \angle\left(2G_1G_2s_{2,i-n_t}s_{2,i-n_t-1}\right).$$

hold for $i = n_t + 1, ..., N$, we further approximate (4.24) as

$$\begin{aligned} L(\mathbf{r}_{t_{n_t+1}}^N; \Theta_s) &= -(N - n_t)\log\left(\pi\sigma^2\right) \\ &- \frac{\sum_{i=n_t+1}^N \left(\left|\left(r_t(i) - Hs_{1,i}\right)^2 - G_1^2 - G_2^2\right| - 2\left|G_1G_2\right|\right)^2}{\sigma^2}. \end{aligned} \tag{4.26}$$

After two steps of approximations, we eliminate unknown signal $s_{2,i}$ from the objective function. Therefore, the semi-blind channel estimation is made possible by these approximations. Maximising the above objective function (4.26) in terms of $\sigma^2$ yields,

$$\hat{\sigma}_s^2 = \frac{\sum_{i=n_t+1}^N \left(\left|\left(r_t(i) - Hs_{1,i}\right)^2 - G_1^2 - G_2^2\right| - 2\left|G_1G_2\right|\right)^2}{N - n_t}. \tag{4.27}$$

Substituting (4.20) and (4.27) into (4.26), we obtain $\hat{H}_s$ as,

$$\hat{H}_s^{BPSK} = \underset{\alpha\in\mathbb{C}}{\operatorname{argmin}} \frac{\sum_{i=n_t+1}^N \left(\left|\left(r_t(i) - \alpha s_{1,i}\right)^2 - \hat{G}_1^2 - \hat{G}_2^2\right| - 2\left|\hat{G}_1\hat{G}_2\right|\right)^2}{A(N - n_t)}. \tag{4.28}$$

#### 4.4.2.2 MPSK($M > 2$)

In this section, we propose the SACE algorithm for MPSK, where modulation order $M > 2$. The condition (4.23) implies that the estimated parameters also make $\angle\left(r_t(i) - Hs_{1,i}\right) - \angle\left(G_1s_{2,i-n_t} + G_2s_{2,i-n_t-1}\right) = 0$ hold for $i = n_t + 1, ..., N$.

Therefore, (4.22) is approximated as

$$L(\mathbf{r}_{t_{n_t+1}}^{N};\Theta_s) = -(N-n_t)\log(\pi\sigma^2) \\ -\frac{\sum_{i=n_t+1}^{N}\left(|r_t(i)-Hs_{1,i}|^2-\left|G_1e^{j\phi_{2,i-n_t}}+G_2e^{j\phi_{2,i-n_t-1}}\right|^2\right)^2}{\sigma^2}.$$

The condition (4.23) also suggests that the estimated parameters satisfy $|r_t(i)-Hs_{1,i}|^2 = |G_1s_{2,i-n_t}+G_2s_{2,i-n_t-1}|^2$ for $i=n_t+1,...,N$. We make another approximation $|G_1s_{2,i-n_t}+G_2s_{2,i-n_t-1}|^2 = \frac{\sum_{i=n_t+1}^{N}|r_t(i)-Hs_{1,i}|^2}{N-n_t}$ and obtain

$$L(\mathbf{r}_{t_{n_t+1}}^{N};\Theta_s) = -(N-n_t)\log(\pi\sigma^2) \\ -\frac{\sum_{i=n_t+1}^{N}\left(|r_t(i)-Hs_{1,i}|^2-\frac{\sum_{k=n_t+1}^{N}\left|r_t(k)-Hs_{1,k}\right|^2}{N-n_t}\right)^2}{\sigma^2}. \tag{4.29}$$

Maximising the approximate objective function (4.29), we get $\hat{H}_s^{MPSK} = \Re\{\hat{H}_s^{MPSK}\}+ j\Im\{\hat{H}_s^{MPSK}\}$, where $\Re\{\hat{H}_s^{MPSK}\}$ and $\Im\{\hat{H}_s^{MPSK}\}$ denote real and imaginary parts of the complex number $\hat{H}_s^{MPSK}$, respectively.

$$\begin{aligned}
\Im\{\hat{H}_s^{MPSK}\} = & \frac{\mathbf{C}_1^T\mathbf{C}_2\left(\mathbf{C}_3^T\mathbf{C}_3+\mathbf{C}_2^T\mathbf{C}_3\right)}{2j\left(\mathbf{C}_2^T\mathbf{C}_2\mathbf{C}_3^T\mathbf{C}_3-\left(\mathbf{C}_2^T\mathbf{C}_3\right)^2\right)} \\
& -\frac{\mathbf{C}_1^T\mathbf{C}_3\left(\mathbf{C}_2^T\mathbf{C}_2+\mathbf{C}_2^T\mathbf{C}_3\right)}{2j\left(\mathbf{C}_2^T\mathbf{C}_2\mathbf{C}_3^T\mathbf{C}_3-\left(\mathbf{C}_2^T\mathbf{C}_3\right)^2\right)}, \\
\Re\{\hat{H}_s^{MPSK}\} = & \; j\Im\{\hat{H}_{MPSK}\}\frac{\left(\mathbf{C}_2^T\mathbf{C}_2-\mathbf{C}_3^T\mathbf{C}_3\right)}{(\mathbf{C}_2+\mathbf{C}_3)^T(\mathbf{C}_2+\mathbf{C}_3)} \\
& -\frac{\mathbf{C}_1^T\mathbf{C}_2+\mathbf{C}_1^T\mathbf{C}_3}{(\mathbf{C}_2+\mathbf{C}_3)^T(\mathbf{C}_2+\mathbf{C}_3)}.
\end{aligned} \tag{4.30}$$

where

$$\begin{cases}
\mathbf{C}_1 \triangleq [C_{1,n_t+1},...,C_{1,N}]^T, \quad C_{1i} = |r_t(i)|^2 - \frac{\sum_{k=n_t+1}^{N}|r_t(k)|^2}{N-n_t}, \\
\mathbf{C}_2 \triangleq [C_{2,n_t+1},...,C_{2,N}]^T, C_{2i} = \frac{\sum_{k=n_t+1}^{N}s_{1k}^*r_t(k)}{N-n_t} - s_{1i}^*r_t(i), \\
\mathbf{C}_3 \triangleq [C_{3,n_t+1},...,C_{3,N}]^T, C_{3i} = \frac{\sum_{k=n_t+1}^{N}s_{1k}r_t^*(k)}{N-n_t} - s_{1i}r_t^*(i), \forall\ i=n_t+1,..,N.
\end{cases}$$

## 4.5 Simulation Results

In this section, we will evaluate the performance of the proposed GLCML, FACE and JSCE algorithms numerically by Monte Carlo simulations over flat-fading channels. In the simulations, we employ MPSK signal modulation and assume $P_r = P_1 = P_2 = P$. The SNR is defined as $\frac{P}{\sigma_n^2}$, where $\sigma_n^2$ denotes the AWGN power. The channel parameters $h_1$, $h_2$, $g_1$ and $g_2$ are modelled as i.i.d in $\mathcal{CN}(0, 1)$ and remain fixed during one frame.

Fig. 4.5 shows the frame synchronisation error in BPSK and QPSK of the FACE algorithm, which is defined as $\frac{|\hat{n}_t - n_t|}{n_t}$, versus $\frac{n_t}{N}$ for SNR=20dB. The synchronisation performance improves with the frame length $N$, which confirms the theoretical result in Section 4.3.2 that the synchronisation error approaches 0 if $N \to \infty$. As the signal power detection and the cross-correlation method are employed in the FACE algorithm to determine the frame offset, the FACE algorithm achieves the same frame synchronisation error performance in the cases of different modulation orders.

The MSE performance of the GLCML algorithm with timing offset $n_t = 5$ and $n_t = 25$ for QPSK is shown in Fig. 4.6. When $n_t = 25$, the ESSC (4.16) holds. Then the non overlapped signal is selected to obtain channel estimation that gives a better estimation MSE than the overlapped signal. If $n_t = 5$, (4.16) does not hold any more. Thus the overlapped signal is used to estimate channel parameters. Fig. 4.6 shows that the GLCML algorithm always selects the samples producing a channel estimation with the minimum MSE in the timing asynchronous system.

The MSE performance of the JSCE algorithm for different modulation orders is plotted versus SNR for frame length $N = 45$ in Figs. 4.7 and 4.8. For simplicity, the rectangular pulse shaping filter is used. In both cases where the frame offset $n_t = 0$ and $n_t \neq 0$, the JSCE algorithm is able to achieve accurate symbol offset estimations. Figs. 4.5, 4.7 and 4.8 show that the JSCE achieves joint channel and timing offset estimation in the asynchronous system.

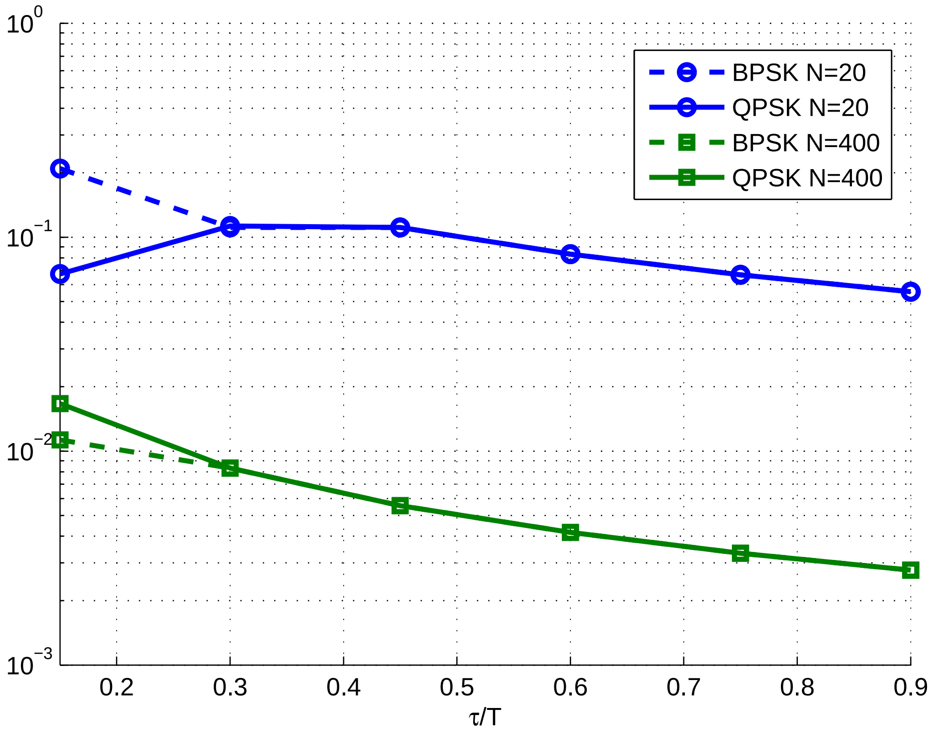


Figure 4.5: The frame synchronization performance of the FACE algorithm VS. frame offset for SNR=20dB.

## 4.6 Conclusion

In this chapter, we proposed channel estimation algorithms, which are referred to as the generalised low complexity maximum likelihood (GLCML) channel estimation, frame asynchronous channel estimation (FACE) and joint synchronisation and channel estimation (JSCE) algorithms, for channel estimation in AF-TWRNs without the assumption of perfect synchronisation among all the nodes. In the presence of a relative time offset between both source nodes, the GLCML algorithm was proposed for channel estimation in the asynchronous TWRNs by

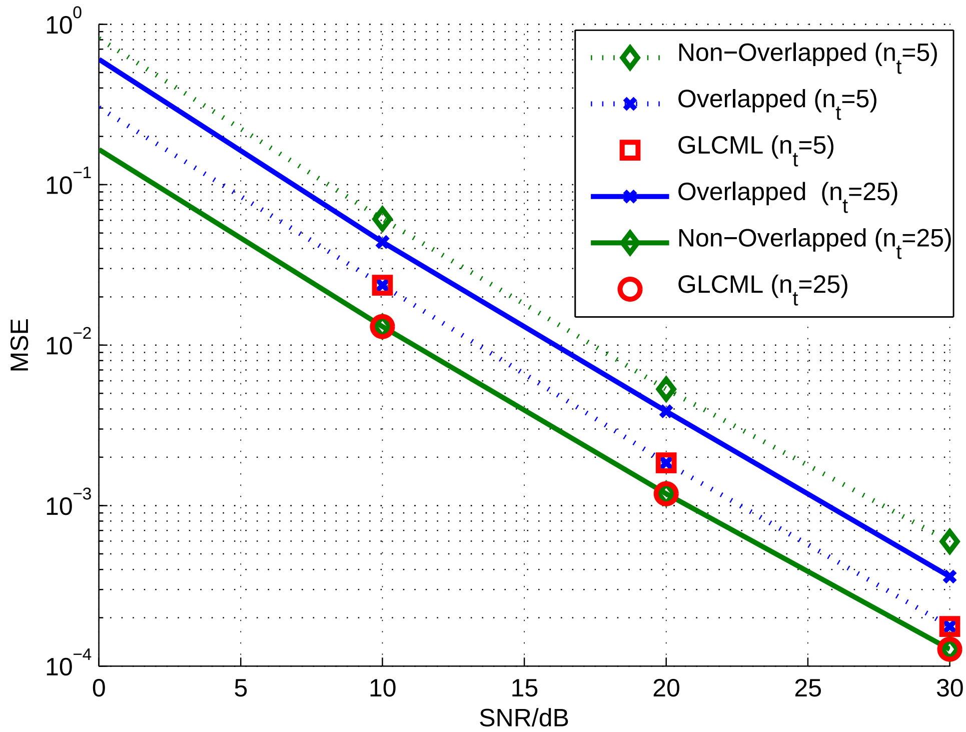


Figure 4.6: The MSE performance of the GLCML channel estimator VS. SNR for $N$=45 in QPSK.

extending the LCML algorithm. The frame offset is estimated by the FACE algorithm and the JSCE algorithm was proposed to estimate the symbol offset and channel parameters jointly. The numerical results show that the GLCML algorithm achieves channel estimation performance as good as the LCML algorithm in the presence of the time offset. The FACE and JSCE algorithms are able to achieve accurate timing offset and channel estimations jointly. The proposed algorithms in this chapter achieve channel estimation and timing synchronisation. However, the carrier frequency synchronisation is assumed among all the nodes. Hence, the joint frequency and timing synchronisation and channel estimation will be performed in the future work.

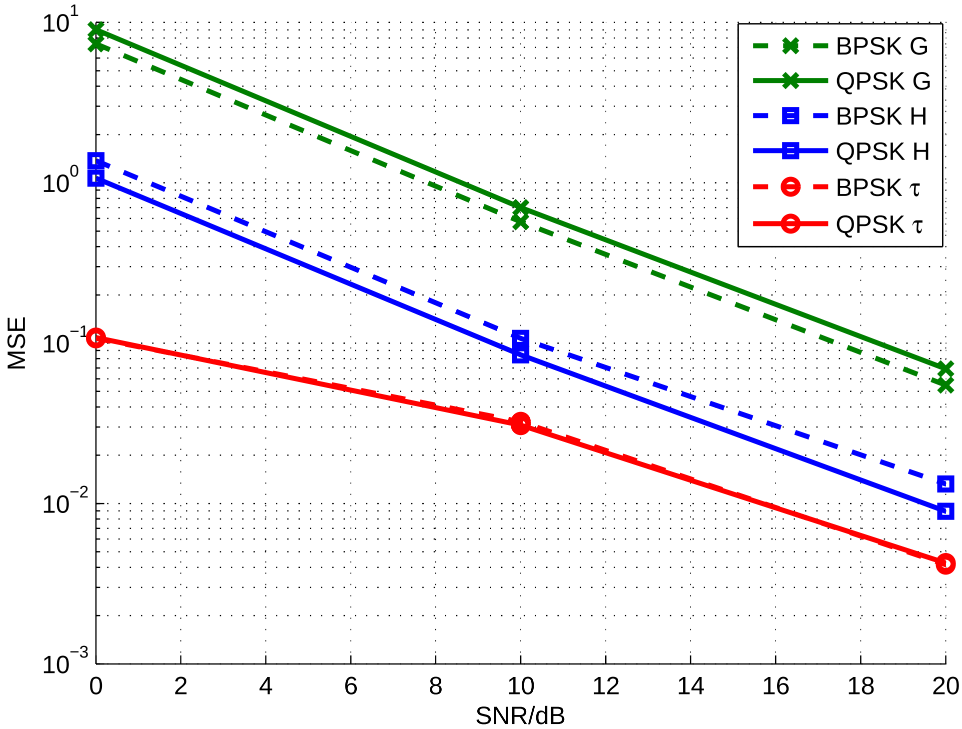


Figure 4.7: The MSE performance of the JSCE channel estimator VS. SNR for $N$=45 in the case of frame offset $n_t \neq 0$.

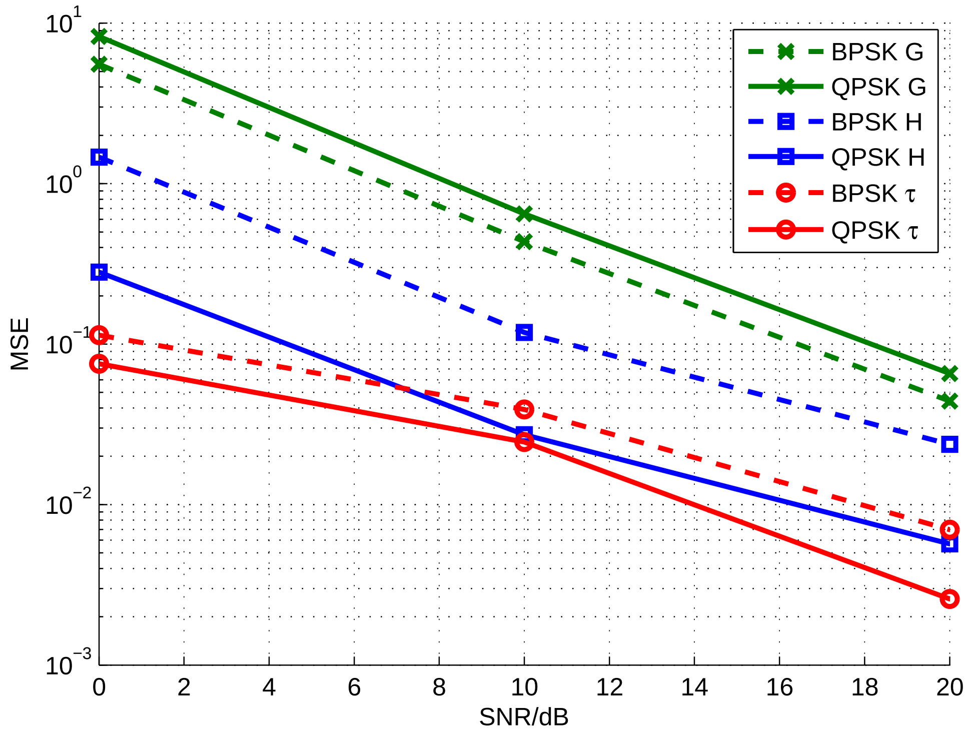


Figure 4.8: The MSE performance of the JSCE channel estimator VS. SNR for $N$=45 in the case of frame offset $n_t = 0$.

# Chapter 5

# Contention Resolution Algorithm

To improve the spectral efficiency in the physical (PHY) layer, the relay schemes has been considered in Chapters 3 and 4. In the media access control (MAC) layer, the multiple access schemes are employed to allocate limited resources to improve the spectral efficiency. One of the challenges facing the multiple access networks is the contention and interference due to multiple transmissions from multiple nodes, sharing the common communication medium. In this chapter, we propose a self-adaptive backoff (SAB) algorithm to resolve contention and mitigate signal interference by adjusting the contention window length in the contention-based multiple access networks.

To derive the optimal contention window length, given the average local packet arrival rate and the total number of nodes in the network, the states of the node is modelled as a discrete-time Markov chain [86] to analyse the network contention. Firstly, we derive the mathematical relationship of the contention window length, the number of nodes in the network, the Markov state probability that a node performs the channel sensing, which is referred as the channel access probability, and the buffer condition at the nodes. Secondly, we obtain the mathematical relationship between the average local packet arrival rate, the number of nodes in the network and the buffer condition at the nodes based on the queue theory [83]. Based on the derived mathematical relationships, we achieve a mathematical relationship of the channel access probability, the contention window length, the average local packet arrival rate and the number of nodes in the network. Then we formulate the system throughput and optimise it with contention window length as a variable.

## 5.1 Network Contention Model

The multiple access network considered in this paper has $N$ nodes, contending to communicate with one access point over a single communication channel, under the contention-based access mechanism CSMA. The distance from each node to the access point is assumed the same, the total number of the nodes in the network is assumed known to all the nodes, and all the nodes share the same average packet arrival rate $\lambda$. In this section, we model the network contention between nodes in CSMA networks by representing them as the Markov state probability and the Markov transition probability [86].

The state transition of a node is illustrated in the Markov Chain model shown in Fig. 5.1. The states of a node are denoted by $\mathbf{S}_1$, $\mathbf{S}_{2,w}$, $\mathbf{S}_{3,l}$ and $\mathbf{S}_{4,l}$. $\mathbf{S}_1$ represents the state when a node is waiting for packets to arrive to its buffer. $\mathbf{S}_{2,w}$ represents the backoff states, where the node counts down from $w$ to 1, and then performs channel sensing. The backoff time is $w$ and $w = 1, 2, ..., W$, where $W$ is the contention window length. $w$ is chosen uniformly from [1 $W$] with the probability $\frac{1}{W}$. $\mathbf{S}_{3,l}$ and $\mathbf{S}_{4,l}$ represent the transmission failure state and transmission success state in time slot $l$, respectively, where $l = 1, 2, ..., L$ and $L$ is the packet length. Here, the packet transmission is assumed to take $L$ time slots.

In the following, the transitions going out of the waiting state $\mathbf{S}_1$ are explained. If there is no new packet arrival and there is currently no packet in the buffer, the node remains in the waiting state with a transition probability from $\mathbf{S}_1$ back to $\mathbf{S}_1$, $\Pr(\mathbf{S}_1|\mathbf{S}_1) = p_0$ where $p_0$ denotes the probability that there is no packet in the buffer and no new packet arrival. Otherwise, the state of the node moves from$\mathbf{S}_1$ to one of the backoff states, $\mathbf{S}_{2,w}$, $w = 1, 2, ..., W$ with a probability of $\Pr(\mathbf{S}_{2,w}|\mathbf{S}_1) = \frac{1-p_0}{W}$, as the node choose the backoff time $w$ uniformly from $[1\ W]$ with the probability $\frac{1}{W}$.

The transitions going out of the backoff state $\mathbf{S}_{2,w}$ are explained in the following. At the backoff state $\mathbf{S}_{2,w}$, the node waits a backoff time $w$ with the probability $\frac{1}{W}$. The backoff counter decreases by one at a time from $w$ to 1 with a probability of 1. This is represented by a state transition from $\mathbf{S}_{2,w}$ to $\mathbf{S}_{2,w-1}$,,...,$\mathbf{S}_{2,1}$. Once $w = 1$, the node is in state $\mathbf{S}_{2,1}$ and performs channel sensing to detect if the channel is occupied or not. We refer to the state $\mathbf{S}_{2,1}$ as the channel access state. If the channel is busy, the node states will move from $\mathbf{S}_{2,1}$ to one of the backoff states $\mathbf{S}_{2,w}$, $w = 1, ..., W$ with a probability of $\Pr(\mathbf{S}_{2,w}|\mathbf{S}_{2,1}) = \frac{\alpha}{W}$ where $\alpha$ denotes the probability that a node senses the channel and finds it busy. If there is no transmission when the node stays in $\mathbf{S}_{2,1}$ and performs channel sensing, an idle channel is detected with the probability $1 - \alpha$.

The node then starts packet transmissions. We assume that it takes $L$ time slot to transmit a packet. If the transmission of a node is successful, its state goes from $\mathbf{S}_{2,1}$ to $\mathbf{S}_{4,1}$, with a probability of $\Pr(\mathbf{S}_{4,1}|\mathbf{S}_{2,1}) = (1 - \alpha)(1 - p_c)$, where $\mathbf{S}_{4,1}$ represents the first time slot of a successful transmission, and $p_c$ and $1 - \alpha$ represent the probability of collision and an idle channel, respectively. The node then continues to transmit the remaining $L - 1$ packets. This successful transmission is represented by the transition probability $\Pr(\mathbf{S}_{4,l}|\mathbf{S}_{4,l-1}) = 1$, where $l = 2, 3, ..., L$. On the other hand, if the transmission of a node collides with other nodes' transmissions, its state goes from $\mathbf{S}_{2,1}$ to $\mathbf{S}_{3,1}$, with a probability of $\Pr(\mathbf{S}_{3,1}|\mathbf{S}_{2,1}) = (1-\alpha)p_c$, where $\mathbf{S}_{3,1}$ represents the first time slot of a fail transmission. The node then continues to transmit the remaining $L-1$ packets. This L packet transmission loss is represented by transition probability $\Pr(\mathbf{S}_{3,l}|\mathbf{S}_{3,l-1}) = 1$, where $l = 2, 3, ..., L$. This is shown in Fig. 5.1.

After a packet transmissions in $L$ time slots, regardless it is a success or failure, if the buffer of the node is empty, the node will move to state $\mathbf{S}_1$ from $\mathbf{S}_{4,L}$ or $\mathbf{S}_{3,L}$ with a probability of $\Pr(\mathbf{S}_1|\mathbf{S}_{3,L}) = \Pr(\mathbf{S}_1|\mathbf{S}_{4,L}) = \pi_0$, where $\pi_0$ represents the probability that the queue of a node is empty after a packet departure. Otherwise, if the node buffer is not empty, the state goes from $\mathbf{S}_1$ to one of the backoff states, $\mathbf{S}_{2,w}$ and $w = 1, ..., W$, with a probability of $\frac{1-\pi_0}{W}$ as the node waits a backoff time $w$ with the probability $\frac{1}{W}$ and $1-\pi_0$ is the probability of non-empty buffer after a packet departure.

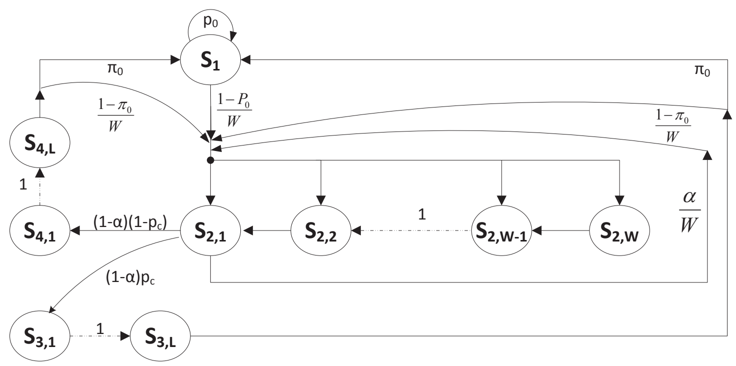


Figure 5.1: Markov Model

## 5.2 Network Contention Analysis

In this section, we derive the expression of the state probability in terms of the contention window length, $W$, the number of nodes in the system, $N$, and the average local packet arrival rate, $\lambda$. First, we derive a mathematical relationship between contention window length, $W$, the state probability and the transition probability by using the Markov based contention model developed in the previous section. Then, we derive the analytical expression for the average service time per packet, including the duration of transmission, backoff and channel sensing, according to the Markov chain model in Fig. 5.1. After that, we use the derived average service time and the derived mathematical relationship to derive an analytical function that relates the network contention model and the traffic load.

### 5.2.1 Contention Window Analysis

In this section, we derive the relation of the contention window length, $W$, the state probability and the transition probability based on the Markov model. We define the state probability [86] as $b_{i,j} = \Pr(\mathbf{S}_{i,j})$, where $i = 1, 2, 3, 4$ and $j = 1, 2, ..., \mathrm{Max}(W, L)$. According to the balance equations, which balance the probability of leaving and entering a state in equilibrium [86], we can write the following equations,

$$\begin{cases} b_1 = b_1 p_0 + (b_{3,1} + b_{4,1})\pi_0, \quad \text{balance equation at } b_1 \\ b_{2,w} = p(W + 1 - w), \quad w = 1, ..., W, \quad \text{balance equation of Backoff States} \\ b_{3,l} = (1 - \alpha) p_c b_{2,1}, \quad l = 1, ..., L, \quad \text{balance equation at } b_{3,l} \\ b_{4,l} = (1 - \alpha)(1 - p_c) b_{2,1}, \quad l = 1, ..., L, \quad \text{balance equation at } b_{4,l}\ . \end{cases} \tag{5.1}$$

where $p = \frac{b_1(1-p_0)+(b_{3,1}+b_{4,1})(1-\pi_0)+\alpha b_{2,1}}{W}$. As the total probability of states is equal to 1, we get

$$1 = b_1 + b_2 + b_3 + b_4. \tag{5.2}$$

where $b_2 = \sum_{w=1}^{W} b_{2,w}$,$b_3 = \sum_{i=1}^{L} b_{3,i}$, and $b_4 = \sum_{j=1}^{L} b_{4,j}$.

Based on the Markov model, we derive the expressions of the Markov transition probabilities $\alpha$ and $p_c$ in the following, where $\alpha$ denotes the probability that a node senses the channel and finds it busy and $p_c$ represents the probability that the transmission of the node collides with other nodes' transmissions. $\alpha$ and $p_c$ also indicate the observed network condition and the actions of other nodes.

As a node performs channel sensing if it stays in state $\mathbf{S}_{2,1}$, the state probability $b_{2,1}$ is defined as the channel access probability. We assume all the nodes share the same channel access probability $b_{2,1}$, so that the fairness of channel access among all the nodes in the network can be guaranteed. If the channel is observed busy by a node, whose probability is denoted as $\alpha$, there is at least one transmission in the channel when the node performs the channel sensing. Hence, we obtain $\alpha$ as

$$\alpha = \left(1 - (1 - b_{2,1})^{N-1}\right)(1 - \alpha). \tag{5.3}$$

In Eq.(5.3), the term $1 - (1 - b_{2,1})^{N-1}$ represents the probability that at least one of the remaining $N - 1$ nodes stay in state $\mathbf{S}_{2,1}$ to sense the channel. And the term $1 - \alpha$ is the probability that the remaining $N - 1$ nodes find the channel is idle. In the network of a large number of nodes, the channel access probability $b_{2,1}$ will be very small relative to $N$. Hence, we make an approximation

$\lim_{b_{2,1}\to 0}(1-b_{2,1})^{N-1} = 1-(N-1)b_{2,1}$ [78] and obtain $\alpha$ as

$$\alpha = \frac{(N-1)\,b_{2,1}}{1+(N-1)\,b_{2,1}}. \tag{5.4}$$

To derive the collision probability, $p_c$, we use the fact that for the collision to happen, there must be another packet transmission from other nodes. This is equivalent with the probability of at least one of the remaining $N-1$ nodes stay in the state $\mathbf{S}_{2,1}$ to sense the channel, described in Eq.(5.3).

$$p_c = 1-(1-b_{2,1})^{N-1}. \tag{5.5}$$

Eq.(5.5) means that transmission collisions result from the fact that at least two nodes perform channel sensing simultaneously and meanwhile the channel is idle.

By using the balance equations described in Eqs.(5.1) and (5.2), the probability of busy channel in Eq.(5.4) and collision probability in Eq.(5.5), we can express the state probabilities $b_{i,j}$ in terms of $p_0$, $\pi_0$, $\alpha$, $p_c$ and the contention window length $W$ as follows,

$$\begin{cases} b_1 = \dfrac{(1-\alpha)\,\pi_0}{1-p_0} b_{2,1}, \\ b_{2,1} = Wp, \quad b_2 = \dfrac{W+1}{2} b_{2,1}, \\ b_{3,l} = (1-\alpha)p_c b_{2,1}, \quad b_3 = \dfrac{Lb_{2,1}\left(1-(1-b_{2,1})^{N-1}\right)}{1+(N-1)\,b_{2,1}}, l = 1,2,...,L, \\ b_{4,l} = (1-\alpha)(1-p_c)b_{2,1}, \quad b_4 = \dfrac{Lb_{2,1}(1-b_{2,1})^{N-1}}{1+(N-1)\,b_{2,1}}, l = 1,2,...,L. \end{cases} \tag{5.6}$$

Based on Eq.(5.6), the mathematical relationship between contention window length $W$, the number of nodes $N$, the probability that the buffer of the node is empty after a packet transmission and due to no new packet arrival, represented by $\rho_0$ and $p_0$, respectively, is given as follows,

$$\left(\frac{\pi_0}{1-p_0}+L\right)\frac{1}{1+(N-1)\,b_{2,1}}+\frac{W+1}{2}-\frac{1}{b_{2,1}}=0. \tag{5.7}$$

### 5.2.2 Service Time Analysis

The traffic load is defined as $\rho \triangleq \lambda E\left[t_{service}\right]$, which represents the number of packets arriving during the average service time. Here $\lambda$ represents the average local packet arrival rate and the service time $t_{service}$ is the instant service time per packet, including backoff, channel sensing and packets transmission durations. $E\left[t_{service}\right]$ is the average service time per packet, including the duration of transmission, backoff and channel sensing. Here $E[x]$ is defined as the expectation of the random variable $x$. In this section, the average service time $E\left[t_{service}\right]$ is derived according to the Markov chain model in Fig. 5.1. As a packet transmission is either successful or failure, the transmission duration is assumed fixed. Therefore, the channel sensing and backoff duration mainly affect the service time of a packet, which is closely related to the contention window length $W$.

The instant service time per packet is expressed as

$$t_{service}=t_i+t_x,$$

where $t_i$ denotes the instant transmission duration and $t_x$ is the instant backoff and sensing duration. The expressions of $E\left[t_i\right]$ and $E\left[t_x\right]$ will be derived in the following.

#### 5.2.2.1 Average Transmission Time $E[t_i]$

To analyse $t_i$, we denote $t_s$ and $t_f$ as the duration of a successful transmission and a failed transmission, respectively and obtain

$$t_i = \begin{cases} t_s, & \Pr(t_i = t_s) = b_4, \\ t_f, & \Pr(t_i = t_f) = b_3. \end{cases}$$

Therefore, $t_i$ follows the Bernoulli distribution [97] and the average duration of a transmission is

$$E[t_i] = b_4 t_s + b_3 t_f. \tag{5.8}$$

#### 5.2.2.2 Average Backoff and Sensing Time $E[t_x]$

As $t_x$ includes the backoff duration, denoted as $t_{backoff}$ and sensing duration, denoted as $t_{cs}$, we get,

$$t_x = t_{backoff} + t_{cs}.$$

For simplicity, it is assumed that the node starts a new backoff process if it senses busy channel with probability $\alpha$, until it senses an idle channel with probability $1-\alpha$. Hence, the probability mass function (PMF) [97] of $x$ is

$$f_x \triangleq (1-\alpha)\alpha^{x-1}, x = 1, ..., \infty. \tag{5.9}$$

Hence, $E[x] = \sum_{x=1}^{\infty} f_x x$.

If the node performs $x$ times backoff before it transmits the packet, then $t_{backoff} = w_i x$. $w_i$ is the backoff duration, following uniform distribution [97] $\mathbb{U}[1, W]$, where $\mathbb{U}$ denotes the uniform distribution. Hence, $E[w_i] = \frac{W+1}{2}$. As the number of back-off process does not affect the each backoff duration, the instant backoff duration

$w_i$ and the number of backoff $x$ are independent variables,

$$E[t_{backoff}] = E[w_i]E[x].$$

The total duration of channel sense is $t_{cs} = \sigma_{cs}x$, where $\sigma_{cs}$ is the channel sensing duration, which is a constant.

$$E[t_{cs}] = E[x]\sigma_{cs}.$$

As $t_x = t_{backoff} + t_{cs}$,

$$E[t_x] = E[t_{backoff}] + E[t_{cs}].$$

As the result, the average duration for channel sensing and backoff per transmission is

$$E\left[t_x\right] = \sum_{x=1}^{\infty} f_x \sigma_{cs} x + \sum_{x=1}^{\infty} f_x \frac{(W+1)x}{2} \tag{5.10}$$

Substituting Eq.(5.9) into Eq.(5.10), we get

$$E\left[t_x\right] = \textstyle\sum_{x=1}^{\infty}(1-\alpha)\alpha^{x-1}\sigma_{cs}x + \sum_{x=1}^{\infty}(1-\alpha)\alpha^{x-1}\frac{(W+1)x}{2}.$$

According to the property of the geometric progression, we get

$$\sum_{x=1}^{k} \alpha^{x-1} x = \frac{1-(k+1)\alpha^k + k\alpha^{k+1}}{(1-\alpha)^2}. \tag{5.11}$$

Therefore,

$$E\left[t_x\right] = \frac{\sigma_{cs} + \frac{W+1}{2}}{1-\alpha}. \tag{5.12}$$

#### 5.2.2.3 Average Service Time $E\left[t_{service}\right]$

As the service time $t_{service} = t_i + t_x$, and $E\left[t_i\right]$ and $E\left[t_x\right]$ are derived in Eqs.(5.8) and (5.12), respectively. The average service time per packet can be obtained as $E\left[t_{service}\right] = E\left[t_i\right] + E\left[t_x\right]$, we obtain,

$$\begin{aligned} E\left[t_{service}\right] &= E\left[t_i\right] + E\left[t_x\right] \\ &= b_4 t_s + b_3 t_f + \tfrac{\sigma_{cs} + \frac{W+1}{2}}{1-\alpha}. \end{aligned}$$

Here $t_s$ and $t_f$ are assumed equal to $L$, hence we get,

$$E\left[t_{service}\right] = \quad b_4 L + b_3 L + \tfrac{\sigma_{cs} + \frac{W+1}{2}}{1-\alpha}. \tag{5.13}$$

Substituting $\alpha$ in Eq.(5.4), $b_3$ and $b_4$ in Eqs.(5.6) into Eq.(5.13), $E\left[t_{service}\right]$ can be expressed in terms of $b_{2,1}$ as,

$$E\left[t_{service}\right] = \frac{b_{2,1} L^2}{1 + (N-1)\, b_{2,1}} + \left(\sigma_{cs} + \frac{W+1}{2}\right)\left(1 + (N-1)\, b_{2,1}\right). \tag{5.14}$$

### 5.2.3 Joint Traffic Load and Contention Window Analysis

In Eq.(5.7), the transition probabilities $\Pr(\mathbf{S}_1|\mathbf{S}_{3,1}) = \Pr(\mathbf{S}_1|\mathbf{S}_{4,1}) = \pi_0$ and $\Pr(\mathbf{S}_1|\mathbf{S}_1) = p_0$ depend on the number of packets in the buffer of the node, which is affected by the average local packet arrival rate and the local buffer size. In the following, the relation of $\pi_0$, $p_0$ and the average local packet arrival rate $\lambda$, which follows any distribution, is analysed under the assumption that the buffer size $K$ of the node is sufficiently large, that is, $K = \infty$.

To analyse the traffic load, we define $p_k$ as the probability that there are $k$ packets in the queue of a node at any arbitrary time, where $k = 0, 1, ..., K$ and the buffer size $K = \infty$, and $\pi_k$ as the probability that there are $k$ packets in the queue of a node after a packet departure, where $k = 0, 1, ..., K-1$ and the buffer size $K = \infty$. $E\left[t_{service}\right]$ is the average service time per packet, including the duration of transmission, backoff and channel sensing.

When $\rho > 1$, the packet service time, $E\left[t_{service}\right]$, is smaller the packet arrivals. Under this condition, as defined in [83], the buffer will never be empty and thus the probability that the buffer of the node is empty after a packet transmission is 0, $\pi_0 = 0$. The mathematical relationship in (5.7) can then be simplified as,

$$\frac{L}{1+(N-1)\,b_{2,1}} + \frac{W+1}{2} - \frac{1}{b_{2,1}} = 0. \tag{5.15}$$

In the case that the traffic load $\rho \leq 1$, the traffic queue of the node is stable and will not be infinitely long. The probability that there are $k$ packets in the buffer of the node is

$$(1-p_K)\rho = 1-(1-p_K)\pi_0, \tag{5.16}$$

where $n = 0, 1, ..., K$ and $p_K$ is the blocking probability, due to the fact that arrival packets are dropped if buffer size reaches to $K$. As the buffer size is assumed as $K = \infty$, the blocking probability $p_K = 0$ and we get $\pi_0 = 1 - \rho$.

As both $p_k$ and $\pi_k$ describe the probability that there are $k$ packets in the buffer. However, the observation durations of $p_k$ and $\pi_k$ are different. The observation duration of $p_k$ is arbitrary and that of $\pi_k$ is a specific time slot. Hence, the observation duration of $\pi_k$ is a part of that of $p_k$. Therefore, $p_k$ is proportional to $\pi_k$ and we get

$$p_k = (1-p_K)\pi_k, \quad k = 0, 1, ..., K-1 \tag{5.17}$$

In Eq.(5.17), $p_k$ (the probability that there are always $k$ packets in the queue) equals to $\pi_k$ (there are always $k$ packets after a packet departure), under the condition that the buffer size is not full $(1 - p_K)$, which means that the arriving packets are allowed to go into the queue. Eq.(5.17) indicates that under the assumption of an infinite buffer size, the probability $p_k$ that there are $k$ packets in the queue of a node at any arbitrary time slot is equal to the probability that there are $k$ packets in the queue of a node after a packet departure, that is, $p_k = \pi_k$ for $k = 0, 1, ..., K - 1$, if $p_K = 0$.

Consequently, we obtain $p_0 = \pi_0 = 1 - \rho$ and Eq. (5.7) is updated as follows in the case of $\rho \leq 1$

$$\left(\frac{1 - \lambda E\left[t_{service}\right]}{\lambda E\left[t_{service}\right]} + L\right) \frac{1}{1 + (N-1)\, b_{2,1}} + \frac{W+1}{2} - \frac{1}{b_{2,1}} = 0. \tag{5.18}$$

The relation of the channel access probability $b_{2,1}$, the number of nodes in the network $N$, the average local packet arrival rate $\lambda$, the average packet service time $t_{service}$ the contention window length $W$ has been derived in Eq.(5.15). The average packet service time $t_{service}$ is expressed in Eq.(5.14). Hence, only $N$ and $\lambda$ are known variables.

## 5.3 Self-Adaptive Backoff Algorithm

In this section, we formulate the system throughput as the optimisation function and use it to achieve the optimal contention window length $W$. As the successful transmission probability is $b_4$ derived in Eq.(5.6), the actual data transmitted successfully is $b_4 L$ during the average service time $E\left[t_{service}\right]$ derived in Eq. (5.14). Hence, the system throughput is defined as the ratio of successful actual trans-

Table 5.1: SAB Algorithm

| |
|---|
| **Input** $\lambda$, $N$, |
| **Assume** $\rho > 1$ |
| 1. Derive $W_1$ according to Eqs.(5.15) and (5.20), |
| 2. Calculate $E\left[t_{service}\right]$ according to (5.14). |
| **if** $\lambda > \frac{1}{E[t_{service}]}$ |
| The assumption $\rho > 1$ holds, $W_{opt} = W_1$. |
| **else** |
| Derive $W_2$ according to Eqs.(5.18) and (5.20) |
| **end** |
| **Output** $W_{opt}$. |

missions over the transmission duration as follows

$$S(b_{2,1}, W) = \frac{N b_4 L}{E\left[t_{service}\right]} = \frac{b_{2,1}(1-b_{2,1})^{N-1} L^2}{b_{2,1} L^2 + \left(\sigma_{cs} + \frac{W+1}{2}\right)\left(1+(N-1)\,b_{2,1}\right)^2}. \tag{5.19}$$

Based on the relation of $W$, $N$, $\lambda$ and $b_{2,1}$ derived in Eqs.(5.15) and (5.18), the optimal contention window length can be derived by optimising the objective function in Eq.(5.19) and is obtained as

$$W_{opt} = \underset{W \in \mathbb{N}}{\operatorname{argmax}}\ S(b_{2,1}, W). \tag{5.20}$$

To solve the system of equations (5.15), (5.18) and (5.20), the optimisation tool, like, the grid search, is employed to obtain the numerical solution $W$. The self-adaptive backoff (SAB) algorithm is summarised in Table 5.1. Firstly, we make an assumption that $\rho > 1$ and derive the contention window length $W_1$ according to Eqs.(5.15) and (5.20). Secondly, $E\left[t_{service}\right]$ can be obtained according to (5.14) as $W_1$ and $b_{2,1}$ are known. Then, we need to verify the assumption $\rho > 1$. If $\lambda > \frac{1}{E[t_{service}]}$, the assumption holds and the optimal contention window length $W_{opt} = W_1$. Otherwise, another contention window value $W_2$ is derived according to Eqs.(5.18) and (5.20) and $W_{opt} = W_2$.

## 5.4 Performance Evaluation

In order to evaluate the performance of the proposed SAB algorithm, we compare the proposed self-adaptive backoff algorithm with the binary exponential backoff (BEB) algorithm [73] and the average contention window (Avg CW) algorithm proposed in [78]. The performances are compared in terms of the system throughput, the collision rate and the energy consumption overhead. The system throughput is defined as the percentage of successful transmissions out of all transmissions, which is normalised in all figures. The collision rate is defined as the ratio of the number of failed packet transmissions to the total number of packet transmissions. The energy consumption overhead is the ratio of the energy consumed for channel sensing and transmission failures to the total energy consumption.

### 5.4.1 Simulation Environment

The backoff algorithm is simulated in MATLAB based on the CSMA mechanism. The simulation parameters are set as follows. The data size $L$ is 100 Bytes and the data rate is $250Kbps$. Time is slotted and a unit time slot $\sigma$ is defined as $0.32ms$. The average channel sensing duration $\sigma_{cs} = 2\sigma$.

### 5.4.2 Simulation Results

The system throughput is compared between the BEB, the Avg CW and the proposed SAB algorithms in Figs. 5.2 and 5.3. Fig. 5.2 shows the throughput comparison of three algorithms versus data rate per node for $N = 20$. The throughput performance of the BEB algorithm increases to 60% and then decreases with the increasing traffic load. In contrast, the throughput performance of the Avg CW and SAB algorithms increase with the traffic arrival rate. The Avg CW algorithm achieves 61% system throughput in the case of $250Kbps$ arrival rate, while, the SAB algorithm achieves 65% system throughput.

Fig. 5.3 shows the throughput comparison versus the number of nodes for data rate $250Kbps$. The results in Fig. 5.3 show that the throughput of BEB degrades significantly with an increasing number of nodes. In contrast, the Avg CW and SAB algorithm achieve a stable throughput of 61% and 68%, respectively, even in a large network of 40 nodes. According to the backoff algorithm, the node performs packet transmissions when the channel is probably available, which contributes to 7% and 11% system throughput improvement compared with the Avg CW algorithm proposed in [78] in Fig. 5.2 and 5.3, respectively. Figs. 5.2 and 5.3 show that the system throughput of both algorithms increase with the packet arrival rate per node and the number of nodes in the network. This results from the fact that the contention for channel resources becomes a serious issue when the traffic load is high. In a network with a high traffic load, the ability of backoff algorithms to resolve contention is more significant to the system performance.

The collision rate performances of three algorithms are compared in Fig. 5.4. The collision rate of BEB reaches 85% in the network of 40 nodes, which indicates its inability to provide reliable transmissions. The collision rates of the Avg CW algorithm reaches 30% in the network of 40 nodes. On the other hand, the proposed algorithm achieves a lower collision rate of 19%. This 37% collision reduction compared with [78] is because individual nodes can dynamically adjust contention window lengths based on the channel congestion status. A node takes action backoff when the channel is likely to be occupied, which results in a significant collision reduction.

Fig. 5.5 shows that for a network of 40 nodes, the BEB algorithm and the Avg CW algorithm in [78] consume nearly 88% and 36% energy for channel sensing.

Compared with the Avg CW, the proposed algorithm consumes only 18% energy for channel sensing. The 50% energy saving as compared to [78] will result in a longer battery life of sensor nodes. The reason leading to a large amount of energy reduction is that the node remains silent when it detects a high channel congestion.

In comparison with the BEB and Avg CW algorithms, the proposed algorithm performs a significant collision rate reduction and energy saving. The performance evaluation demonstrates that the proposed algorithm is capable to support reliable and real-time communications in the contention-based multiple access networks.

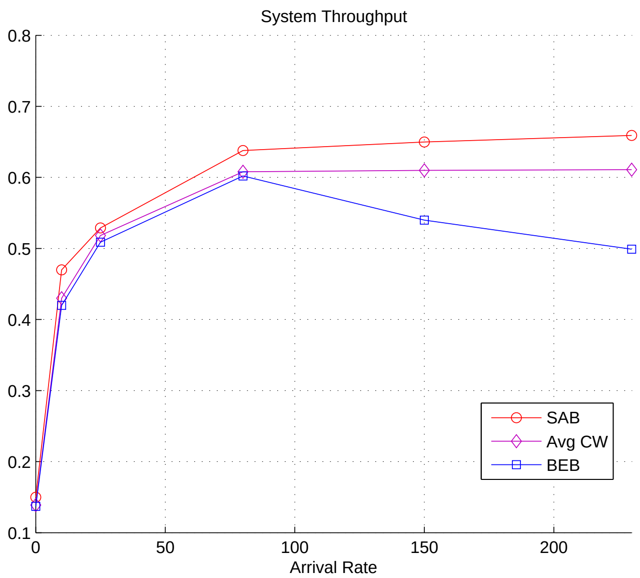


Figure 5.2: System Throughput Comparison of the BEB, Avg CW and SAB algorithms plotted *vs.* Arrival Rate $\lambda$ for $N = 20$

## 5.5 Conclusion

In this chapter, we proposed a self-adaptive backoff algorithm for the random access networks, where the contention window (CW) length is dynamically ad-

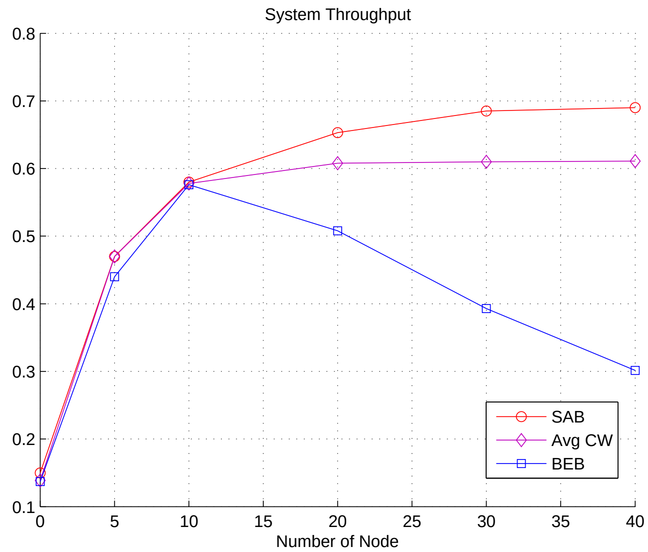


Figure 5.3: Throughput Comparison of the BEB, Avg CW and SAB algorithms plotted *vs.* the number of node $N$ for $\lambda = 250Kbps$

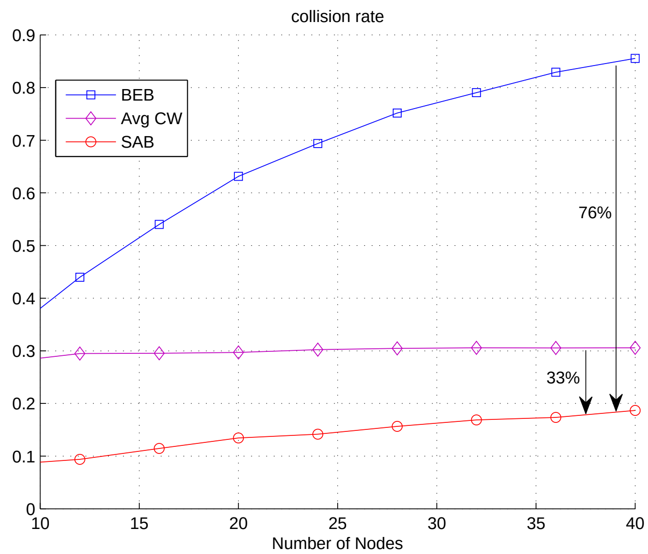


Figure 5.4: Collision Rate Comparison of the BEB, Avg CW and SAB algorithms plotted *vs.* the number of node $N$

justed by each node and adapted to channel congestion conditions. We derived a probabilistic analytical expression of the optimal channel access probability of each node, based on the criteria of maximising the system throughput and minimising collisions. The optimal channel access probability is then used to derive the expression for the CW length adapted to real-time measurements of channel

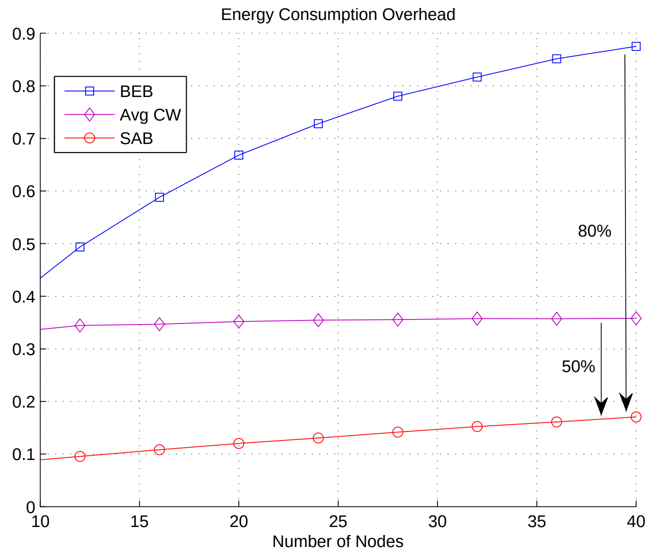


Figure 5.5: Energy Consumption Overhead Comparison of the BEB, Avg CW and SAB algorithms plotted *vs*. the number of node $N$

congestion conditions. Performance comparison with the Avg CW algorithm proposed in [78] shows that the proposed algorithm significantly reduces the collision rate by 37% and the energy consumption by 50%, when the number of nodes is 40, while achieving an 11% higher throughput than [78]. The proposed self-adaptive backoff algorithm can be used in any contention-based multiple access networks, such as, ZigBee, WiFi and WiMax.

# Chapter 6

# Conclusions

This thesis has investigated the methods that are capable to improve the spectral efficiency for wireless communication networks. In particular, relay schemes, employed in the physical (PHY) layer of the open systems interconnect (OSI) model, and multiple access schemes, applied in the media access control (MAC) layer of the OSI model, are considered.

In the physical layer, the channel estimation issue was investigated in the two-way relay networks (TWRNs) under the assumption of the perfect synchronisation. The main challenge is to design a low complexity channel estimation algorithm, which is also independent of training symbols. Hence, we proposed two low complexity semi-blind channel estimation algorithms by deriving convex maximum likelihood estimation functions. To relax the assumption of the perfect synchronisation in the channel estimation for TWRNs, we explored the channel estimation and synchronisation issues in the asynchronous two-way relay networks, where there are timing offsets between nodes. The challenge is to jointly estimate channel coefficients and timing offsets. We proposed the frame asynchronous channel estimation (FACE) and the joint synchronisation and channel estimation (JSCE) algorithms to detect channel parameters, frame offsets and symbol offsets jointly.

In the media access control layer, the backoff algorithm is investigated to resolve contention in the multiple access networks. The challenge here is to adjust the contention window length according to the average local packet arrival rate and the channel congestion. We proposed a self-adaptive backoff (SAB) algorithm that achieves the optimal contention window length that maximise the system throughput by considering the number of nodes, the local packet arrival rate and the channel congestion condition.

In Chapter 3 of the thesis, we proposed two low complexity semi-blind channel estimation algorithms, referred to as the low complexity maximum likelihood (LCML) estimator and the modified low complexity maximum likelihood (MLCML) estimator. Both channel estimators use only one training symbol in each channel estimation to estimate general non-reciprocal flat-fading channels in AF-TWRNs. We proposed the LCML algorithm with a convex optimisation function that produces a closed-form channel estimator. By taking into account the modulation structure, the MLCML channel estimation algorithm with the closed-form channel estimation is proposed to further improved the MSE performance of the LCML algorithm in BPSK. In the case of a high SNR, the LCML and MLCML channel estimation algorithms approach the real channel parameter values with the probability of $1 - \left(\frac{2}{M}\right)^{N-1}(M-1)$ and $1 - \frac{1}{M^{N-1}}$, respectively, where $M$ is the modulation order and $N$ denotes the frame length of signals. Additionally, the LCML channel estimator is proved to be consistent and unbiased [85]. The closed-form MSE expressions of the LCML and MLCML channel estimator with respect to the SNR and $N$ are derived as, $MSE \propto \frac{2}{SNR\ N}$ and $MSE \propto \frac{1}{SNR\ N}$, respectively. Both the analytical MSE expression and Monte-Carlo simulations show that the average MSE performance of the proposed channel estimators improve as either SNR, frame length of signals or modulation order increases. In

[60], a deterministic maximum likelihood (DML) channel estimator and a modified constrained maximum likelihood (MCML) estimator are proposed for semi-blind channel estimation in the synchronous AF-TWRNs. Due to the non-convex optimisation functions for channel estimation, the DML and MCML algorithms have to rely on numerical solutions by using optimisation tools. As closed-form channel estimation is achieved by the LCML and MLCML algorithms, the computational complexity of the LCML and MLCML estimation algorithms is $\mathcal{O}(N)$, where $N$ is the frame length of signals. In addition, the LCML channel estimator noticeably decreases the average MSE of the DML channel estimator by 89.84% in BPSK. Compared with the DML and MCML channel estimators in the literature, the LCML and MLCML estimators not only achieve a better MSE and SER performance, but also significantly reduce the computational load. However, the perfect synchronisation is assumed in this chapter. As a result, the channel impairments result from asynchronization are not considered.

In Chapter 4 of the thesis, the assumption of the perfect synchronisation is relaxed and the channel impairments result from asynchronization are considered. We considered the joint synchronisation and channel estimation in the asynchronous AF-TWRNs and proposed algorithms to estimate the timing offsets and channel parameters jointly. In the asynchronous AF-TWRNs, we developed a generalised low complexity maximum likelihood (GLCML) algorithm to perform channel estimation in the presence of a timing offset. The optimal channel estimation is achieved in GLCML algorithm based on the MSE expressions derived in Chapter 3. Then a joint synchronisation and channel estimation (JSCE) algorithm is proposed to estimate the timing offset. We firstly proposed a sub-algorithm to achieve frame synchronisation, referred to as the frame asynchronous channel estimation (FACE) algorithm, to estimate the frame offset by energy detection and the cross correlation of the received and transmitted signals. The analysis shows that the error probability of the FACE algorithm approaches zero in a large frame length scenario. After frame boundaries are determined by the FACE algorithm, we proposed a sub-algorithm, named the symbol asynchronous channel estimation (SACE) algorithm, to estimate the symbol offset (fractional timing offset). In addition, the SACE algorithm achieves joint symbol synchronisation and channel estimation. In the GLCML and JSCE algorithms, only few training symbols are needed per estimation and low computational complexity is achieve by the closed-form solutions. Monte-Carlo simulation results demonstrate that the GLCML algorithm always select the optimal channel estimation in the cases of varying timing offsets and the JSCE algorithm is able to achieve accurate timing offset estimations. Compared with the best known channel estimation algorithm for TWRNs, the modified constrained maximum likelihood (MCML) estimator in [60], the proposed GLCML and JSCE algorithm are capable to achieve a similar MSE performance of channel parameter estimation in the presence of the timing offset. Different from the MCML algorithm, which depend on optimisation tools to derive channel estimation, the GLCML and JSCE algorithm derive the closed-form channel estimation. Thus, the computational complexity of the MCML algorithm is reduced. Moreover, the timing offset and channel parameters can be jointly estimated for the AF-TWRNs in the proposed GLCML and JSCE algorithms. The proposed algorithms in this chapter achieve channel estimation and timing synchronisation. However, the carrier frequency synchronisation is assumed among all the nodes. Hence, the joint frequency and timing synchronisation and channel estimation will be studied in the future work.

In Chapter 5, we propose a self-adaptive backoff (SAB) algorithm to resolve contention in the contention-based multiple access networks. We model the states of a node as a discrete-time Markov chain [86] and use the queue theory [83] to analyse the traffic load. The contention window length expression is obtained given the average local packet arrival rate and the total number of nodes in the network and provides specific directions on the CW length adjustment. As the average local packet arrival rate is considered, the assumption that all the nodes always have packets to transmit is relaxed in the proposed algorithm. Based on the derived contention window length expression, the system throughput is formulated as the optimisation function with the contention window length as the variable. Compared with the algorithm proposed in [78], the proposed algorithm significantly reduces the collision rate by 37% and the energy consumption by 50%, when the number of nodes is 40, while achieving an 11% higher throughput than [78]. The proposed self-adaptive backoff algorithm can be used in any contention-based multiple access networks, such as, ZigBee, WiFi and WiMax.

# Appendix A

In this appendix, we will derive $V(v)$, which is the variance of $|z_i(v)|^2$ as stated in (C.1). $|z_i(v)|^2$ could be expanded as,

$$\begin{aligned}|z_i(v)|^2 &= A^2 |v|^2 + A^2 |G|^2 + vG^* s_{1i} s_{2i}^* + v^* G s_{1i}^* s_{2i} \\ &+ |n_i|^2 + (vs_{1i} + Gs_{2i})\, n_i^* + (v^* s_{1i}^* + G^* s_{2i}^*)\, n_i. \end{aligned} \tag{A.1}$$

Firstly, assuming that $s_{1i}$ and $s_{2i}$ are deterministic, the conditional expectation and variance [98] of $|z_i(v)|^2$ are obtained as,

$$\begin{gathered} \mathrm{E}\left\{|z_i(v)|^2 \,|\, (s_{1i}, s_{2i})\right\} = \\ A^2 |v|^2 + A^2 |G|^2 + vG^* s_{1i} s_{2i}^* + v^* G s_{1i}^* s_{2i} + |h_2|^2 \sigma_n^2 + \sigma_n^2, \\ \mathrm{Var}\left\{|z_i(v)|^2 \,|\, (s_{1i}, s_{2i})\right\} = \\ \mathrm{E}\left\{|z_i(v)|^4 \,|\, (s_{1i}, s_{2i})\right\} - \mathrm{E}\left\{|z_i(v)|^2 \,|\, (s_{1i}, s_{2i})\right\}^2 \\ = 2\left(K^2 |h_2|^2 \sigma_n^2 + \sigma_n^2\right) \\ \left(A^2 |v|^2 + A^2 |G|^2 + vG^* s_{1i} s_{2i}^* + v^* G s_{1i}^* s_{2i}\right). \end{gathered} \tag{A.2}$$

According to **The Total Law of Variance** [98],

$$\begin{aligned} Var\left\{|z_i(v)|^2\right\} &= \mathrm{E}\left\{\mathrm{Var}\left\{|z_i(v)|^2 \,|\, (s_{1i}, s_{2i})\right\}\right\} \\ &+ \mathrm{Var}\left\{\mathrm{E}\left\{|z_i(v)|^2 \,|\, (s_{1i}, s_{2i})\right\}\right\}, \end{aligned}$$

$$
\begin{aligned}
&\mathrm{E}\left\{Var\left\{\left|z_i(v)\right|^2 \mid (s_{1i}, s_{2i})\right\}\right\} \\
&= 2\left(K^2|h_2|^2\sigma_n^2 + \sigma_n^2\right)\left(A^2\left|v\right|^2 + A^2\left|G\right|^2\right), \\
&\mathrm{Var}\left\{\mathrm{E}\left\{\left|z_i(v)\right|^2 \mid (s_{1i}, s_{2i})\right\}\right\} \\
&= \mathrm{E}\left\{\mathrm{E}\left\{\left|z_i(v)\right|^2 \mid (s_{1i}, s_{2i})\right\}^2\right\} - \mathrm{E}\left\{\mathrm{E}\left\{\left|z_i(v)\right|^2 \mid (s_{1i}, s_{2i})\right\}\right\}^2 \\
&= 2A^4\left|v\right|^2\left|G\right|^2.
\end{aligned}
$$

Expand $V(v)$ with respect to $(\Re\{v\}, \Im\{v\})$, we get

$$
\begin{aligned}
V(v) &= 2A^2\left|G\right|^2\left(K^2|h_2|^2\sigma_n^2 + \sigma_n^2\right) \\
&+2A^2\left(K^2A^2|h_2|^2\sigma_n^2 + A^2\left|G\right|^2 + \sigma_n^2\right)\left|v\right|^2,
\end{aligned} \tag{A.3}
$$

where $\left|v\right|^2 = (\Re\{v\}^2 + \Im\{v\}^2)$ and $(\Re\{v\}, \Im\{v\}) \in \mathbb{R}^2$.

# Appendix B

**Lemma B.1.** *Assume $H$ and $G$ both belong to compact set $\Omega$, then $V_N(v)$ converges uniformly to $V(v)$ as $N \to \infty$.*

*Proof.* We use *the Uniform Law of Large Numbers* (**Lemma B.2**) [92] to prove **Lemma B.1**. Let $g(x_i, \theta)$ be a function of the parameter $\theta \in \Omega$ and a sequence of i.i.d random variables $x_i \in \mathbb{C}, i = 1, ..., N$, we have **Lemma B.2** as follows,

**Lemma B.2.** *Suppose for all $x_i$, $(a)$ $g(x_i, \theta)$ is continuous at each $\theta \in \Omega$ with probability one, $(b)$ $g(x_i, \theta)$ is dominated by a function $D(x_i)$ for all $\theta \in \Omega$, i.e. $|g(x_i, \theta)| \leq D(x_i), \forall \theta \in \Omega$, and $(c)$ $E\{D(x_i)\} < \infty$, then $\frac{1}{N}\sum_{i=1}^{N} g(x_i, \theta)$ converges uniformly to $E\{g(x_i, \theta)\}$ when $N \to \infty$: $\boldsymbol{sup}_{\theta \in \Omega} \left| \frac{1}{N}\sum_{i=1}^{N} g(x_i, \theta) - E\{g(x_i, \theta)\} \right|$ $\xrightarrow{p} 0$, $N \to \infty$.*

First of all, we will prove that **Lemma B.2** is applicable to $|z_i(v)|^2$. Since $z_i(v) \triangleq vs_{1i} + Gs_{2i} + n_i, i = 1, ..., N$ and $|z_i(v)|^2$ is derived in **Appendix A**,

$$
\begin{aligned}
|z_i(v)|^2 = A^2 |v|^2 + A^2 |G|^2 + vG^* s_{1i} s_{2i}^* + v^* G s_{1i}^* s_{2i} \\
+ |n_i|^2 + vs_{1i} n_i^* + Gs_{2i} n_i^* + v^* s_{1i}^* n_i + G^* s_{2i}^* n_i.
\end{aligned}
$$

$|z_i(v)|^2$ is a function of fixed parameters $v$ and $G$, and i.i.d random variables $s_{1i}$, $s_{2i}$ and $n_i$. Define vector $\mathbf{z} \triangleq [A^2 |v|^2, A^2 |G|^2, vG^* s_{1i} s_{2i}^*, v^* G s_{1i}^* s_{2i}, |n_i|^2, vs_{1i} n_i^*, Gs_{2i} n_i^*, v^* s_{1i}^* n_i, G^* s_{2i}^* n_i]$. Note **Lemma B.2** can be extended to multivariate cases with multiple fixed parameters and random variables [60]. Condition $(a)$

is met, as $|z_i(v)|^2$ is continuous at each $v, G \in \Omega$ with probability one. Using the *triangle inequality* [85], we obtain $|z_i(v)|^2 \leq (|vs_{1i}| + |Gs_{2i}| + |n_i|)^2$. As $|H|, |G| < \xi$ is assumed in condition 1.1, $|z_i(v)|^2 \leq 4A^2\xi^2 + |n_i|^2 + 4A\xi\,|n_i|$, then condition $(b)$ is satisfied. Define $d(n_i) \triangleq 4A^2\xi^2 + |n_i|^2 + 4A\xi\,|n_i|$, we get $E\{d(n_i)\} = 4A^2\xi^2 + (K^2|h_2|^2 + 1)\sigma_n^2 + \sqrt{\frac{2\sigma_n^2(K^2|h_2|^2+1)}{\pi}}$. Since channel coefficient $h_2$ and noise power $\sigma_n$ are bounded, $E\{d(n_i)\} < \infty$ and condition $(c)$ is met. Therefore, **Lemma B.2** can be applied to $|z_i(v)|^2$ to prove that $\mathbf{sup}_{v\in\Omega}\left|\frac{1}{N}\sum_{i=1}^{N}|z_i(v)|^2 - E\left\{|z_i(v)|^2\right\}\right| \xrightarrow{p} 0$ as $N \to \infty$.

It has been proved that the sample mean $\frac{1}{N}\sum_{i=1}^{N}|z_i(v)|^2$ converges uniformly to the expectation $E\left\{|z_i(v)|^2\right\}$ as $N \to \infty$. If we define random i.i.d $g_i(v) \triangleq \left(|z_i(v)|^2 - \frac{\sum_{k=1}^{N}|z_k(v)|^2}{N}\right)^2$, $i = 1, ..., N$, then $g_i(v)$ converges uniformly to $g_i^{'}(s_{1i}, s_{2i}, n_i; v, G) = \left(|z_i(v)|^2 - E\{|z_k(v)|^2\}\right)^2$. Here, $g_i^{'}(s_{1i}, s_{2i}, n_i; v, G)$ is a function of parameters $v$ and $G$, and random variables $s_{1i}$, $s_{2i}$ and $n_i$. Next we will validate that **Lemma B.2** can be applied to $g_i^{'}(s_{1i}, s_{2i}, n_i; v, G)$. By inspection, $g_i^{'}(s_{1i}, s_{2i}, n_i; v, G)$ is continuous at each $v, G \in \Omega$ with probability one, hence, condition $(a)$ is met. Using triangle inequality, we get the dominant function of $\left|g_i^{'}(s_{1i}, s_{2i}, n_i; v, G)\right|$ from (A.1) (See **Appendix A**),

$$\begin{aligned}
\left|g_i^{'}(s_{1i}, s_{2i}, n_i; v, G)\right| &= |vG^* s_{1i}s_{2i}^* + v^* G s_{1i}^* s_{2i} + |n_i|^2 \\
&+ (vs_{1i} + Gs_{2i})\, n_i^* + (v^* s_{1i}^* + G^* s_{2i}^*)\, n_i - K^2|h_2|^2\sigma_n^2 - \sigma_n^2|^2, \\
&\leq (|vG^* s_{1i}s_{2i}^*| + |v^* G s_{1i}^* s_{2i}| + |n_i|^2 + |(vs_{1i} + Gs_{2i})\, n_i^*| \\
&+ |(v^* s_{1i}^* + G^* s_{2i}^*)\, n_i| + K^2|h_2|^2\sigma_n^2 + \sigma_n^2)^2, \\
&< \left(2A^2\xi^2 + |n_i|^2 + 4A\xi\,|n_i| + K^2\xi^2\sigma_n^2 + \sigma_n^2\right)^2.
\end{aligned}$$

Define $D(n_i) \triangleq \left(2A^2\xi^2 + |n_i|^2 + 4A\xi\,|n_i| + K^2\xi^2\sigma_n^2 + \sigma_n^2\right)^2$, condition $(b)$ is met. Since noise power $\sigma^2 = (K^2|h_2|^2 + 1)\sigma_n^2$ and $|h_2| < \xi$, $E\{D(n_i)\} < \infty$ and condition $(c)$ is met. As a result, we obtain

$\mathbf{sup}_{v\in\Omega}\left|\frac{1}{N}\sum_{i=1}^{N} g_i^{'}(s_{1i}, s_{2i}, n_i; v, G) - E\left\{g_i^{'}(s_{1i}, s_{2i}, n_i; v, G)\right\}\right| \xrightarrow{p} 0$ as $N \to \infty$.

The conclusion that $\mathbf{sup}_{v\in\Omega}\left|\frac{1}{N}\sum_{i=1}^{N} |z_i(v)|^2 - E\left\{|z_i(v)|^2\right\}\right| \xrightarrow{p} 0$ as $N \to \infty$ implies that $V_N(v)$ (3.22) converges uniformly to $\frac{1}{N}\sum_{i=1}^{N} g_i^{'}(s_{1i}, s_{2i}, n_i; v, G)$. Since $V(v) = E\left\{g_i^{'}(s_{1i}, s_{2i}, n_i; v, G)\right\}$ and it has been proved that $\frac{1}{N}\sum_{i=1}^{N} g_i^{'}(s_{1i}, s_{2i}, n_i; v, G)$ converges uniformly to $E\left\{g_i^{'}(s_{1i}, s_{2i}, n_i; v, G)\right\}$ as $N \to \infty$, therefore, $V_N(v)$ converges uniformly to $V(v)$ as $N \to \infty$. $\square$

# Appendix C

**Lemma C.1.** *$V(v)$ has a unique global minimum with respect to $v$ occurring at $v_o = 0$.*

*Proof.* To demonstrate condition 1.3, we will prove that $v = 0$ is a local minimum of $V(v)$ first (See **Lemma C.2**) and then the convexity of $V(v)$ (See **Lemma C.3**). □

**Lemma C.2.** *$v = 0$ is a local minimum of $V(v)$.*

*Proof.* Expanding $V(v)$ and we obtain (See **Appendix A** ),

$$V(\Re\{v\}, \Im\{v\}) = 2A^2 |G|^2 (|h_2|^2\sigma_n^2 + \sigma_n^2) +$$
$$2A^2 \left(A^2|h_2|^2\sigma_n^2 + A^2 |G|^2 + \sigma_n^2\right) (\Re\{v\}^2 + \Im\{v\}^2). \tag{C.1}$$

with $(\Re\{v\}, \Im\{v\}) \in \mathbb{R}^2$ where $\mathbb{R}$ denotes real number field. The first partial derivative [85] of $V(v)$ is

$$\frac{\partial V}{\partial \Re\{v\}} = 4A^2 \left(A^2|h_2|^2\sigma_n^2 + A^2 |G|^2 + \sigma_n^2\right) \Re\{v\},$$
$$\frac{\partial V}{\partial \Im\{v\}} = 4A^2 \left(A^2|h_2|^2\sigma_n^2 + A^2 |G|^2 + \sigma_n^2\right) \Im\{v\}.$$

which are equal to 0 at the critical point $(0, 0)$, that is, $v = 0$ is a local extrema. According to the *Second Partial Derivative Test* [85], the second derivative test discriminant is

$$\nabla^2 V(v) = \begin{vmatrix} \dfrac{\partial^2 V}{\partial \Re\{v\}^2} & \dfrac{\partial V}{\partial \Re\{v\} \partial \Im\{v\}} \\ \dfrac{\partial V}{\partial \Re\{v\} \partial \Im\{v\}} & \dfrac{\partial^2 V}{\partial \Im\{v\}^2} \end{vmatrix},$$

where the second partial derivatives of $V(v)$ are,

$$\frac{\partial V}{\partial \Re\{v\} \partial \Im\{v\}} = 0,$$
$$\frac{\partial^2 V}{\partial \Re\{v\}^2} = \frac{\partial^2 V}{\partial \Im\{v\}^2} = 4A^2 \left( A^2 |h_2|^2 \sigma_n^2 + A^2 |G|^2 + \sigma_n^2 \right).$$

Then we get $\nabla^2 V(v) = 16A^4 \left( A^2 |h_2|^2 \sigma_n^2 + A^2 |G|^2 + \sigma_n^2 \right)^2 > 0$ and $\frac{\partial^2 V}{\partial \Re\{v\}^2} > 0$ at $v = 0$. Hence, the local extrema $v = 0$ is a local minimum of $V(v)$. $\square$

Then, we will prove this local minimum is also the global minimum of $V(v)$ by demonstrating the convexity of $V(v)$ according to **Lemma C.3** [62].

**Lemma C.3.** *Define* $\boldsymbol{dom}V$ *as the domain of* $V$*, then* $V(v)$ *is convex if and only if* $\boldsymbol{dom}V$ *is convex and its Hessian is positive semidefinite: for all* $v \in \boldsymbol{dom}V$*,* $\nabla^2 V(v) \geq 0$*.*

It has been proved in **Lemma C.2** that $\nabla^2 V > 0$ for all $(\Re\{v\}, \Im\{v\}) \in \mathbb{R}^2$. Since $\mathbf{dom}\, V = \mathbb{R}^2$ is convex, $V(v)$ is a convex function according to **Lemma C.3**. For a convex function, its local minimum is also the global minimum, therefore, the local minimum point $v = 0$ is the global minimum of $V(v)$. We complete the proof based on **Lemma C.2** and **Lemma C.3**.

# Appendix D

**Theorem 3.1**.

*Proof.* Regarding condition 1.1, there are no upper bounds on $H$ and $G$, strictly speaking, if we treat $h_1$, $h_2$, $g_1$ and $g_2$ as ideal complex Gaussian random variables. However, we can always choose a sufficiently large $\xi$ such that $\Pr(|H|, |G| < \xi) = 1 - \epsilon$ , where $\epsilon$ can be made arbitrarily small. Therefore, condition 1.1 can be satisfied by assuming that the amplitude of channel coefficients $h_1$, $h_2$, $g_1$ and $g_2$ are bounded. Conditions 1.2 and 1.3 have been proved in **Lemma B.1** (See **Appendix B**) and **Lemma C.1** (See **Appendix C**), respectively. Since **Conditions** $[1.1, 1.2, 1.3]$ are satisfied, **Theorem 3.1** holds. □

# Appendix E

**Theorem 3.2**.

*Proof.* For simplicity, we define the estimation error $v_2 \triangleq H - \hat{H}_{lcml}^{BPSK}$. Then (3.19) is expressed as,

$$\begin{aligned} F_{sync}^{BPSK}(v_2) &= \tfrac{1}{N}\textstyle\sum_{i=1}^{N}\left|z_i^2(v_2) - \frac{\sum_{k=1}^{N} z_k^2(v_2)}{N}\right|^2, \\ &= \tfrac{1}{N}\textstyle\sum_{i=1}^{N}\left(\Re\left\{z_i^2(v_2)\right\} - \frac{\sum_{k=1}^{N}\Re\left\{z_k^2(v_2)\right\}}{N}\right)^2 \\ &+ \tfrac{1}{N}\textstyle\sum_{i=1}^{N}\left(\Im\left\{z_i^2(v_2)\right\} - \frac{\sum_{k=1}^{N}\Im\left\{z_k^2(v_2)\right\}}{N}\right)^2, \end{aligned} \tag{E.1}$$

where $z_i(v_2) \triangleq v_2 s_{1i} + G s_{2i} + n_i, i = 1, ..., N$. (E.1) represents the sum of sample variance of the real and imaginary parts of random variable $z_i^2(v_2)$. $z_i(v_2)$ in (E.1) is approximated as $z_i(v_2) = v_2 s_{1i} + G s_{2i}, i = 1, ..., N$ as SNR $\to \infty$. As $s_{1i}, s_{2i} = \pm 1$ in BPSK, we obtain

$$z_i^2(v_2) = v_2^2 + G^2 + 2v_2 G s_{1i} s_{2i},$$

$$\Re\left\{z_i^2(v_2)\right\} = \Re\left\{v_2^2 + G^2\right\} + 2\Re\left\{v_2 G\right\}\cos\left(\phi_{1i} + \phi_{2i}\right), \tag{E.2}$$

$$\Im\left\{z_i^2(v_2)\right\} = \Im\left\{v_2^2 + G^2\right\} + 2\Im\left\{v_2 G\right\}\cos\left(\phi_{1i} + \phi_{2i}\right). \tag{E.3}$$

Since the objective function (E.1) is the sum of the sample variance of $\Re\left\{z_i^2(v_2)\right\}$ and $\Im\left\{z_i^2(v_2)\right\}$, it is obvious that $F_{sync}^{BPSK}(v_2) \geq 0$ with equality if and only if the terms $z_i^2(v_2), i = 1, ..., N$ are all equal. This is equivalent to either of the following two conditions given $G \neq 0$,

$$\begin{cases} \texttt{Condition 1:} v_2 = 0, \quad \texttt{Condition 2:} \quad x_i = x_j, \\ x_i = \cos\left(\phi_{1i} + \phi_{2i}\right), \quad x_j = \cos\left(\phi_{1j} + \phi_{2j}\right), \\ \texttt{where} \quad i \neq j \quad \texttt{and} \ i, j = 1, ..., N. \end{cases} \tag{E.4}$$

**Condition 1** indicates that there is a unique global minimum of the objective function at $v_2 = 0$, that is, $\hat{H}_{lcml}^{BPSK} = H$. While, on the other hand, there are infinite number of global minimum if **Condition 2** holds. In BPSK, $x_i, x_j = \pm 1$ as $\phi_{1i}, \phi_{2i} = [0, \pi]$. As a result, Pr(**Condition 2**) $= \frac{1}{2^{N-1}}$. The probability that there exists an unique global minimum of the objective function (E.1) conditioned on SNR $\to \infty$ is $1 - \frac{1}{2^{N-1}}$, $\square$

# Appendix F

In the following, we will validate **Lemma 3.2** by proving $\Im\left\{\hat{H}\right\}$ equals its Taylor series expansion $T(x, y)$ if either SNR or $N \to \infty$ (**See Lemma F.1**) at first and then demonstrating $T(x, y) = \frac{\mu_x}{\mu_y} + \frac{x}{\mu_y} - \frac{\mu_x y}{\mu_y^2}$ if SNR $\to \infty$ (**See Lemma F.2**).

Since the multivariate function $f(x, y) = \frac{x}{y}$ where $(x, y) \in \mathbb{C}^2$ is k+1 times continuously differentiable at the point $(\mu_x, \mu_y) \in \mathbb{C}^2$, its Taylor series expansion at the point $(\mu_x, \mu_y)$ is expressed as,

$$\begin{aligned} T(x, y) = \quad & \textstyle\sum_{n_x+n_y=0}^{k} \frac{\partial^{n_x+n_y} f(\mu_x,\mu_y)}{\partial x^{n_x} \partial y^{n_y}} \frac{(x-\mu_x)^{n_x} (y-\mu_y)^{n_y}}{n_x! n_y!} \\ + \quad & \textstyle\sum_{n_x'+n_y'=k+1} R_{n_x'+n_y'}(x, y)(x-\mu_x)^{n_x'}(y-\mu_y)^{n_y'}, \end{aligned}$$

where $n_x, n_y, n_x', n_y' \in \mathbb{N}$ and $R_{k+1}(x, y)$ is the remainder of $k^{th}$ degree Taylor polynomial approximation [94].

**Lemma F.1.** *The Taylor series expansion $T(x, y)$ about the point $(\mu_x, \mu_y)$ is equal to $f(x, y) = \frac{x}{y}$ for $(x, y) \in \mathbb{C}^2$, if and only if either SNR or frame length $N \to \infty$.*

*Proof.* Since $f(x, y) = \frac{x}{y}$ is infinitely differentiable at the point $(\mu_x, \mu_y)$, its Taylor series expansion is summed up as

$$T(x, y) = \lim_{k\to\infty} \frac{x}{y} \left(1 - \left(1 - \frac{y}{\mu_y}\right)^k\right),$$

which shows if $|y-\mu_y|<|\mu_y|$ holds, then $T(x,y)=f(x,y)$. Next, we will prove that $\Pr\left(|y-\mu_y|<|\mu_y|\right)=1$, if either SNR or $N\to\infty$.

As $y$ is a complex normal distributed variable in $\mathcal{CN}(\mu_y,\sigma_y^2)$, where

$$\begin{aligned}\mu_y &= \frac{-j2A^4(A^2|G|^2+\sigma^2)^2(N^2-3N+2)}{N^2},\\ \sigma_y^2 &= \frac{8A^7\sigma(A^2|G|^2+\sigma^2)^4(N^2-3N+2)^2}{|G|^4N^5},\end{aligned} \tag{F.1}$$

according to its cumulative distribution function (CDF), we get,

$$\Pr\left(|y-\mu_y|<|\mu_y|\right)=\mathrm{erf}\left(\frac{|\mu_{\mathrm{y}}|}{\sqrt{2\sigma_{\mathrm{y}}^2}}\right), \tag{F.2}$$

where erf(x) denotes the error function [84]. Substituting (F.1) into (F.2), we obtain $\Pr\left(|y-\mu_y|<|\mu_y|\right)=\mathrm{erf}\left(\frac{|\mathrm{G}|^2}{2}\sqrt{\frac{\mathrm{AN}}{\sigma}}\right)$. The values of error function state that if $\frac{|G|^2}{2}\sqrt{\frac{AN}{\sigma}}\to\infty$, then $\Pr\left(|y-\mu_y|<|\mu_y|\right)=1$, which implies that Taylor series expansion $T(x,y)$ equals the function $f(x,y)$ for $(x,y)\in\mathbb{C}^2$ in either high SNR or large frame length scenario. □

Actually, there is no need to meet the strict requirement of $\frac{|G|^2}{2}\sqrt{\frac{AN}{\sigma}}\to\infty$. As long as $\frac{|G|^2}{2}\sqrt{\frac{AN}{\sigma}}$ is not too small, $T(x,y)=f(x,y)$ holds. For example, $\mathrm{erf}\left(\frac{|\mathrm{G}|^2}{2}\sqrt{\frac{\mathrm{AN}}{\sigma}}\right)=0.9953$ when $\frac{|G|^2}{2}\sqrt{\frac{AN}{\sigma}}=2$. In practical applications, it is possible to adjust SNR or frame length $N$, in order to satisfy the condition for $\Pr\left(|y-\mu_y|<|\mu_y|\right)=1$.

**Lemma F.2.** *If SNR $\to\infty$, the Taylor series $T(x,y)$ equals its first degree Taylor polynomial approximation at the point $(\mu_x,\mu_y)$, namely,*

$$T(x,y)=\frac{\mu_x}{\mu_y}+\frac{x}{\mu_y}-\frac{\mu_x y}{\mu_y^2}. \tag{F.3}$$

*Proof.* Expand $T(x,y)$ to its first order Taylor polynomial approximation, we get,

$$T(x,y) = \frac{\mu_x}{\mu_y} + \frac{x}{\mu_y} - \frac{\mu_x y}{\mu_y^2} + R_2(x,y).$$

where $R_2(x,y)$ is the remainder [94]. According to *Taylor's theorem for multivariate functions* [94], the upper bound of the remainder $R_{k+1}(x,y)$ is

$$|R_{k+1}(x,y)| \leq \max_{n_x^{'}+n_y^{'}=k+1} \max_{(x,y)\in\mathbb{R}^2} \frac{k+1}{n_x^{'}!n_y^{'}!} \left| \frac{\partial^{k+1} f(x,y)}{\partial x^{n_x^{'}} \partial y^{n_y^{'}}} \right|, \tag{F.4}$$

where $R_{k+1}(x,y)$ represents the remainder of the $k^{th}$ degree Taylor polynomial approximation. (F.4) indicates that the upper bound of $|R_{k+1}(x,y)|$ is related to the maximum norm of the $k+1^{th}$ partial derivative of $f(x,y)$. As we expand Taylor series $T(x,y)$ to its first order, $k=1$ in this case. Calculate the second order partial derivative of $f(x,y)$ and we obtain the upper bound of the remainder $|R_2(x,y)|$,

$$|R_2(x,y)|_{up} = \mathbf{max}\left\{ \left|\frac{2x}{y^3}\right|, \left|\frac{2}{y^2}\right| \right\}.$$

Expanding $x$ and $y$ from (3.13) and approximating $x$ and $y$ under the condition of SNR $\to \infty$ yields,

$$\begin{aligned} x &= -2j|G|^4 \Im\{H\} * \left( \begin{array}{l} A^8 - \frac{2A^4}{N^2} s_2^T s_1^* s_1^T s_2^* - \frac{\left(s_2^T\right)_.^2 \left(s_1^*\right)_.^2 \left(s_1^T\right)_.^2 \left(s_2^*\right)_.^2}{N^2} \\ + \frac{\left(s_2^T\right)_.^2 \left(s_1^*\right)_.^2 \left(s_1^T s_2^*\right)^2}{N^3} + \frac{\left(s_1^T\right)_.^2 \left(s_2^*\right)_.^2 \left(s_2^T s_1^*\right)^2}{N^3} \end{array} \right), \\ y &= -2j|G|^4 * \left( \begin{array}{l} A^8 - \frac{2A^4}{N^2} s_2^T s_1^* s_1^T s_2^* - \frac{\left(s_2^T\right)_.^2 \left(s_1^*\right)_.^2 \left(s_1^T\right)_.^2 \left(s_2^*\right)_.^2}{N^2} \\ + \frac{\left(s_2^T\right)_.^2 \left(s_1^*\right)_.^2 \left(s_1^T s_2^*\right)^2}{N^3} + \frac{\left(s_1^T\right)_.^2 \left(s_2^*\right)_.^2 \left(s_2^T s_1^*\right)^2}{N^3} \end{array} \right) \end{aligned} \tag{F.5}$$

Here we define $\mathbf{s}_.^2 \triangleq [s_1^2, s_2^2, ..., s_N^2]$, in which $\mathbf{s} = [s_1, s_2, ..., s_N]$. (F.5) shows

$|R_2(x,y)|_{up} \propto \frac{1}{|y|^2}$, which approaches 0 as SNR $\to \infty$. Then, we conclude that $T(x,y) = \frac{\mu_x}{\mu_y} + \frac{x}{\mu_y} - \frac{\mu_x y}{\mu_y^2}$ if SNR $\to \infty$. $\square$

# Appendix G

As frequency is perfect synchronised between both source nodes, source node $T_1$ down converts the received signal to the baseband signal

$$
\begin{aligned}
r(t) = H \textstyle\sum_{i=n_t+1}^{N} s_{1,i} f(t - iT - \tau) \\
+G \textstyle\sum_{i=n_t+1}^{N} s_{2,i} f(t - iT) + Kh_2 n_1(t) + n_2(t),
\end{aligned}
\tag{G.1}
$$

where $H = Kh_1h_2$ and $G = Kg_1h_2$. As $T_1$ is able to synchronize with $s_2(t)$, it filters the baseband signal with a matched filter $f'(t) = f(T-t)$ and then samples it every $T$ period to get,

$$
\begin{aligned}
r_{async}(i) = H \left[f_1(\tau)s_{1,i} + f_2(\tau)s_{1,i+1}\right] \\
+Gs_{2,i-n_t} + Kh_2 n_{1i} + n_{2i}, i = n_t + 1, ..., N.
\end{aligned}
\tag{G.2}
$$

where $f_1(\tau)$ and $f_2(\tau)$ are the factors resulting from the symbol offset $\tau$ and the use of a matched filter. $f_1(\tau)$ and $f_2(\tau)$ are estimated together with $H$ by the GLCML algorithm.

In the following, we will show the derivation from (G.1) to (G.2) step by step and conclude that the values of $f_1(\tau)$ and $f_2(\tau)$ are related to the filter type and symbol offset $\tau$. In addition, it is proved that $f_1(\tau), f_2(\tau) < 1$ regardless of the filter type.

As different type of filters do not affect the noise part in the received samples, we consider the noise free signal is received by $T_1$ for simplicity.

$$r(t) = H \sum_{i=n_t+1}^{N} s_{1,i} f(t - iT - \tau) + G \sum_{i=n_t+1}^{N} s_{2,i} f(t - iT).$$

Let $r(t)$ pass through the matched filter $f'(t)$, we obtain

$$\begin{aligned} r'(t) = r(t) * f'(t) &= \left(H \textstyle\sum_{i=n_t+1}^{N} s_{1,i} f(t - iT - \tau)\right) * f'(t) \\ &+ \left(G \textstyle\sum_{i=n_t+1}^{N} s_{2,i} f(t - iT)\right) * f'(t) \\ &= H \textstyle\int_{-\infty}^{\infty} \left(\sum_{i=n_t+1}^{N} s_{1,i} f(\mu - iT - \tau)\right) f'(t-\mu)\mathrm{d}\mu \\ &+ G \textstyle\int_{-\infty}^{\infty} \left(\sum_{i=n_t+1}^{N} s_{2,i} f(\mu - iT)\right) f'(t-\mu)\mathrm{d}\mu \\ &= H \textstyle\int_{-\infty}^{\infty} \left(\sum\limits_{i=1}^{N} s_{1,i} f(\mu - iT - \tau)\right) f(T - t + \mu)\mathrm{d}\mu \\ &+ G \textstyle\int_{-\infty}^{\infty} \left(\sum\limits_{i=1}^{N} s_{2,i} f(\mu - iT)\right) f(T - t + \mu)\mathrm{d}\mu \\ &= H \sum\limits_{i=n_t+1}^{N} \left(s_{1,i} \textstyle\int_{-\infty}^{\infty} f(\mu - iT - \tau) f(\mu + T - t)\mathrm{d}\mu\right) \\ &+ G \sum\limits_{i=n_t+1}^{N} \left(s_{2,i} \textstyle\int_{-\infty}^{\infty} f(\mu - iT) f(\mu + T - t)\mathrm{d}\mu\right). \end{aligned}$$

Define $x \triangleq \mu + T - t$, $r'(t)$ is updated as

$$\begin{aligned} r'(t) = H &\sum\limits_{i=n_t+1}^{N} \left(s_{1,i} \textstyle\int_{-\infty}^{\infty} f(x) f\left(x - (i+1)\,T + t - \tau\right)\mathrm{d}x\right) \\ +G &\sum\limits_{i=n_t+1}^{N} \left(s_{1,i} \textstyle\int_{-\infty}^{\infty} f(x) f\left(x - (i+1)\,T + t\right)\mathrm{d}x\right). \end{aligned}$$

Note that there exist auto-correlation terms of $f(x)$ in (G.3), we denote the auto-correlation of $f(x)$ as $R(\Delta x) = \int_{-\infty}^{\infty} f(x) f\left(x + \Delta x\right)\mathrm{d}x$ and obtain,

$$\begin{aligned} r'(t) = H &\textstyle\sum_{i=n_t+1}^{N} R(t - (i+1)\,T - \tau) s_{1,i} \\ +G &\textstyle\sum_{i=n_t+1}^{N} R(t - (i+1)\,T) s_{2,i}. \end{aligned}$$

Then sampling the signal every $T$ period yields,

$$r_{async}(i) = R(\tau)Hs_{1,i} + R(T-\tau)Hs_{1,i-1} + Gs_{2,i},$$
$$i = n_t + 1, ..., N.$$

Hence, $f_1(\tau) = R(\tau)$ and $f_2(\tau) = R(T-\tau)$, whose values are related to the filter type and symbol offset $\tau$. As the normalized value of $R(\Delta x)$ has the following property that $R(\Delta x) = 1$ if $\Delta x = 0$,otherwise $R(\Delta x) < 1$. Therefore, $f_1(\tau), f_2(\tau) < 1$. In the case of rectangle pulse shaping filters, $f_1(\tau) = \frac{T-\tau}{T}$ and $f_2(\tau) = \frac{\tau}{T}$.

# Bibliography

[1] T. Cover and A. E. Gamal, "Capacity theorems for the relay channel," *IEEE Transactions on Information Theory*, vol. 25, no. 5, pp. 572–584, 1979.

[2] H. Zimmermann, "Osi reference model–the iso model of architecture for open systems interconnection," *IEEE Transactions on Communications*, vol. 28, no. 4, pp. 425–432, 1980.

[3] R. Rom, M. Sidi, and R. R. M. Sidi, "Multiple access protocols: performance and analysis," 1990.

[4] E. Van der Meulen, "A survey of multi-way channels in information theory: 1961-1976," *IEEE Transactions on Information Theory*, vol. 23, no. 1, pp. 1–37, 1977.

[5] B. Yupeng Jia, "Channel estimation and optimal resource allocation of relay assisted communication systems," Ph.D. dissertation, University of Rochester.

[6] J. Zander, S.-L. Kim, M. Almgren, and O. Queseth, *Radio resource management for wireless networks.* Artech House, Inc., 2001.

[7] A. W. Scott and R. Frobenius, "Multiple access techniques: Fdma, tdma, and cdma," *RF Measurements for Cellular Phones and Wireless Data Systems*, pp. 413–429, 2010.

[8] J. N. Laneman, D. N. Tse, and G. W. Wornell, "Cooperative diversity in wireless networks: Efficient protocols and outage behavior," *IEEE Transactions on Information Theory*, vol. 50, no. 12, pp. 3062–3080, 2004.

[9] S. Y. Hui and K. H. Yeung, "Challenges in the migration to 4g mobile systems," *Communications Magazine, IEEE*, vol. 41, no. 12, pp. 54–59, 2003.

[10] J. Yick, B. Mukherjee, and D. Ghosal, "Wireless sensor network survey," *Computer networks*, vol. 52, no. 12, pp. 2292–2330, 2008.

[11] G. R. Hiertz, D. Denteneer, S. Max, R. Taori, J. Cardona, L. Berlemann, and B. Walke, "Ieee 802.11 s: the wlan mesh standard," *Wireless Communications, IEEE*, vol. 17, no. 1, pp. 104–111, 2010.

[12] V. Genc, S. Murphy, Y. Yu, and J. Murphy, "Ieee 802.16 j relay-based wireless access networks: an overview," *Wireless Communications, IEEE*, vol. 15, no. 5, pp. 56–63, 2008.

[13] S. W. Peters and R. W. Heath, "The future of wimax: multihop relaying with ieee 802.16 j," *Communications Magazine, IEEE*, vol. 47, no. 1, pp. 104–111, 2009.

[14] V. Chandrasekhar, J. Andrews, and A. Gatherer, "Femtocell networks: a survey," *Communications Magazine, IEEE*, vol. 46, no. 9, pp. 59–67, 2008.

[15] S. Parkvall, E. Dahlman, A. Furuskar, Y. Jading, M. Olsson, S. Wanstedt, and K. Zangi, "Lte-advanced-evolving lte towards imt-advanced," in *IEEE 68th Vehicular Technology Conference, 2008. VTC 2008-Fall.* IEEE, 2008, pp. 1–5.

[16] S. W. Peters, A. Y. Panah, K. T. Truong, and R. W. Heath, "Relay architectures for 3gpp lte-advanced," *EURASIP Journal on Wireless Communications and Networking*, vol. 2009, p. 1, 2009.

[17] J. Parikh and A. Basu, "Lte advanced: The 4g mobile broadband technology," *spectrum*, vol. 5, no. 2.5, p. 30, 2011.

[18] T. Cover and A. E. Gamal, "Capacity theorems for the relay channel," *IEEE Trans. Inform. Theory*, vol. 25, no. 5, pp. 572–584, Sep. 1979.

[19] J. N. Laneman, D. N. C. Tse, and G. W. Wornell, "Cooperative diversity in wireless networks: Efficient protocols and outage behavior," *IEEE Trans. Inform. Theory*, vol. 50, no. 12, pp. 3062–3080, Dec. 2004.

[20] B. Rankov and A. Wittneben, "Spectral efficient protocols for half-duplex fading relay channels," *IEEE Journal on Selected Areas in Communications*, vol. 25, no. 2, pp. 379–389, 2007.

[21] P. Popovski and H. Yomo, "Physical network coding in two-way wireless relay channels," in *IEEE International Conference on Communications, 2007. ICC'07.* IEEE, 2007, pp. 707–712.

[22] S. J. Kim, P. Mitran, and V. Tarokh, "Performance bounds for bidirectional coded cooperation protocols," *IEEE Transactions, Information Theory*, vol. 54, no. 11, pp. 5235–5241, 2008.

[23] T. J. Oechtering, C. Schnurr, I. Bjelakovic, and H. Boche, "Broadcast capacity region of two-phase bidirectional relaying," *IEEE Transactions, Information Theory*, vol. 54, no. 1, pp. 454–458, 2008.

[24] C. Schnurr, S. Stanczak, and T. J. Oechtering, "Achievable rates for the restricted half-duplex two-way relay channel under a partial-decode-and-forward protocol," in *Information Theory Workshop, 2008. ITW'08. IEEE.* IEEE, 2008, pp. 134–138.

[25] S. Katti, S. Gollakota, and D. Katabi, "Embracing wireless interference: analog network coding," in *ACM SIGCOMM Computer Communication Review*, vol. 37, no. 4. ACM, 2007, pp. 397–408.

[26] S. Massoud Amin and B. F. Wollenberg, "Toward a smart grid: power delivery for the 21st century," *Power and Energy Magazine, IEEE*, vol. 3, no. 5, pp. 34–41, 2005.

[27] P. P. Parikh, M. G. Kanabar, and T. S. Sidhu, "Opportunities and challenges of wireless communication technologies for smart grid applications," in *Power and Energy Society General Meeting, 2010 IEEE*. IEEE, 2010, pp. 1–7.

[28] H. J. Fowler and W. E. Leland, "Local area network characteristics, with implications for broadband network congestion management," *IEEE Journal on Selected Areas in Communications*, vol. 9, no. 7, pp. 1139–1149, 1991.

[29] P. A. Morreale and G. Campbell, "Metropolitan-area networks," *Spectrum, IEEE*, vol. 27, no. 5, pp. 40–42, 1990.

[30] V. Garg, *Wireless Communications & Networking*. Morgan Kaufmann, 2010.

[31] N. Bandeira and L. Poulsen, "Scalable wireless network topology systems and methods," Apr. 27 2004, uS Patent 6,728,514.

[32] I. F. Akyildiz, X. Wang, and W. Wang, "Wireless mesh networks: a survey," *Computer networks*, vol. 47, no. 4, pp. 445–487, 2005.

[33] I. F. Akyildiz, W. Su, Y. Sankarasubramaniam, and E. Cayirci, "A survey on sensor networks," *Communications magazine, IEEE*, vol. 40, no. 8, pp. 102–114, 2002.

[34] T. T. Ha, *Digital satellite communications*, 1986, vol. 86.

[35] A. J. Viterbi *et al.*, *CDMA: principles of spread spectrum communication.* Addison-Wesley Reading, 1995, vol. 129.

[36] C. Pemble, "Time division satellite acquisition," May 21 2002, uS Patent 6,392,593.

[37] I. F. B. H. V. Poor, "Communications and networks," *Urbana*, vol. 51, 1986.

[38] L. Georgiadis, "Carrier-sense multiple access (csma) protocols," *Encyclopedia of Telecommunications*, 2003.

[39] K. Christensen, P. Reviriego, B. Nordman, M. Bennett, M. Mostowfi, and J. A. Maestro, "Ieee 802.3 az: the road to energy efficient ethernet," *IEEE Communications Magazine*, vol. 48, no. 11, pp. 50–56, 2010.

[40] P. Kinney *et al.*, "Zigbee technology: Wireless control that simply works," in *Communications design conference*, vol. 2, 2003.

[41] A. V. Dolikian, "Synchronizing means for a two-way communication system," Oct. 28 1980, uS Patent 4,231,114.

[42] F. Gao, R. Zhang, and Y.-C. Liang, "On channel estimation for amplify-and-forward two-way relay networks," in *Global Telecommunications Conference, 2008. IEEE GLOBECOM 2008. IEEE.* IEEE, 2008, pp. 1–5.

[43] S. Benedetto and E. Biglieri, *Digital Transmission Theory: With Wireless Applications.* Springer, 1999.

[44] J. G. Proakis, *Intersymbol Interference in Digital Communication Systems.* Wiley Online Library, 1995.

[45] C. Helmberg, F. Rendl, R. J. Vanderbei, and H. Wolkowicz, "An interior-point method for semidefinite programming," *SIAM Journal on Optimization*, vol. 6, no. 2, pp. 342–361, 1996.

[46] T. Unger and A. Klein, "Applying relay stations with multiple antennas in the one-and two-way relay channel," in *18th International Symposium on Personal, Indoor and Mobile Radio Communications, 2007. PIMRC 2007. IEEE*. IEEE, 2007, pp. 1–5.

[47] R. Zhang, Y.-C. Liang, C. C. Chai, and S. Cui, "Optimal beamforming for two-way multi-antenna relay channel with analogue network coding," *IEEE Journal on Selected Areas in Communications*, vol. 27, no. 5, pp. 699–712, 2009.

[48] K. Jitvanichphaibool, R. Zhang, and Y.-C. Liang, "Optimal resource allocation for two-way relay-assisted ofdma," *IEEE Transactions on Vehicular Technology*, vol. 58, no. 7, pp. 3311–3321, 2009.

[49] D. Zeng, S. Guo, Y. Xiang, and H. Jin, "On the throughput of two-way relay networks using network coding," 2014.

[50] Y. Jing and H. Jafarkhani, "Network beamforming using relays with perfect channel information," *IEEE Transactions on Information Theory*, vol. 55, no. 6, pp. 2499–2517, 2009.

[51] V. Havary-Nassab, S. Shahbazpanahi, and A. Grami, "Optimal distributed beamforming for two-way relay networks," *IEEE Transactions on Signal Processing*, vol. 58, no. 3, pp. 1238–1250, 2010.

[52] F. Gao, T. Cui, and A. Nallanathan, "On channel estimation and optimal training design for amplify and forward relay networks," *IEEE Transactions, Wireless Communications*, vol. 7, no. 5, pp. 1907–1916, 2008.

[53] G. Wang, F. Gao, and C. Tellambura, "Joint frequency offset and channel estimation methods for two-way relay networks," in *Global Telecommunications Conference, 2009. GLOBECOM 2009. IEEE*. IEEE, 2009, pp. 1–5.

[54] K. Zhong, X. Lei, S. Hu, and S. Li, “On channel estimation and detection for amplify-and-forward orthogonal frequency division multiplexing-based two-way relay systems under unknown non-reciprocal doubly selective fading channels,” *Institution of Engineering and Technology*, 2014.

[55] C. Shin, R. W. Heath, and E. J. Powers, “Blind channel estimation for mimo-ofdm systems,” *IEEE Transactions, Vehicular Technology*, vol. 56, no. 2, pp. 670–685, 2007.

[56] F. Gao, R. Zhang, and Y.-C. Liang, “Optimal channel estimation and training design for two-way relay networks,” *IEEE Transactions on Communications*, vol. 57, no. 10, pp. 3024–3033, 2009.

[57] F. Roemer and M. Haardt, “Tensor-based channel estimation and iterative refinements for two-way relaying with multiple antennas and spatial reuse,” *IEEE Transactions on Signal Processing*, vol. 58, no. 11, pp. 5720–5735, 2010.

[58] F. Gao, R. Zhang, and Y.-C. Liang, “Channel estimation for ofdm modulated two-way relay networks,” *Signal Processing, IEEE Transactions on*, vol. 57, no. 11, pp. 4443–4455, 2009.

[59] S. Abdallah and I. N. Psaromiligkos, “Semi-blind channel estimation for amplify-and-forward two-way relay networks employing constant-modulus constellations,” in *Information Sciences and Systems (CISS), 2010 44th Annual Conference on.* IEEE, 2010, pp. 1–5.

[60] S. Abdallah and I. Psaromiligkos, “Blind channel estimation for amplify-and-forward two-way relay networks employing m -psk modulation,” *IEEE Transactions, Signal Processing*, vol. 60, no. 7, pp. 3604–3615, 2012.

[61] D. Tse and P. Viswanath, *Fundamentals of wireless communication.* Cambridge university press, 2005.

[62] S. P. Boyd and L. Vandenberghe, *Convex optimization.* Cambridge university press, 2004.

[63] J. Barnes, "The measurement of linear frequency drift in oscillators," in *In NRL Proc. of the 15th Ann. Precise Time and Time Interval (PTTI) Appl. and Planning Meeting p 551-582 (SEE N85-28287 17-35)*, vol. 1, 1985, pp. 551–582.

[64] A. A. Nasir, *Synchronization in Cooperative Communication Systems.* The Australian National University, 2012.

[65] U. Mengali and A. N. D'Andrea, *Synchronization techniques for digital receivers.* Springer, 1997.

[66] X. Liao, L. Fan, and F. Gao, "Blind channel estimation for ofdm modulated two-way relay network," in *Wireless Communications and Networking Conference (WCNC), 2010 IEEE.* IEEE, 2010, pp. 1–5.

[67] Y.-C. Liang, H. Garg, A. Nallanathan *et al.*, "Joint channel estimation and data detection for mimo-ofdm two-way relay networks," in *Global Telecommunications Conference (GLOBECOM 2010), 2010 IEEE.* IEEE, 2010, pp. 1–5.

[68] G. Wang, F. Gao, Y.-C. Wu, and C. Tellambura, "Joint cfo and channel estimation for ofdm-based two-way relay networks," *IEEE Transactions on Wireless Communications*, vol. 10, no. 2, pp. 456–465, 2011.

[69] K. Sohraby, D. Minoli, and T. Znati, *Wireless sensor networks: technology, protocols, and applications.* John Wiley & Sons, 2007.

[70] Z. Ding and G. Y. Li, *Blind channel equalization and identification.* CRC press, 2001, vol. 9.

[71] Y. Tian, X. Lei, Y. Xiao, and S. Li, "Ml synchronization algorithm and estimation bounds for cooperative systems," in *Circuits, Communications and System (PACCS), 2010 Second Pacific-Asia Conference on*, vol. 1. IEEE, 2010, pp. 379–382.

[72] Y. Tian, X. Lei, , and S. Li, "Sage based joint timing-frequency offsets and channel estimation in distributed mimo systems," *Computer Communications*, vol. 33, no. 17, pp. 2125–2131, 2010.

[73] B.-J. Kwak, N.-O. Song, and L. E. Miller, "Performance analysis of exponential backoff," *IEEE/ACM Transactions on Networking*, vol. 13, no. 2, pp. 343–355, 2005.

[74] C. Ye, Y. Li, and A. Reznik, "Performance analysis of exponential increase exponential decrease back-off algorithm," in *Global Telecommunications Conference (GLOBECOM 2010), 2010 IEEE*. IEEE, 2010, pp. 1–6.

[75] G. Bianchi, L. Fratta, and M. Oliveri, "Performance evaluation and enhancement of the csma/ca mac protocol for 802.11 wireless lans," in *Seventh IEEE International Symposium on Personal, Indoor and Mobile Radio Communications, 1996. PIMRC'96.*, vol. 2. IEEE, 1996, pp. 392–396.

[76] F. Cali, M. Conti, and E. Gregori, "Ieee 802.11 protocol: design and performance evaluation of an adaptive backoff mechanism," *IEEE Journal on Selected Areas in Communications*, vol. 18, no. 9, pp. 1774–1786, 2000.

[77] M. Heusse, F. Rousseau, R. Guillier, and A. Duda, "Idle sense: an optimal access method for high throughput and fairness in rate diverse wireless lans," in *ACM SIGCOMM Computer Communication Review*, vol. 35, no. 4. ACM, 2005, pp. 121–132.

[78] K. Hong, S. Lee, K. Kim, and Y. Kim, “Channel condition based contention window adaptation in ieee 802.11 wlans,” *IEEE Transactions on Communications*, vol. 60, no. 2, pp. 469–478, 2012.

[79] F. Daneshgaran, M. Laddomada, F. Mesiti, and M. Mondin, “Unsaturated throughput analysis of ieee 802.11 in presence of non ideal transmission channel and capture effects,” *IEEE Transactions on Wireless Communications*, vol. 7, no. 4, pp. 1276–1286, 2008.

[80] D. Malone, K. Duffy, and D. Leith, “Modeling the 802.11 distributed coordination function in nonsaturated heterogeneous conditions,” *IEEE/ACM Transactions on Networking*, vol. 15, no. 1, pp. 159–172, 2007.

[81] O. Tickoo and B. Sikdar, “Modeling queueing and channel access delay in unsaturated ieee 802.11 random access mac based wireless networks,” *IEEE/ACM Transactions on Networking (TON)*, vol. 16, no. 4, pp. 878–891, 2008.

[82] J. Misic, V. B. Misic, and S. Shafi, “Performance of ieee 802.15. 4 beacon enabled pan with uplink transmissions in non-saturation mode-access delay for finite buffers,” in *Broadband Networks, 2004. BroadNets 2004. Proceedings. First International Conference on.* IEEE, 2004, pp. 416–425.

[83] L. Kleinrock, “Queueing systems. volume 1: Theory,” 1975.

[84] U. Mengali and A. N. D’Andrea, *Synchronization techniques for digital receivers.* Springer, 1997.

[85] J. M. Wooldridge, *Introductory econometrics: a modern approach.* Cengage Learning, 2012.

[86] W. R. Gilks, S. Richardson, and D. J. Spiegelhalter, *Markov chain Monte Carlo in practice.* CRC press, 1996, vol. 2.

[87] A. D. Kucar, "Mobile radio: An overview," *Communications Magazine, IEEE*, vol. 29, no. 11, pp. 72–85, 1991.

[88] R. Prasad, *CDMA for wireless personal communications.* Artech House, Inc., 1996.

[89] W. Ye, "Carrier sense multiple access protocols," *Handbook of Computer Networks: LANs, MANs, WANs, the Internet, and Global, Cellular, and Wireless Networks, Volume 2*, pp. 779–789, 2008.

[90] C. E. Shannon, "Two-way communication channels," in *Proc. 4th Berkeley Symp. Math. Stat. Prob*, vol. 1, 1961, pp. 611–644.

[91] S. S. Rao and S. Rao, *Engineering optimization: theory and practice.* John Wiley & Sons, 2009.

[92] W. K. Newey and D. McFadden, "Large sample estimation and hypothesis testing," *Handbook of econometrics*, vol. 4, pp. 2111–2245, 1994.

[93] K. Itō, *Encyclopedic dictionary of mathematics.* The MIT Press, 1993, vol. 1.

[94] A. I. Markuševič, *Theory of functions of a complex variable.* AMS Bookstore, 2005, vol. 1.

[95] P. Dent, G. E. Bottomley, and T. Croft, "Jakes fading model revisited," *Electronics Letters*, vol. 29, no. 13, pp. 1162–1163, 1993.

[96] J. Lewis, "Fast normalized cross-correlation," in *Vision interface*, vol. 10, no. 1, 1995, pp. 120–123.

[97] H. Cramér, *Random variables and probability distributions.* Cambridge University Press, 2004, no. 36.

[98] N. A. Weiss, P. T. Holmes, and M. Hardy, *A course in probability.* Pearson Addison Wesley, 2006.